An exact Riemann solver for one-dimensional multi-material elastic-plastic flows with Mie-Grüneisen equation of state without vacuum

Li Liu [1], Jun-Bo Cheng [1,*], Yongxing Shen [2]

[1] *Laboratory of Computational Physics, Institute of Applied Physics and Computational Mathematics, Beijing 100094, China*

[2] *University of Michigan - Shanghai Jiao Tong University Joint Institute, Shanghai Jiao Tong University, Shanghai, 200240, China*

Abstract

In this paper, we present exact Riemann solvers for the Riemann problem and the half Riemann problem, respectively, for one-dimensional multi-material elastic-plastic flows with the Mie-Grüneisen equation of state(EOS), hypo-elastic constitutive model and the von Mises' yielding condition. We firstly analyze the Jacobian matrices in the elastic and plastic states, and then build the relations of different variables across different type of waves. Based on these formulations, an exact Riemann solver is constructed with totally thirty-six possible cases of wave structures. A large number of tests prove the rightness of the new exact Riemann solver. Moreover, an exact Riemann solver is also deduced for the half Riemann problem and its validity is tested by two examples.

Keywords: Elastic-plastic flows, Riemann problem, hypo-elastic model, exact Riemann solver, Mie-Grüneisen equation

1. Introduction

In this paper, an exact Riemann solver is built for one-dimensional multi-material elastic-plastic flows modeled by the Mie-Grüneisen equation of state (EOS) [1, 2], hypo-elastic constitutive model and the von Mises' yielding condition.

The elastic-plastic flow is used to describe the deformation process of solid materials, especially metals, under strong dynamics loading, such as explosive or high-speed impact. The simulation of elastic-plastic flows has important application backgrounds, especially in the Implosion Dynamics weapon and Inertial Confine Fusion (ICF). The first try of simulating the elastic-plastic flows was given by Wilkins [3] in 1960s. In his work, the hypo-elastic constitutive model with the von Mises' yielding condition (so-called the elastic-perfectly plastic model) is considered with a simple EOS that pressure only depends on density. Following [3], Maire et.al [4] developed a high-order cell-centered Lagrangian scheme with the same elastic-plastic constitutive model with the Mie-Grüneisen EOS which is widely used in characterring real materials [1]. Besides the elastic-perfectly plastic model, there are other more complex models for elastic-plastic deformations, such as the

*Correspondence to: Jun-Bo Cheng, Institute of Applied Physics and Computational Mathematics, Beijing 100094, China. E-mail: Cheng_junbo@iapcm.ac.cn

September 12, 2020

hypo-elastic constitutive model with strain hardening (HCMSH) [5] and Steinberg-Guinan (SG) constitutive model [6] and so on. In this paper, only the elastic-perfectly plastic model with the Mie-Grüneisen EOS is considered for its general applications in the numerical study of elastic-plastic flows [7, 8, 9].

Riemann problems and the corresponding solvers have been viewed as essential problems for the study of computational fluid dynamics (CFD) since the introduction of Godunov schemes [10] and their high-order extensions [11]. In the following two decades, a lot of famous and widely used approximate Riemann solvers are proposed, such as the Roe Riemann solver [12], the HLL [13], HLLC [14] and HLLE Riemann solvers[15]. Even recently, Riemann problems still attract much attention, especially in the following three aspects. The first is to reduce numerical dissipation and to approve the robustness of schemes [16, 17]; the second is to develop two-dimensional Riemann solvers [18, 19, 20]; and the third is to extend the existin approximate solvers to other systems, such as the magnetohydrodynamic (MHD) [21, 18] and elastic-plastic flows [22, 23, 24, 25]. In the study of Riemann problems, the exact Riemann solver has also played a very important role as it not only can give a guide and reference in constructing approximate Riemann solvers, but also can be used to determine the convergence and stability of numerical schemes. Besides the exact Riemann solver for Euler equations which is used in the first Godunov scheme given by Godunov [10], some exact Riemann solvers are also constructed for other systems, for example, for highly transient mixed flows [26], for two-phase flows containing non-conservative products [27] and for shallow water equations system [28]. In solving the Riemann problems of these systems, solving procedures are different. For example, for the shallow water equations with discontinuous bottom geometry [28], we only need to solve algebraic equations; but for general hyperbolic equations [10, 26, 27, 29, 30, 31], the iteration procedures are necessary. Recently, the exact Riemann solver for elastic-plastic flows also attracts much attention [29, 30, 31]. However, building the exact Riemann solver for elastic-plastic flows is not easy. Comparing with the governing equations of 1D pure fluids, for 1D elastic-plastic flows, there are two more equations, a non-conservative constitutive equation and the von Mises yielding condition, needed to be considered. The non-conservative character of the constitutive equation increases the difficulty in constructing Riemann solvers, while the von Mises yielding condition may lead to more non-linear waves in the wave structure of Riemann solvers. Moreover, in a general way, the equation of state(EOS) for solid materials is more complex than that for pure fluids, which directly increases the difficulty in solving the Riemann problem.

For the elastic-plastic flow with the hypo-elastic constitutive model and the von Mises' yielding condition, some approximate Riemann solvers[22, 23, 24, 25, 20] have been developed recently. However, for the exact Riemann solver, the research is relatively few, and focuses mainly on the problems with relatively simple constitutive models or relatively simple EOSs. For example, Garaizar [32] and Miller [30] introduced an exact Riemann solver for elastic or hyper-elastic materials, Gao and Liu [33, 34] firstly considered the yielding effect and developed an exact elastic-perfectly plastic solid Riemann solver. In Gao and Liu works [33, 34], a five-equation Eulerian governing system is constructed, and a complete list of sixty-four cases of wave type

is presented.

In this paper, we construct an exact Riemann solver for the system of 1D elastic-plastic flows with the Mie-Grüneisen EOS, the hypo-elastic constitutive model and the von Mises' yielding condition. Although Gao and Liu [33, 34] have developed a comprehensive exact Riemann solver for a five-equation system with 1D elastic-perfectly plastic solid, but their exact Riemann solver is not suitable for a general four-equation system because there are big differences between these two systems. In the four-equation system in Section 2.1, the elastic and plastic states are treated with same equations of mass, momentum, total energy and the same complex Mie-Grneisen EOS, but only different in deviatoric stress. While in the five-equation system, two states are separated and they have their own densities, velocities and EOSs. For example, in the elastic state, the pressure is only a function of density and the internal energy is not necessarily considered; in the plastic state, a linear stiffened-gas EOS is used, which is the simplified form of the Mie-Grneisen EOS. Moreover, the four-equation system is widely used in many engineering areas since the seminal work by Wilkins [3] and the following works [4, 35, 36, 23, 37, 38]. For these reasons, we want to construct an exact Riemann solver for the common used four-equation system and with a more general case of real materials characterized by the Mie-Grüneisen EOS [3].

This paper is organized as follows. In Section 2, we introduce the governing equations to be studied. In Section 3, the Riemann problem and the relations for every wave type (contact wave, shock wave and rarefaction wave) are derived. Then, the exact Riemann solver is given in Section 4. The half Riemann problem and its solver is introduced in Section 5. Some numerical examples are presented to validate our Riemann solvers in Section 6. Conclusions are shown in Section 7.

2. Governing equations

In this paper, the elastic energy is not included in the total energy. The exclusion of the elastic energy is usual for practical engineering problems [4] and is different from that in Ref.[22].

2.1. Motion equations

For a continuous one-dimensional homogeneous solid, the motion equations in the differential form are

$$\partial_t \mathbf{U} + \partial_x \boldsymbol{F}(\mathbf{U}) = 0,\ x \in\ \Omega \subset \mathbf{R},\ t > 0,$$

where

$$\mathbf{U} = \begin{bmatrix} \rho \\ \rho u \\ \rho E \end{bmatrix}, \quad \mathbf{F} = \begin{bmatrix} \rho u \\ \rho u^2 - \sigma \\ (\rho E - \sigma) u \end{bmatrix}, \tag{2.1}$$

ρ, u, σ and E are the density, velocity in $x-$direction, Cauchy stress and total energy per unit volume, respectively, E has the relation with the specific internal energy e as

$$E = e + \frac{1}{2}u^2, \tag{2.2}$$

$$\sigma = -p + s_{xx}, \tag{2.3}$$

where p and s_{xx} denote the hydrostatic pressure and the deviatoric stress in the $x-$ direction, respectively.

2.2. The equation of state (EOS)

The relation of the pressure with the density and the specific internal energy is gotten from the equation of state (EOS). In this paper, we consider the Mie-Grüneisen EOS,

$$p(\rho, e) = \rho_0 a_0^2 f(\eta) + \rho_0 \Gamma_0 e, \tag{2.4}$$

where $f(\eta) = \frac{(\eta-1)(\eta-\Gamma_0(\eta-1)/2)}{(\eta-s(\eta-1))^2}$, $\eta = \frac{\rho}{\rho_0}$, ρ_0, a_0, s and Γ_0 are the constant parameters of the Mie-Grüneisen EOS.

2.3. The constitutive relation

Hooke's law is used here to describe the relationship between the deviatoric stress and the strain [39, 40],

$$\dot{s}_{xx} = 2\mu\left(\dot{\varepsilon}_x - \frac{1}{3}\frac{\dot{V}}{V}\right), \tag{2.5}$$

where μ is the shear modulus, V is the volume, and the dot means the material time derivative,

$$\dot{()} = \frac{\partial()}{\partial t} + u\frac{\partial()}{\partial t}, \tag{2.6}$$

and

$$\dot{\varepsilon}_x = \frac{\partial u}{\partial x}, \quad \frac{\dot{V}}{V} = \frac{\partial u}{\partial x}. \tag{2.7}$$

By using Eq.(2.7), Eq.(2.5) can be rewritten as

$$\frac{\partial s_{xx}}{\partial t} + u\frac{\partial s_{xx}}{\partial t} = \frac{4}{3}\mu\frac{\partial u}{\partial x}. \tag{2.8}$$

2.4. The yielding condition

The Von Mises' yielding condition is used here to describe the elastic limit. In one spatial dimension, the von Mises' yielding criterion is given by

$$|s_{xx}| \leq \frac{2}{3}Y_0, \tag{2.9}$$

where Y_0 is the yield strength of the material in simple tensions.

3. The Riemann problem

The Riemann problem for 1D time dependent elastic-plastic equations is given as follows:

$$\begin{cases} \partial_t \rho + \partial_x(\rho u) = 0, \\ \partial_t(\rho u) + \partial_x(\rho u^2 + p - s_{xx}) = 0, \\ \partial_t(\rho E) + \partial_x\left[(\rho E + p - s_{xx})u\right] = 0, \\ \begin{cases} \partial_t s_{xx} + u\partial_x s_{xx} - \frac{4}{3}\partial_x u = 0, \\ |s_{xx}| \le \frac{2}{3}Y_0, \end{cases} \\ Q(x, t=0) = \begin{cases} Q_L, \text{ if } x < 0, \\ Q_R, \text{ if } x > 0, \end{cases} \end{cases} \tag{3.1}$$

where $Q = (\rho, \rho u, \rho E, s_{xx})^T$.

Firstly, we assume that the wave structure of this Riemann problem is self-similar [20, 41].

If the material is in the plastic state, the above forth equation can be simplified. Correspondingly, sonic velocity is different from that in the elastic state, which will be discussed in the following.

3.1. Elastic state

3.1.1. Jacobian matrix in elastic regions

For the Mie-Grüneisen EOS, if the material is not yielding,

$$|s_{xx}| < \frac{2}{3}Y_0,$$

the system (3.1) can be written as

$$\partial_t \mathbf{Q} + \mathbf{J}_e(\mathbf{Q})\partial_x \mathbf{Q} = 0,$$

where $Q = (\rho, \rho u, \rho E, s_{xx})$, and the Jacobian matrix is

$$\mathbf{J}_e(Q) = \begin{bmatrix} 0 & 1 & 0 & 0 \\ -u^2 + \frac{\partial p}{\partial \rho} + \Gamma(\frac{u^2}{2} - e) & u(2-\Gamma) & \Gamma & -1 \\ (\Gamma(\frac{u^2}{2} - e) - e - \frac{u^2}{2} + \frac{\sigma}{\rho} + \frac{\partial p}{\partial \rho})u & -\Gamma u^2 - \frac{\sigma}{\rho} + \frac{u^2}{2} + e & (1+\Gamma)u & -u \\ \frac{4}{3}\mu\frac{u}{\rho} & -\frac{4}{3}\mu\frac{1}{\rho} & 0 & u \end{bmatrix}, \tag{3.2}$$

where $\Gamma = \frac{\Gamma_0 \rho_0}{\rho}$.

The eigenvalues of $\mathbf{J}_e(\mathbf{Q})$ are given as

$$\lambda_1 = \lambda_2 = u, \quad \lambda_3 = u - c_e, \quad \lambda_4 = u + c_e,$$

where c_e means the sonic speed of the solid in the elastic state,

$$\begin{cases} c_e = \sqrt{a^2 - \dfrac{\rho_0}{\rho^2}\Gamma_0 s_{xx} + \dfrac{4}{3}\dfrac{\mu}{\rho}}, \\ a^2 = \dfrac{\partial p}{\partial \rho} + \dfrac{p}{\rho^2}\dfrac{\partial p}{\partial e} = a_0^2\dfrac{\partial f}{\partial \eta} + \dfrac{p}{\rho^2}\rho_0\Gamma_0. \end{cases} \tag{3.3}$$

Corresponding right eigenvectors are

$$r_1 = \begin{bmatrix} \frac{1}{b_1} \\ \frac{u}{b_1} \\ 0 \\ 1 \end{bmatrix}, \quad r_2 = \begin{bmatrix} -\frac{\Gamma}{b_1} \\ -\frac{\Gamma u}{b_1} \\ 1 \\ 0 \end{bmatrix}, \quad r_3 = \frac{1}{\phi^2}\begin{bmatrix} 1 \\ u - c_e \\ h - uc_e \\ \phi^2 \end{bmatrix}, \quad r_4 = \frac{1}{\phi^2}\begin{bmatrix} 1 \\ u + c_e \\ h + uc_e \\ \phi^2 \end{bmatrix}, \tag{3.4}$$

where

$$b_1 = \frac{\partial p}{\partial \rho} - \Gamma E, \quad h = E + \frac{p - s_{xx}}{\rho},$$

and

$$\phi^2 = a^2 - \frac{\rho_0}{\rho^2}\Gamma_0 s_{xx} - c_e^2 = -\frac{4\mu}{3}\frac{1}{\rho}.$$

3.1.2. Relations across the contact wave

For a system without molecular diffusion, there is no materials convecting across the contact wave or interface, so the velocities on two sides of the discontinuity are always equal. This can also be verified by eigenvectors in Eq.(3.4) and Eq.(3.51).

Use $\mathbf{Q}_L^*$ and $\mathbf{Q}_R^*$ to denote the two states connected by the contact wave in the solution, where $\mathbf{Q} = (\rho, u, p, s_{xx})$.

Thanks to Eq.(3.4), based on the theory of Generalised Riemann Invariants introduced by [41, 42], for the λ_1-wave we have

$$\frac{d\rho}{\frac{1}{b_1}} = \frac{d\rho u}{\frac{u}{b_1}} = \frac{d\rho E}{0} = \frac{ds_{xx}}{1}. \tag{3.5}$$

From above equations, we can easily deduce that

$$du = 0, \quad d(s_{xx} - p) = 0, \tag{3.6}$$

which means

$$u_L^* = u_R^*, \tag{3.7}$$

and

$$\sigma_{x,L}^* = \sigma_{x,R}^*, \tag{3.8}$$

where $()_L^*$ and $()_R^*$ denote $()$ in the regions of $\mathbf{Q}_L^*$ and $\mathbf{Q}_R^*$, respectively. Here we do not show the details of the derivation for a simple presentation.

Similarly, for the λ_2-wave one has

$$\frac{d\rho}{\frac{-\Gamma}{b_1}} = \frac{d\rho u}{\frac{-u\Gamma}{b_1}} = \frac{d\rho E}{1} = \frac{ds_{xx}}{0}. \tag{3.9}$$

From the above equations, we can easily deduce that

$$du = 0, \quad dp = 0, \quad ds_{xx} = 0, \tag{3.10}$$

which means

$$u_L^* = u_R^*, \tag{3.11}$$

$$p_L^* = p_R^*, \quad s_{xx,L}^* = s_{xx,R}^*. \tag{3.12}$$

From Eq.(3.12), we get that

$$\sigma_{x,L}^* = \sigma_{x,R}^*. \tag{3.13}$$

At last, for the λ_1 and λ_2 waves, one can find that the following two relations always hold:

$$u_L^* = u_R^*, \quad \sigma_{x,L}^* = \sigma_{x,R}^*. \tag{3.14}$$

For convenience, we define

$$s^* = u_L^* = u_R^*. \tag{3.15}$$

where s^* denotes the velocity of the contact wave.

3.1.3. Relations across rarefaction waves

Left-going rarefaction wave

Across the left wave associated with λ_3-wave, ($\lambda_3 = u - c_e$), we have

$$\frac{d\rho}{1} = \frac{d(\rho u)}{u - c_e} = \frac{d(\rho E)}{h - uc_e} = \frac{ds_{xx}}{-\frac{4\mu}{3}\frac{1}{\rho}}. \tag{3.16}$$

which leads to

$$\mathrm{d}u = -\frac{c_e}{\rho}\mathrm{d}\rho, \tag{3.17}$$

$$\mathrm{d}E = -\frac{\sigma + \rho u c_e}{\rho^2}d\rho, \tag{3.18}$$

$$\mathrm{d}s_{xx} = -\frac{4}{3}\frac{\mu}{\rho}d\rho. \tag{3.19}$$

Using (2.4), one can get

$$dE = de + udu. \tag{3.20}$$

Substituting (3.17) and (3.18) into the above equation yields

$$de = -\frac{\sigma}{\rho^2}d\rho = \frac{p - s_{xx}}{\rho^2}d\rho. \tag{3.21}$$

Thanks to (2.4), one can get

$$dp = \frac{\partial p}{\partial \rho}d\rho + \frac{\partial p}{\partial e}de = a_0^2\frac{\partial f}{\partial \eta}d\rho + \rho_0\Gamma_0 de, \tag{3.22}$$

Substituting (3.21) into the above equation yields

$$dp = \left(a_0^2\frac{\partial f}{\partial \eta} + \frac{p}{\rho^2}\rho_0\Gamma_0 - \frac{\rho_0}{\rho^2}\Gamma_0 s_{xx}\right)d\rho. \tag{3.23}$$

The above equation can be rewritten as a differential equation of $p(\rho)$

$$p'(\rho) - \lambda\frac{p}{\rho^2} = f_2(\rho), \tag{3.24}$$

where

$$\lambda = \rho_0\Gamma_0 \quad f_2(\rho) = a_0^2\frac{\partial f}{\partial \eta} - \lambda\frac{s_{xx}(\rho)}{\rho^2}. \tag{3.25}$$

By integrating (3.24) across the left rarefaction wave, the pressure can be solved out as

$$pe^{\frac{\lambda}{\rho}} - \int f_2(\rho)e^{\frac{\lambda}{\rho}}d\rho = \text{constant}. \tag{3.26}$$

Integrating (3.17) across the left rarefaction wave yields

$$u + \int \frac{c_e}{\rho}d\rho = \text{constant}. \tag{3.27}$$

Right-going rarefaction wave

Across the right wave associated with λ_4-wave, ($\lambda_3 = u + c_e$), we have

$$\frac{d\rho}{1} = \frac{d(\rho u)}{u + c_e} = \frac{d(\rho E)}{h + uc_e} = \frac{ds_{xx}}{-\frac{4\mu}{3}\frac{1}{\rho}}. \tag{3.28}$$

which leads to

$$\mathrm{d}u = \frac{c_e}{\rho}\mathrm{d}\rho, \tag{3.29}$$

$$\mathrm{d}E = -\frac{\sigma + \rho u c_e}{\rho^2}d\rho, \tag{3.30}$$

$$\mathrm{d}s_{xx} = -\frac{4}{3}\frac{\mu}{\rho}d\rho. \tag{3.31}$$

By using the same method as the left wave, one can get

$$pe^{\frac{\lambda}{\rho}} - \int f_2(\rho)e^{\frac{\lambda}{\rho}}d\rho = \text{constant}. \tag{3.32}$$

$$u - \int \frac{c_e}{\rho}d\rho = \text{constant}. \tag{3.33}$$

3.1.4. Relations across shock waves

Now we consider a shock wave moving with the speed of s. The data in front of the shock is $(\rho_1, u_1, p_1, s_{xx1})$ and that after the shock is $(\rho_2, u_2, p_2, s_{xx2})$.

We transform the equations to a frame of reference moving with the shock. The Rankine-Hugoniot conditions are given as

$$\rho_2(u_2 - s) = \rho_1(u_1 - s), \tag{3.34}$$

$$\rho_2 u_2(u_2 - s) = \rho_1 u_1(u_1 - s) + \sigma_2 - \sigma_1, \tag{3.35}$$

$$\rho_2 E_2(u_2 - s) = \rho_1 E_1(u_1 - s) + \sigma_2 u_2 - \sigma_1 u_1. \tag{3.36}$$

Substituting (3.34) into (3.35) yields

$$\rho_1(u_2 - u_1)(u_1 - s) = \sigma_2 - \sigma_1. \tag{3.37}$$

From (3.34), one has

$$u_1 - s = \frac{(u_1 - u_2)\rho_2}{\rho_2 - \rho_1}, \tag{3.38}$$

then substituting it into (3.37) yields

$$-t(u_2 - u_1)^2 = \sigma_2 - \sigma_1, \tag{3.39}$$

where $t = \frac{\rho_1\rho_2}{\rho_2 - \rho_1}$.

By using the same methods for (3.39), (3.36) can be written as

$$t(u_1 - u_2)(E_2 - E_1) = \sigma_2 u_2 - \sigma_1 u_1. \tag{3.40}$$

Because of $E = e + \frac{1}{2}u^2$, we can get

$$e_2 - e_1 = -\frac{\sigma_1 + \sigma_2}{2t}. \tag{3.41}$$

Using the EOS of Mie-Grüneisen (2.4), can get

$$e = c_0 p - c_1 f(\rho/\rho_0), \tag{3.42}$$

where $c_0 = \frac{1}{\rho_0 \Gamma_0}$ and $c_1 = \frac{a_0^2}{\Gamma_0}$. Put the above equation into (3.41), we can formulate the pressure p_2 in terms of ρ_2.

$$p_2 = \frac{2t(c_1 f(\rho_2/\rho_0) + e_1) - (\sigma_1 + s_{xx2})}{2tc_0 - 1}. \tag{3.43}$$

Thanks to (3.66), s_{xx2} can be written as

$$s_{xx2} = s_{xx1} - \frac{4}{3}\mu \ln(\frac{\rho_2}{\rho_1}). \tag{3.44}$$

Then, the Cauchy stress can be written as

$$\sigma_2 = -p_2 + s_{xx2}. \tag{3.45}$$

We can use (3.39) to solve the velocity after the shock

$$u_2 = \begin{cases} u_1 - \sqrt{\dfrac{\sigma_1 - \sigma_2}{t}} & \text{Left-going,} \\ u_1 + \sqrt{\dfrac{\sigma_1 - \sigma_2}{t}} & \text{Right-going.} \end{cases} \tag{3.46}$$

And the shock speed is given as

$$s = \frac{\rho_2 u_2 - \rho_1 u_1}{\rho_2 - \rho_1}. \tag{3.47}$$

3.2. Plastic state

When the material is yielding,

$$|s_{xx}| = \frac{2}{3} Y_0, \tag{3.48}$$

the equations of Riemann problem can be simplified as

$$\begin{cases} \partial_t \rho + \partial_x(\rho u) = 0, \\ \partial_t(\rho u) + \partial_x(\rho u^2 + p - s_{xx}) = 0, \\ \partial_t(\rho E) + \partial_x\left[(\rho E + p - s_{xx})u\right] = 0, \\ |s_{xx}| = \dfrac{2}{3} Y_0, \\ U(x, t=0) = \begin{cases} U_L, \text{ if } x < 0, \\ U_R, \text{ if } x > 0, \end{cases} \end{cases} \tag{3.49}$$

where $\mathbf{U} = (\rho, \rho u, \rho E)$.

3.2.1. Jacobian matrix in plastic regions

Motion equations of (3.49) can be written as

$$\partial_t \mathbf{U} + \mathbf{J}_p(\mathbf{U})\partial_x \mathbf{U} = 0,$$

where the Jacobian matrix is

$$\mathbf{J}_p(\mathbf{U}) = \begin{bmatrix} 0 & 1 & 0 \\ -u^2 + \frac{\partial p}{\partial \rho} + \Gamma(\frac{u^2}{2} - e) & u(2-\Gamma) & \Gamma \\ (\Gamma(\frac{u^2}{2} - e) - e - \frac{u^2}{2} + \frac{\sigma}{\rho} + \frac{\partial p}{\partial \rho})u + \frac{u^2}{2} & -\Gamma u^2 - \frac{\sigma}{\rho} + e & (1+\Gamma)u \end{bmatrix}.$$

Eigenvalues of $\mathbf{J}_p(\mathbf{Q})$ are given as

$$\lambda_1 = u, \quad \lambda_2 = u - c_p, \quad \lambda_3 = u + c_p,$$

where c_p shows the sonic speed in the plastic state,

$$c_p = \sqrt{a^2 - \frac{\rho_0}{\rho^2}\Gamma_0 s_{xx}}. \tag{3.50}$$

The corresponding right eigenvectors are

$$r_1 = \begin{bmatrix} -\frac{\Gamma}{b_1} \\ -\frac{\Gamma u}{b_1} \\ 1 \end{bmatrix}, \quad r_2 = \frac{1}{h - uc_p}\begin{bmatrix} 1 \\ u - c_p \\ h - uc_p \end{bmatrix}, \quad r_3 = \frac{1}{h + uc_p}\begin{bmatrix} 1 \\ u + c_p \\ h + uc_p \end{bmatrix}. \tag{3.51}$$

Comparing Eq.(3.3) with Eq.(3.50), we notice that the sonic speed is not continuous between the elastic state and plastic state. As the shear modulus μ is always positive, the elastic wave runs always faster than the plastic wave.

3.2.2. Relations across the contact wave

According to the eigenvectors in Eq.(3.51), for the λ_1-wave ($\lambda_1 = u$), we have

$$\frac{d\rho}{\frac{-\Gamma}{b_1}} = \frac{d(\rho u)}{\frac{-u\Gamma}{b_1}} = \frac{d(\rho E)}{1}. \tag{3.52}$$

From the above equations, we can easily deduce that

$$du = 0, \quad dp = 0,$$

which means that

$$u_L^* = u_R^*, \quad p_L^* = p_R^*.$$

Because $s^*_{xxL} = s^*_{xxR}$, thanks to (2.3), one can get

$$\sigma^*_L = \sigma^*_R.$$

For convenience, we define

$$s^* = u^*_L = u^*_R.$$

3.2.3. Relations across rarefaction waves

Left-going rarefaction wave

Across the left wave associated with λ_2-wave, ($\lambda_2 = u - c_p$), we have

$$\frac{d\rho}{1} = \frac{d(\rho u)}{u - c_p} = \frac{d(\rho E)}{h - uc_p}. \tag{3.53}$$

Similar to Section 3.1.3, we can get the relations

$$pe^{\frac{\lambda}{\rho}} - \int f_2(\rho) e^{\frac{\lambda}{\rho}} d\rho = \text{constant}. \tag{3.54}$$

and

$$u + \int \frac{c_p}{\rho} d\rho = \text{constant}. \tag{3.55}$$

Right-going rarefaction wave

Across the right wave associated with λ_3-wave, ($\lambda_3 = u + c_p$), we have

$$\frac{d\rho}{1} = \frac{d(\rho u)}{u + c_p} = \frac{d(\rho E)}{h + uc_p}. \tag{3.56}$$

Similarly, we can get

$$pe^{\frac{\lambda}{\rho}} - \int f_2(\rho) e^{\frac{\lambda}{\rho}} d\rho = \text{constant}. \tag{3.57}$$

$$u - \int \frac{c_p}{\rho} d\rho = \text{constant}. \tag{3.58}$$

3.2.4. Relations across a shock wave

By using the same deducing process as Section 3.1.4, we can get the state after the shock wave:

$$s_{xx2} = s_{xx1}, \tag{3.59}$$

$$p_2 = \frac{2t(c_1 f(\rho_2/\rho_0) + e_1) - (\sigma_1 + s_{xx2})}{2tc_0 - 1}, \tag{3.60}$$

where $c_0 = \frac{1}{\rho_0 \Gamma_0}$, $c_1 = \frac{a_0^2}{\Gamma_0}$, $\sigma_2 = -p_2 + s_{xx2}$,

$$u_2 = \begin{cases} u_1 - \sqrt{\dfrac{\sigma_1 - \sigma_2}{t}} & \text{Left-going,} \\ u_1 + \sqrt{\dfrac{\sigma_1 - \sigma_2}{t}} & \text{Right-going.} \end{cases} \tag{3.61}$$

And the shock speed is given as

$$s = \frac{\rho_2 u_2 - \rho_1 u_1}{\rho_2 - \rho_1}. \tag{3.62}$$

3.3. A relation between ρ and s_{xx}

Thanks to (2.6), the equations of the density and the deviatoric stress in Eq.(3.1) can be written as

$$\frac{\partial u}{\partial x} = -\frac{1}{\rho}\frac{d\rho}{dt}, \tag{3.63}$$

and

$$\frac{ds_{xx}}{dt} = \frac{4}{3}\mu\frac{\partial u}{\partial x}. \tag{3.64}$$

Substituting (3.63) into (3.64) yields

$$\frac{ds_{xx}}{dt} = -\frac{4}{3}\mu\frac{1}{\rho}\frac{d\rho}{dt}. \tag{3.65}$$

Integrate the above equation from the data in front of a wave to the data behind the wave and perform some simple algebraic manipulations, one can get

$$s_{xx} + \frac{4}{3}\mu\ln(\rho) = \text{constant}. \tag{3.66}$$

Analyzing (3.66), one can find, $\frac{\partial s_{xx}}{\partial \rho} < 0$. So, if the material is compressed and ρ increases, s_{xx} will decrease; if the material is expanded and ρ decreases, s_{xx} will increase. According to the compressed or expanded process of the material, even if the initial material is in the plastic state, the material can be into a different state. With considering of the von Mises yielding condition, all cases are shown as follows:

1. If $s_{xx} = \frac{2}{3}Y^0$, initial material reaches the elastic limit. If the material is compressed so that $\rho_{plastic} > \rho^* > \rho$, one can get $|s_{xx}^*| < \frac{2}{3}Y^0$, the compressed material jumps from the plastic state to the elastic state. Here ρ and s_{xx} mean the initial density and deviatoric stress, respectively, $\rho_{plastic} = \rho e^{\left(-\frac{Y_0}{2\mu} + \frac{3s_{xx}}{4\mu}\right)}$, $()^*$ denotes the variable () of the compressed or expanded material.

2. If $s_{xx} = \frac{2}{3}Y^0$ and the material is compressed greatly so that $\rho_{plastic} < \rho^*$, $s_{xx}^* \leq -\frac{2}{3}Y^0$, the compressed material will jump from the positive plastic state to the negative plastic state. Here the positive or negative plastic state means $s_{xx} = \frac{2}{3}Y^0$ or $s_{xx} = -\frac{2}{3}Y^0$, respectively.

3. If $s_{xx} = \frac{2}{3}Y^0$ and the material is expanded, $s_{xx}^* > \frac{2}{3}Y^0$, the material is still in the positive plastic state.

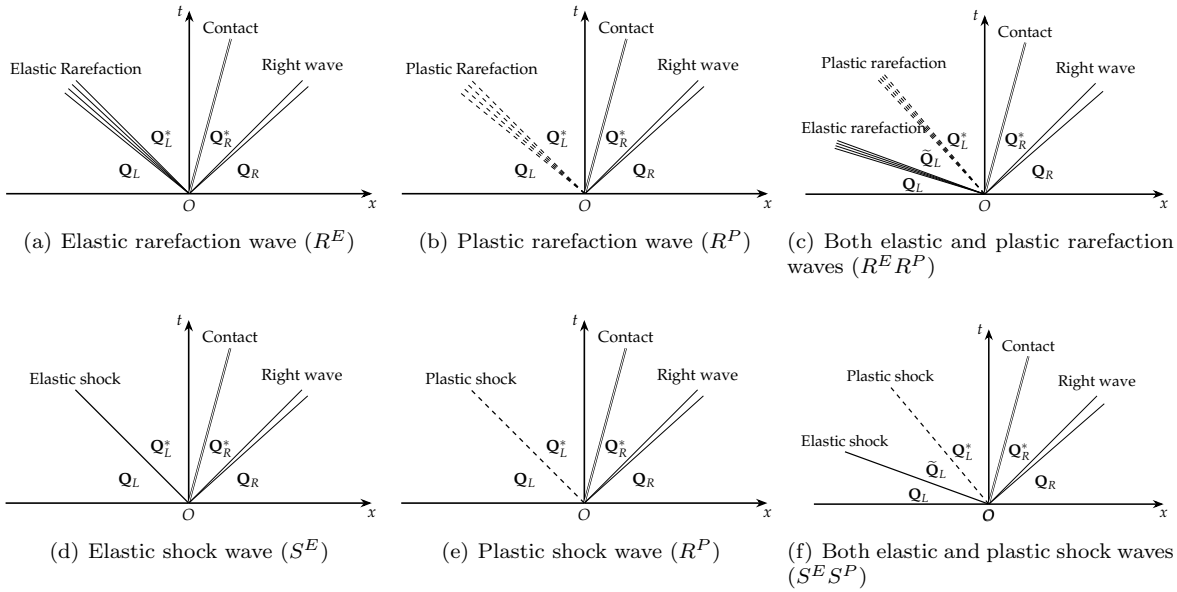

(a) Elastic rarefaction wave (R^E)

(b) Plastic rarefaction wave (R^P)

(c) Both elastic and plastic rarefaction waves ($R^E R^P$)

(d) Elastic shock wave (S^E)

(e) Plastic shock wave (R^P)

(f) Both elastic and plastic shock waves ($S^E S^P$)

Figure 1: The possible cases of Riemann solution structures in the left side.

4. If $s_{xx} = -\frac{2}{3}Y^0$ and the material is expanded so that $\rho_{plastic} < \rho^* < \rho$, one can get $|s^*_{xx}| < \frac{2}{3}Y^0$, the expanded material jumps from the plastic state to the elastic state.

5. If $s_{xx} = -\frac{2}{3}Y^0$ and the material is expanded greatly so that $\rho_{plastic} > \rho^*$, $s^*_{xx} \geq \frac{2}{3}Y^0$, the expanded material will jump from the negative plastic state to the positive plastic state.

6. If $s_{xx} = -\frac{2}{3}Y^0$ and the material is compressed, $s^*_{xx} < -\frac{2}{3}Y^0$, the material is still in the negative plastic state.

4. Exact Riemann solver

Now we consider the constructing details of the exact Riemann solver. For the Riemann problem in Section 3, there are 6×6 possible cases in the Riemann solution with different wave structures. The left six cases are shown in Fig.1. Here we remark that *we do not consider vacuum in building our exact Riemann solver*, for the reason that vacuum hardly ever appears in the elastic-plastic deformation of solid materials that we have studied.

4.1. The solving process

From Section 3, we can find that all variables can be formulated in terms of the density. So we define functions f_u and f_σ:

$$\begin{cases} f_u(\rho_L^*, \rho_R^*, \mathbf{Q}_L, \mathbf{Q}_R) = u_L^*(\rho_L^*, \mathbf{Q}_L) - u_R^*(\rho_R^*, \mathbf{Q}_R), \\ f_\sigma(\rho_L^*, \rho_R^*, \mathbf{Q}_L, \mathbf{Q}_R) = \sigma_L^*(\rho_L^*, \mathbf{Q}_L) - \sigma_R^*(\rho_R^*, \mathbf{Q}_R). \end{cases} \tag{4.1}$$

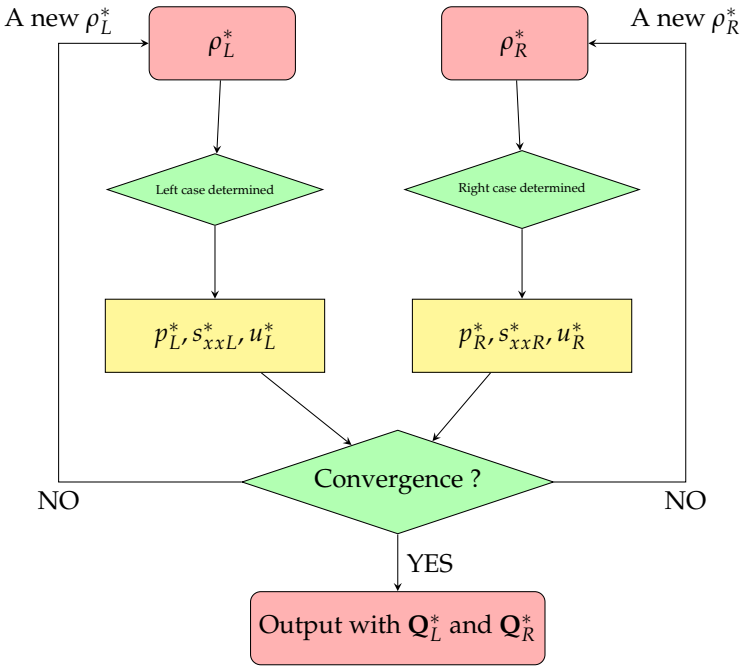

Figure 2: A flow chat of the Newton iteration process.

By using the relations across the contact wave in Section 3.1.2 and Section 3.2.2, we can get

$$\begin{cases} f_u(\rho_L^*, \rho_R^*, \mathbf{Q}_L, \mathbf{Q}_R) = u_L^*(\rho_L^*, \mathbf{Q}_L) - u_R^*(\rho_R^*, \mathbf{Q}_R) = 0, \\ f_\sigma(\rho_L^*, \rho_R^*, \mathbf{Q}_L, \mathbf{Q}_R) = \sigma_L^*(\rho_L^*, \mathbf{Q}_L) - \sigma_R^*(\rho_R^*, \mathbf{Q}_R) = 0. \end{cases} \tag{4.2}$$

Obviously, this system is uniquely solvable, but we can not get the analytical solution of (4.2). We have to use an iteration procedure to solve (4.2) and the solving process is shown in Fig.2. The details are introduced in the following.

Initial:

The initial densities are given as

$$\rho_{L(1)}^* = \frac{\rho_L + \rho_R}{2} \quad \rho_{R(1)}^* = \frac{\rho_L + \rho_R}{2}. \tag{4.3}$$

Iterations begin:

Step 1 Determining the case of the wave structure:

Given $\rho_{L(k)}^*$ and $\rho_{R(k)}^*$ in the k-th iteration step, we can use the method introduced in Section 4.2 to determine the case of wave structure of this Riemann problem. In the procedure for solving the Riemann problem, the subscript (k) means the variable in the k-th iteration step.

Step 2 Evaluating $f_{u(k)}$ and $f_{\sigma(k)}$:

After determining the structures case, we need to solve Cauchy stresses and velocities in regions $\mathbf{Q}_L^*$

and $\mathbf{Q}_R^*$ and the details are given in Section 4.4.

Step 3 Evaluating the derivatives of $f_{u(k)}$ and $f_{\sigma(k)}$.

The derivatives of $f_{u(k)}$ and $f_{\sigma(k)}$ are given as

$$\frac{\partial f_{u(k)}}{\partial \rho^*_{L(R)}} = \frac{f_{u(k)} - f_{u(k-1)}}{\rho^*_{L(R)(k)} - \rho_{L(R)(k-1)}}, \quad \frac{\partial f_{\sigma(k)}}{\partial \rho^*_{L(R)}} = \frac{f_{\sigma(k)} - f_{\sigma(k-1)}}{\rho^*_{L(R)(k)} - \rho_{L(R)(k-1)}}. \tag{4.4}$$

At the first step, we use a simple numerical difference method to evaluate

$$\frac{\partial f_{u(1)}}{\partial \rho^*_{L(R)}} = \frac{f_u(\rho^*_{L(R)(1)} + \Delta\rho) - f_u(\rho^*_{L(R)(1)})}{\Delta\rho_{L(R)(1)}}, \quad \frac{\partial f_{u(1)}}{\partial \rho^*_{L(R)}} = \frac{f_u(\rho^*_{L(R)(1)} + \Delta\rho) - f_u(\rho^*_{L(R)(1)})}{\Delta\rho_{L(R)(1)}}, \tag{4.5}$$

where $\Delta\rho$ is a small quantity, here we define it as

$$\Delta\rho = \frac{\rho^*_{L(R)(1)}}{100}. \tag{4.6}$$

Step 4 Evaluating $\rho^*_{L(k+1)}$ and $\rho^*_{R(k+1)}$:

$$\begin{bmatrix} \rho^*_{L(k+1)} \\ \rho^*_{R(k+1)} \end{bmatrix} = \begin{bmatrix} \rho^*_{L(k)} \\ \rho^*_{R(k)} \end{bmatrix} - \begin{bmatrix} \frac{\partial f_{u(k)}}{\partial \rho^*_L} & \frac{\partial f_{u(k)}}{\partial \rho^*_R} \\ \frac{\partial f_{\sigma(k)}}{\partial \rho^*_L} & \frac{\partial f_{\sigma(k)}}{\partial \rho^*_R} \end{bmatrix}^{-1} \begin{bmatrix} f_{u(k)} \\ f_{\sigma(k)} \end{bmatrix} \tag{4.7}$$

Step 5 Convergence test:

The iteration is convergent if

$$\mathrm{CHA} \le \mathrm{TOL}, \tag{4.8}$$

where

$$\mathrm{CHA} = \max\left[\frac{|\rho^*_{L(k+1)} - \rho^*_{L,(k)}|}{\frac{1}{2}|\rho^*_{L(k+1)} + \rho^*_{L(k)}|}, \frac{|\rho^*_{R(k+1)} - \rho^*_{R,(k)}|}{\frac{1}{2}|\rho^*_{R(k+1)} + \rho^*_{R(k)}|}, |f_u|, |f_\sigma| \right], \tag{4.9}$$

$$\mathrm{TOL} = 10^{-4}.$$

If not, go to Step 1 and continue the iteration procedure until convergent. Numerical examples show, after 2-4 iterations, the condition (4.8) is satisfied.

Iterations end

4.2. Determining the case of structures

Given the value of density $\rho^*_{L(R)}$, we can distinguish the non-linear wave is a shock or rarefaction wave. This is done easily by comparing $\rho^*_{L(R)}$ with $\rho_{L(R)}$, the subscript $_{L(R)}$ means in the left(right) side of the contact wave.

$$\begin{cases} \text{a rarefaction wave:} & \text{if } \rho_{L(R)} > \rho^*_{L(R)}, \\ \text{a shock wave:} & \text{if } \rho_{L(R)} < \rho^*_{L(R)}. \end{cases} \tag{4.10}$$

Table 4.1: The condition of cases classification.

$\hat{\rho^*} < \rho$	$\hat{s}_{xx} < \frac{2}{3}Y_0$	$s_{xx} = \frac{2}{3}Y_0$ and $\hat{s}_{xx} \geq \frac{2}{3}Y_0$	other
	Case a: R^E	Case b: R^P	Case c: $R^E R^P$
$\hat{\rho^*} > \rho$	$\hat{s}_{xx} > -\frac{2}{3}Y_0$	$s_{xx} = -\frac{2}{3}Y_0$ and $\hat{s}_{xx} \leq -\frac{2}{3}Y_0$	other
	Case d: S^E	Case e: S^P	Case f: $S^E S^P$

Thanks to (3.66), the deviatoric stress can be evaluated as

$$\hat{s}_{xxL(R)} = -\frac{4}{3}\mu \ln\left(\frac{\rho^*_{L(R)}}{\rho_{L(R)}}\right) + s_{xxL(R)}. \tag{4.11}$$

According to the values of initial and evaluated deviatoric stresses in (4.11) in one side of the contact wave, the non-linear wave in this side may be:

$$\begin{cases} \text{an elastic rarefaction} & \text{if } \hat{s}_{xxL(R)} < \frac{2}{3}Y^0, \\ \text{a plastic rarefaction} & \text{if } s_{xxL(R)} = \frac{2}{3}Y^0 \text{ and } \hat{s}_{xxL(R)} \geq \frac{2}{3}Y_0, \\ \text{an elastic rarefaction and a following plastic rarefaction} & \text{if } s_{xxL(R)} < \frac{2}{3}Y_0 \text{ and } \hat{s}_{xxL(R)} \geq \frac{2}{3}Y_0, \\ \text{an elastic shock} & \text{if } \hat{s}_{xxL(R)} > -\frac{2}{3}Y_0, \\ \text{a plastic shock} & \text{if } s_{xxL(R)} = -\frac{2}{3}Y_0 \text{ and } \hat{s}_{xxL(R)} \leq -\frac{2}{3}Y_0, \\ \text{an elastic shock and a following plastic shock} & \text{if } s_{xxL(R)} > -\frac{2}{3}Y_0 \text{ and } \hat{s}_{xxL(R)} \leq -\frac{2}{3}Y_0. \end{cases} \tag{4.12}$$

Combining (4.10) and (4.12), we can find, in any side of the wave structures of this Riemann problem, there are six cases showed in Table 4.1, where capital letters "S" and "R" mean the shock and rarefaction wave, respectively; superscript letters "E" and "P" indicate the elastic and plastic state of a wave, respectively. Otherwise, the subscript L or R are omitted for simplification.

4.3. Evaluating states in middle regions ($\tilde{\mathbf{Q}}_L$ and $\tilde{\mathbf{Q}}_R$)

Cases (R^E, R^P, S^E and S^P)

For cases (R^E, R^P, S^E and S^P) in Fig.1, the material is totally yielding or totally not yielding, there is no midlle state $\tilde{\mathbf{Q}}_{L(R)}$. For expression convenience, we let

$$(\tilde{\rho}_{L(R)}, \tilde{u}_{L(R)}, \tilde{p}_{L(R)}, \tilde{s}_{xx}) = (\rho_{L(R)}, u_{L(R)}, p_{L(R)}, s_{xxL(R)}), \tag{4.13}$$

Case ($R^E R^P$)

Using the methods introduced in the Section (3.1.3), we can easily deduce the formulation of all unknown variables after the rarefaction wave. Here we do not show the details of the deduction.

For the case ($R^E R^P$), after the elastic rarefaction wave, the deviatoric stress achieves the elastic limit. Thanks to (4.10) and (4.12), one can easily deduce that

$$\tilde{s}_{xxL(R)} = \frac{2}{3}Y_0.$$

By using (3.66), the density in $\tilde{\mathbf{Q}}_{L(R)}$ is given as

$$\tilde{\rho}_{L(R)} = \rho_{L(R)}\exp\left(-\frac{Y_0}{2\mu} + \frac{3s_{xxL(R)}}{4\mu}\right).$$

From (3.26) and (3.32), for the case ($R^E R^P$), the pressure is rearranged as

$$\tilde{p}_{L(R)} = p_{L(R)}e^{\frac{\lambda}{\rho_{L(R)}} - \frac{\lambda}{\tilde{\rho}_{L(R)}}} + e^{-\frac{\lambda}{\tilde{\rho}_{L(R)}}}\int_{\rho_{L(R)}}^{\tilde{\rho}_{L(R)}} f_2(x)e^{\frac{\lambda}{x}}dx, \tag{4.14}$$

where

$$\lambda = \rho_0\Gamma_0 \quad f_2(\rho) = a_0^2\frac{\partial f}{\partial \eta} - \lambda\frac{s_{xx}(\rho)}{\rho^2},\ s_{xx}(\rho) = -\frac{4}{3}\mu\ln\left(\frac{\rho}{\rho_{L(R)}}\right) + s_{xxL(R)}.$$

Thanks to (3.27) and (3.33), for the rarefaction wave case ($R^E R^P$), the velocity is given as

$$\tilde{u}_{L(R)} = \begin{cases} u_L - \displaystyle\int_{\rho_L}^{\tilde{\rho}_{L(R)}} \frac{c_e(x)}{x}dx & \text{for the left-going rarefaction wave,} \\ u_R + \displaystyle\int_{\rho_R}^{\tilde{\rho}_{L(R)}} \frac{c_e(x)}{x}dx & \text{for the right-going rarefaction wave,} \end{cases} \tag{4.15}$$

where the sonic speed is given as

$$c_e(\rho) = \sqrt{a_0^2\frac{\partial f}{\partial \eta} + \frac{p(\rho)}{\rho^2}\rho_0\Gamma_0 - \frac{\rho_0}{\rho^2}\Gamma_0 s_{xx}(\rho) + \frac{4}{3}\frac{\mu}{\rho}}.$$

Remark 1: In (4.14) and (4.15), there are two integral terms. Obviously, because of the complexity of the EOS, we can not get the exact integral values. We have to use the numerical methods to approximate the two integral terms with high order accuracy. The approximation methods are introduced in the Appendix A.

Case ***($S^E S^P$)***

Using the methods introduced in the Section (3.1.4), we can easily deduce the formulation of all unknown variables in $\tilde{\mathbf{Q}}_{L(R)}$. In order to shorten the length of our paper, we do not show the details of the deduction.

For the case ($S^E S^P$), after the elastic shock wave, the deviatoric stress achieves the elastic limit. So, by using (4.10) and (4.12), one can easily deduce that

$$\tilde{s}_{xxL(R)} = -\frac{2}{3}Y_0.$$

From (3.66), after the elastic shock wave, the density in $\tilde{\mathbf{Q}}_{L(R)}$ is given as

$$\tilde{\rho}_{L(R)} = \rho_{L(R)} \exp\left(\frac{Y_0}{2\mu} + \frac{3s_{xxL(R)}}{4\mu}\right).$$

By using (3.43), the pressure can be solved as

$$\tilde{p}_{L(R)} = \frac{2t(c_1 f(\tilde{\rho}_{L(R)}/\rho_0) + e_{L(R)}) - (\sigma_{L(R)} + \tilde{s}_{xxL(R)})}{2tc_0 - 1}, \tag{4.16}$$

where $c_0 = \frac{1}{\rho_0 \Gamma_0}$, $c_1 = \frac{a_0^2}{\Gamma_0}$ and $t = \frac{\rho_{L(R)}\tilde{\rho}_{L(R)}}{\tilde{\rho}_{L(R)} - \rho_{L(R)}}$.

Thanks to (3.46), the velocity can be written as

$$\begin{cases} \tilde{u}_L = u_L - \sqrt{\frac{\sigma_L - \tilde{\sigma}_L}{t}}, \\ \tilde{u}_R = u_R + \sqrt{\frac{\sigma_R - \tilde{\sigma}_R}{t}}, \end{cases} \tag{4.17}$$

where

$$\tilde{\sigma}_{L(R)} = -\tilde{p}_{L(R)} + \tilde{s}_{xxL(R)}. \tag{4.18}$$

4.4. Evaluating states in regions $\mathbf{Q}_L^*$ and $\mathbf{Q}_R^*$

Rarefaction wave cases (R^E, R^P and $R^E R^P$)

For the three rarefaction wave cases, thanks to (3.66) and (3.48), s_{xx} in $\mathbf{Q}_L^*$ and $\mathbf{Q}_R^*$ are

$$s^*_{xxL(R)} = \begin{cases} -\frac{4}{3}\mu \ln\left(\frac{\rho^*_{L(R)}}{\tilde{\rho}_{L(R)}}\right) + s_{xxL(R)} & \text{for case } (R^E), \\ \frac{2}{3}Y_0 & \text{for cases } (R^P \text{ and } R^E R^P). \end{cases}$$

From (4.14), the pressure in the star region is

$$p^*_{L(R)} = \tilde{p}_{L(R)} e^{\frac{\lambda}{\rho_{L(R)}} - \frac{\lambda}{\rho}} + e^{-\frac{\lambda}{\rho^*_{L(R)}}} \int_{\tilde{\rho}_{L(R)}}^{\rho^*_{L(R)}} f_2(x) e^{\frac{\lambda}{x}} dx, \tag{4.19}$$

where

$$\lambda = \rho_0 \Gamma_0 \quad f_2(\rho) = a_0^2 \frac{\partial f}{\partial \eta} - \lambda \frac{s_{xx}(\rho)}{\rho^2}, \ s_{xx}(\rho) = -\frac{4}{3}\mu \ln\left(\frac{\rho}{\rho_{L(R)}}\right) + s_{xxL(R)}.$$

By Equations (3.27) and (3.33) the velocity in regions $\mathbf{Q}_L^*$ and $\mathbf{Q}_R^*$ can be written as

$$u^*_{L(R)} = \begin{cases} \tilde{u}_L - \int_{\rho_L}^{\rho^*_{L(R)}} \frac{c(x)}{x} dx, \\ \tilde{u}_R + \int_{\rho_R}^{\rho^*_{L(R)}} \frac{c(x)}{x} dx, \end{cases} \tag{4.20}$$

where

$$c(\rho)=\begin{cases}\sqrt{a_0^2\dfrac{\partial f}{\partial \eta}+\dfrac{p(\rho)}{\rho^2}\rho_0\Gamma_0-\dfrac{\rho_0}{\rho^2}\Gamma_0 s_{xx}(\rho)+\dfrac{4}{3}\dfrac{\mu}{\rho}} & \text{for case } (R^E),\\ \sqrt{a_0^2\dfrac{\partial f}{\partial \eta}+\dfrac{p(\rho)}{\rho^2}\rho_0\Gamma_0-\dfrac{\rho_0}{\rho^2}\Gamma_0 s_{xx}(\rho)} & \text{for cases } (R^P \text{ and } R^E R^P).\end{cases}$$

Remark 2: Just like **Remark 1**, we have to use numerical integral methods introduced in the Appendix A to evaluate the integral terms in (4.19) and (4.20).

Shock wave cases (S^E, S^P and $S^E S^P$)

For shock wave cases, the deviatoric stresses in $\mathbf{Q}_L^*$ and $\mathbf{Q}_R^*$ are given as

$$s_{xx}(\rho)=\begin{cases}-\dfrac{4}{3}\mu\ln\left(\dfrac{\rho}{\tilde{\rho}_{L(R)}}\right)+\tilde{s}_{xxL(R)}, & \text{for case } (S^E),\\ -\dfrac{2}{3}Y_0, & \text{for cases (} S^P \text{ and } S^E S^P).\end{cases}$$

(3.43) gives direct expression for the the pressure in the star region as

$$p^*_{L(R)}=\frac{2t\left(c_1 f(\rho^*_{L(R)}/\rho_0)+\tilde{e}_{L(R)}\right)-\left(\tilde{\sigma}_{L(R)}+s_{xx}(\rho^*_{L(R)})\right)}{2tc_0-1},$$

where $c_0=\frac{1}{\rho_0\Gamma_0}$, $c_1=\frac{a_0^2}{\Gamma_0}$ and $t=\frac{\rho^*_{L(R)}\tilde{\rho}_{L(R)}}{\rho^*_{L(R)}-\tilde{\rho}_{L(R)}}$.

Thanks to (3.46), the velocities in $\mathbf{Q}_L^*$ and $\mathbf{Q}_R^*$ are

$$u^*_{L(R)}=\begin{cases}\tilde{u}_L-\sqrt{\dfrac{\tilde{\sigma}_L-\sigma^*_{L(R)}}{t}} & \text{for the left-going shock wave,}\\ \tilde{u}_R+\sqrt{\dfrac{\tilde{\sigma}_R-\sigma^*_{L(R)}}{t}} & \text{for the right-going shock wave,}\end{cases}$$

where $\sigma^*_{L(R)}=-p^*_{L(R)}+s^*_{xxL(R)}$.

5. Half Riemann problem and its solver

Sometimes we need to analyse a half Riemann problem with a given velocity or Cauchy stress. Shown in Fig.3, in these cases, we only need to solve states in one side. There are six possible cases which are introduced in Section 3. Here we will use the example shown in Fig.3 to show how to solve the half Riemann problem.

As we know the velocity u^* or the Cauchy stress σ^* on one side, for example , the left side, there is only one equation need to be solved:

$$f(\rho^*,\mathbf{Q}_R)=u(\rho^*,\mathbf{Q}_R)-u^*=0, \tag{5.1}$$

or

$$f(\rho^*,\mathbf{Q}_R)=\sigma(\rho^*,\mathbf{Q}_R)-\sigma^*=0. \tag{5.2}$$

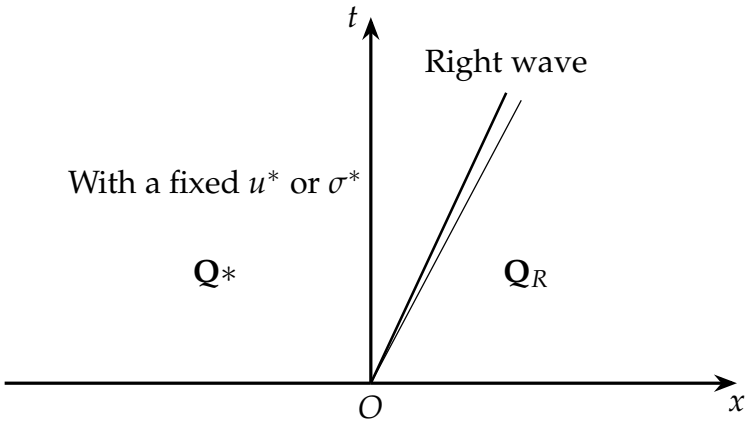

Figure 3: Half Riemann problem with a given left velocity or Cauchy stress.

Similar to the process in Section (4.1), we have to use an iteration procedure to solve (5.1) or (5.2) and the solving process is list in the following.

Initial:

The initial density is given as

$$\rho^*_{(1)} = \rho_R. \tag{5.3}$$

Iterations begin:

Step 1 Determine the case of the wave structures:

Given the value of $\rho^*_{(k)}$ in the k-th iteration step, use the methods introduced in Section 4.2 to determine the case of wave structure of this Riemann problem. Here the subscript (k) means the variable in the k-th iteration step.

Step 2 Elevate $f(\rho^*, \mathbf{Q}_R)$:

After determining the structure case, evaluate the velocity (or the Cauchy stress) in the region $\mathbf{Q}^*$ and the details are given in Section 4.4.

Step 3 Evaluate the derivative of $f(\rho^*, \mathbf{Q}_R)$:

The derivative of f is given by

$$\frac{\partial f_{(k)}}{\partial \rho^*} = \frac{f_{(k)} - f_{(k-1)}}{\rho^*_{(k)} - \rho^*_{(k-1)}}, \text{ for } k > 1$$

At the first step,

$$\frac{\partial f_{(1)}}{\partial \rho^*} = \frac{f(\rho^* + \Delta\rho) - f(\rho^*)}{\Delta\rho},$$

where $\Delta\rho$ is a small quantity, here we set $\Delta\rho = \frac{\rho^*_{(1)}}{100}$.

Step 4 Evaluate $\rho^*_{(k+1)}$:

A new density can be updated by

$$\rho^*_{(k+1)} = \rho^*_{(k)} - f/\frac{\partial f_{(k)}}{\partial \rho}.$$

Step 5 Convergence test:

The iteration is convergent if

$$\text{CHA} \leq \text{TOL}, \tag{5.4}$$

where

$$\text{CHA} = \max\left[\frac{|\rho^*_{(k+1)} - \rho^*_{(k)}|}{\frac{1}{2}|\rho^*_{(k+1)} + \rho^*_{(k)}|}, |f|\right], \quad \text{TOL} = 10^{-4}.$$

If not, go to Step 1 and continue the iteration procedure until convergent. Numerical examples show, after 2-4 iterations, the condition (5.4) is satisfied.

Iterations end.

6. Numerical tests

In this section, we will solve different elastic-plastic Riemann problems with several different wave structures in the Riemann solutions. In order to verify the correctness of our exact Riemann solver, we use a third-order numerical scheme for 1D elastic-plastic flows to evaluate these Riemann problems and compare numerical results with our exact solution. Before considering elastic-plastic Riemann problems, a two-phase impact benchmark problem [43, 1, 44] is firstly taken in to test the correctness of the numerical method [25].

6.1. Two-phase impact benchmark problem

At the beginning of this problem, there is a right-moving copper with the speed $u_1 = 1500$m/s interacting with a solid explosive at the rest on the right of the plate under the uniform atmospheric condition which has pressure $p_0 = 10^5$Pa and temperature $T_0 = 300$K throughout the domain. Cochran-Chan equation of state which is in the form of Mie-Grüneisen form [1] is used but derivative stress is not considered in this problem. The Cochran-Chan EOS is

$$p(\rho, e) = p_{\text{ref}}(\rho) + \Gamma(\rho)[e - e_{\text{ref}}(\rho)].$$

where

$$\begin{aligned}
&\Gamma = \Gamma_0 \\
&p_{\text{ref}}(\rho) = \beta_1 \left(\frac{\rho_0}{\rho}\right)^{-\varepsilon_1} - \beta_2 \left(\frac{\rho_0}{\rho}\right)^{\varepsilon_2}, \\
&e_{\text{ref}}(\rho) = -\frac{\beta_1}{\rho_0(1-\varepsilon_1)}\left[\left(\frac{\rho_0}{\rho}\right)^{1-\varepsilon_1} - 1\right] + \frac{\beta_1}{\rho_0(1-\varepsilon_2)}\left[\left(\frac{\rho_0}{\rho}\right)^{1-\varepsilon_2} - 1\right] - C_\nu T_0
\end{aligned}$$

For the copper and solid explosive, the parameters are given as

$$\begin{cases} (\rho_0, \beta_1, \beta_2, \varepsilon_1, \varepsilon_2, \Gamma_0, C_\nu)_{\text{Copper}} = (8900\text{kg/m}^3, 145.67\text{GPa}, 147.75\text{GPa}, 2.99, 1.99, 2, 393\text{J/kg}\cdot\text{K}) \\ (\rho_0, \beta_1, \beta_2, \varepsilon_1, \varepsilon_2, \Gamma_0, C_\nu)_{\text{Explosive}} = (1840\text{kg/m}^3, 12.87\text{GPa}, 13.42\text{GPa}, 4.1, 3.1, 0.93, 1087\text{J/kg}\cdot\text{K}) \end{cases}$$

In this problem, the yielding strength is set to zero and the 3rd-order cell-centered Lagrangian scheme [25] is used. We solve this problem with 200 grids and CFL number is set as 0.5. The final time is $t = 85\mu$s. Results of density and velocity shown in Fig.4 are compared the exact solution and numerical solution in [16]. This comparison verifies the correctness of our numerical scheme.

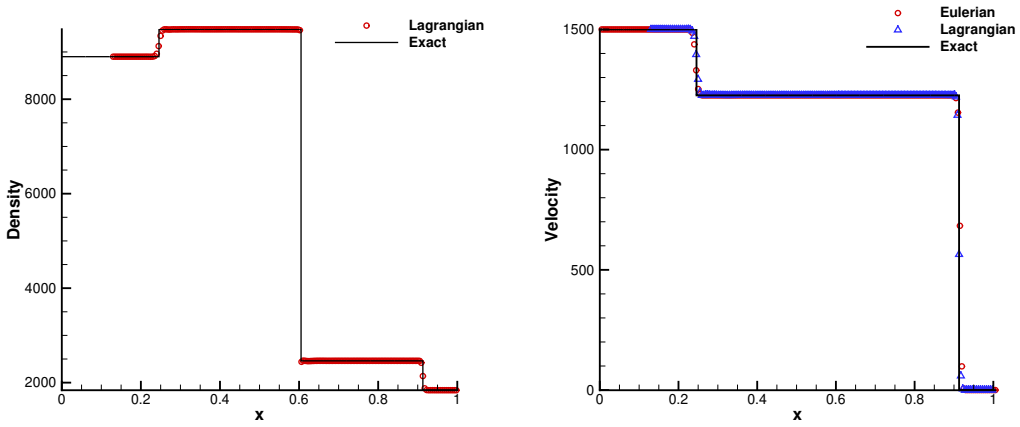

Figure 4: Numerical results for the two-phase impact benchmark [43, 1, 44].(The "Eulerian" and the "Exact" results are extracted from [44] and the "Lagrangian" result are computed by the method in [25])

6.2. Elastic-plastic Riemann problems

By choosing different initial conditions, different Riemann problems are tested in following with several different wave structures in the solutions. Two materials, copper and aluminum are considered with the parameters $(\rho_0, a_0, \Gamma_0, s, \mu)_{\text{Copper}} = (8930\text{kg/m}^3, 3940\text{m/s}, 2, 1.49, 2.76, 2.76\times10^{10}\text{Pa})$ and $(\rho_0, a_0, \Gamma_0, s, \mu)_{\text{Al}} = (2785\text{kg/m}^3, 5328\text{m/s}, 2, 1.338, 4.5\times10^{10}\text{Pa})$, respectively. The yielding strengths of the two materials are $Y_{0,\text{Al}} = 3\times10^8$Pa and $Y_{0,\text{Copper}} = 9\times10^7$Pa, respectively. The computational domain is setted as $[0, 1m]$ with 800 cell points and the initial interface is located at $0.5m$, the terminal time is $t = 5\times10^{-5}s$. Otherwise, in the initial condition, "L" and "R" mean $x < 0.5m$ and $x > 0.5m$, respectively.

Test 1

In this case, the material is yielding at both sides, so there are three waves with two plastic shock waves and one contact. The initial condition is

$$\begin{cases} \text{L: Al}, \quad \rho = 2785\text{kg/m}^3, \quad u = 20\text{m/s}, \quad p = 1.0\text{Pa}, \quad s_{xx} = -2.0\times10^8\text{Pa}, \\ \text{R: Al}, \quad \rho = 2785\text{kg/m}^3, \quad u = 0\text{m/s}, \quad p = 1.0\text{Pa}, \quad s_{xx} = -2.0\times10^8\text{Pa}, \end{cases} \tag{6.1}$$

It can be seen that the exact solution matches the numerical results very well in Fig.5.

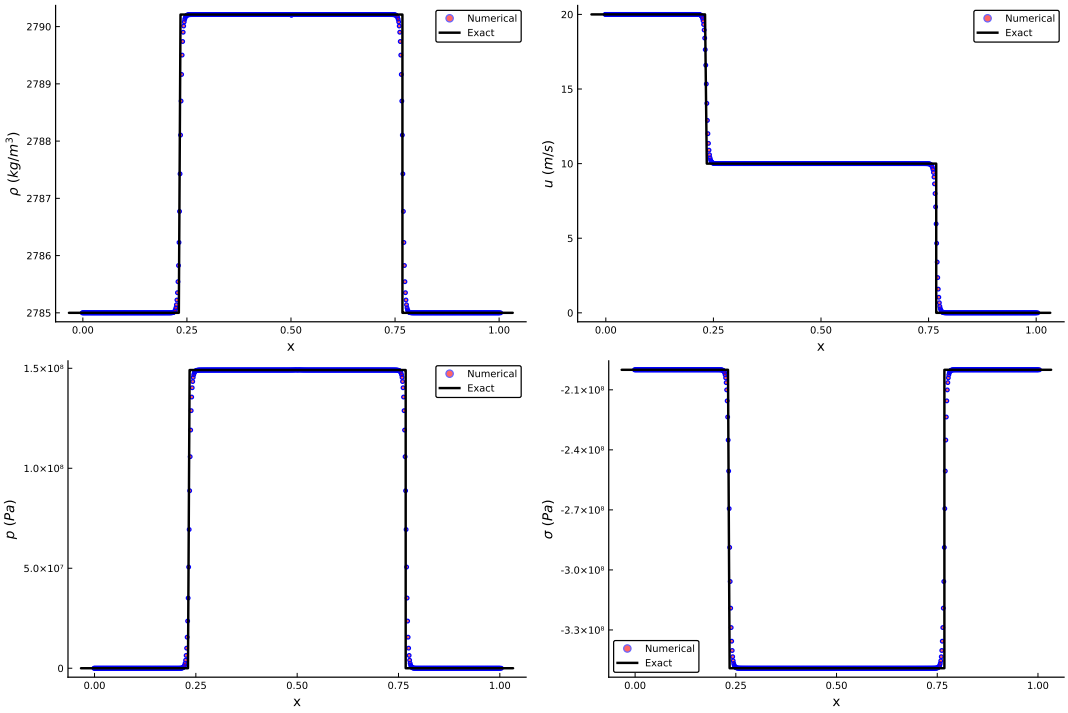

Figure 5: Comparison for Test 1 with the structure of $S^P|S^P$.

Test 2

Here we consider a case with yielding process at both sides, so there are five waves in the wave structure of this Riemann problem. The initial condition is

$$\begin{cases} \text{L: Al}, \quad \rho = 2785\text{kg/m}^3, \quad u = 800\text{m/s}, \quad p = 1.0\text{Pa}, \quad s_{xx} = 0.0\text{Pa}, \\ \text{R: Al}, \quad \rho = 2785\text{kg/m}^3, \quad u = 0\text{m/s}, \quad p = 1.0\text{Pa}, \quad s_{xx} = 0.0\text{Pa}, \end{cases} \tag{6.2}$$

Shown in Fig.6, the exact solution matches the numerical results well generally, except the under-cooling effect performed in the numerical results, but it is not considered in the designing of the exact Riemann solver.

Test 3

In this example, we test the case with two elastic rarefaction waves. In the wave structure there is one elastic rarefaction wave on each side of the contact wave. The initial condition is given as

$$\begin{cases} \text{L: Al}, \quad \rho = 2785\text{kg/m}^3, \quad u = -2.0\text{m/s}, \quad p = 1.0^7\text{Pa}, \quad s_{xx} = 0.0\text{Pa}, \\ \text{R: Al}, \quad \rho = 2785\text{kg/m}^3, \quad u = 2.0\text{m/s}, \quad p = 1.0 \times 10^7\text{Pa}, \quad s_{xx} = 0.0\text{Pa}, \end{cases} \tag{6.3}$$

We can see that the results of the exact solution match the numerical results very well.

Test 4

In this test we test the example with both elastic and plastic rarefaction waves on both sides of contact

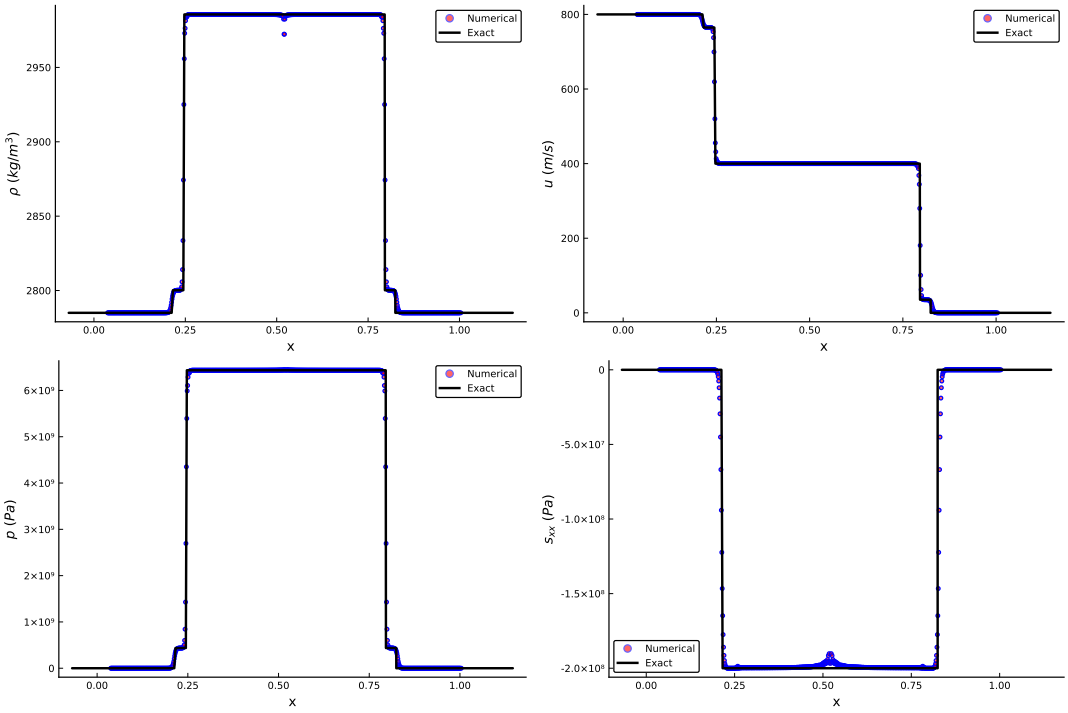

Figure 6: Comparison for Test 2 with the structure of $S^E S^P | S^P S^E$.

wave. The initial condition is

$$\begin{cases} \text{L: Al}, \quad \rho = 2785\text{kg/m}^3, \quad u = -40\text{m/s}, \quad p = 1.0 \times 10^7\text{Pa}, \quad s_{xx} = 0.0\text{Pa}, \\ \text{R: Al}, \quad \rho = 2785\text{kg/m}^3, \quad u = 40\text{m/s}, \quad p = 1.0 \times 10^7\text{Pa}, \quad s_{xx} = 0.0\text{Pa}. \end{cases} \tag{6.4}$$

Results are shown in Fig.8, the results of the exact solver match the numerical results very well.

Test 5

The initial condition of this Riemann problem is

$$\begin{cases} \text{L: Al}, \quad \rho = 2785\text{kg/m}^3, \quad u = -200\text{m/s}, \quad p = 1.0\text{Pa}, \quad s_{xx} = -2.0^8\text{Pa}, \\ \text{R: Al}, \quad \rho = 2785\text{kg/m}^3, \quad u = 0\text{m/s}, \quad p = 1.0\text{Pa}, \quad s_{xx} = -2.0^8\text{Pa}. \end{cases} \tag{6.5}$$

Obviously, at the beginning, the material is in the negative plastic state (i.e. $s_{xxL(R)} = -\frac{2}{3}Y^0$). According to the analysis introduced in Section 3.3, after an expanding process the material will turn back into an elastic state and will yield again into a positive plastic state. Our exact solution in Fig.9 are consistent with the analysis in Section 3.3. Of course, our exact solution matches the numerical solutions very well.

In this case, we also compared the results given with different orders of the Gaussian quadrature method in Fig.10, from which we can see that there is nearly no difference between the results, so the Riemann solver is not sensitive to the accuracy of the Gaussian quadrature method.

Test 6

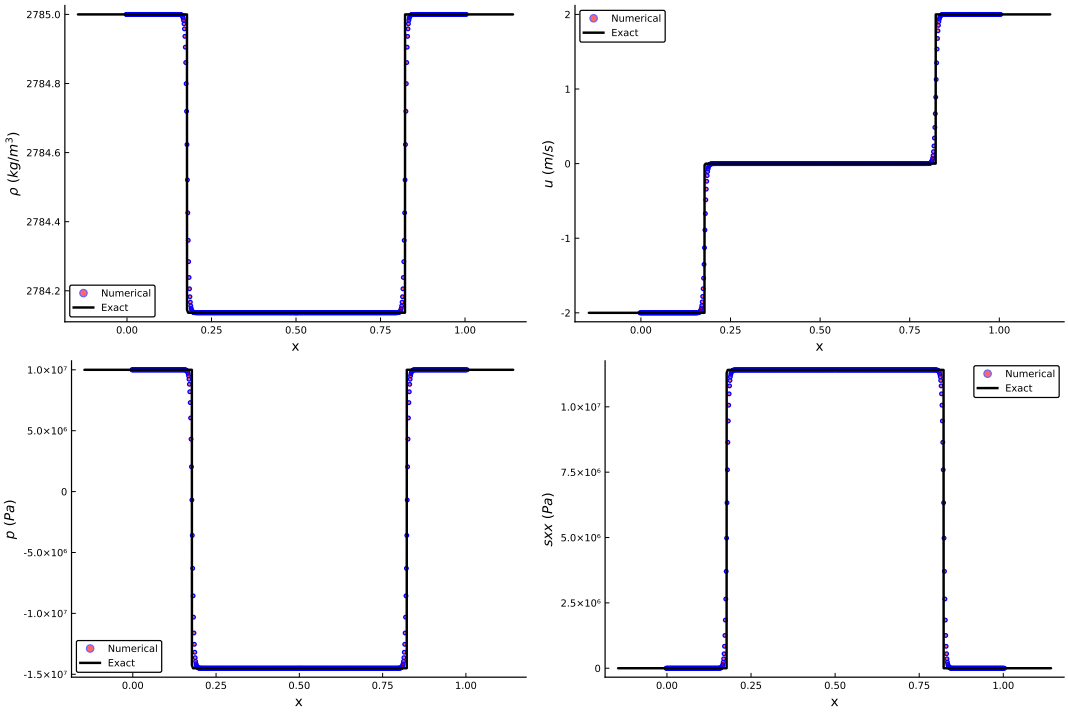

Figure 7: Comparison results for Test 3 with the wave structures of $R^E|R^E$.

The initial condition of this Riemann problem is

$$\begin{cases} \text{L: Al}, \quad \rho = 2785\text{kg/m}^3, \quad u = 200\text{m/s}, \quad p = 1.0\text{Pa}, \quad s_{xx} = 2.0^8\text{Pa}, \\ \text{R: Al}, \quad \rho = 2785\text{kg/m}^3, \quad u = 0\text{m/s}, \quad p = 1.0\text{Pa}, \quad s_{xx} = 2.0^8\text{Pa}. \end{cases} \tag{6.6}$$

Different from Test 5, at the beginning, the material is in the positive plastic state (i.e. $s_{xxL(R)} = \frac{2}{3}Y^0$). According to the analysis introduced in Section 3.3, after an compressing process the material will turn back into an elastic state and will yield again into a negative plastic state. We can get the exact solutions which match the numerical solutions very well in Fig.11.

Test 7

All the above five tests have symmetrical wave structures. Here we will test an example with different structures on two sides: one plastic shock on the left side and both the elastic shock and plastic shock on the right side of one contact wave. The initial condition is given as

$$\begin{cases} \text{L: Al}, \quad \rho = 2785\text{kg/m}^3, \quad u = 40\text{m/s}, \quad p = 1.0 \times 10^8\text{Pa}, \quad s_{xx} = -2.0 \times 10^8\text{Pa}, \\ \text{R: Al}, \quad \rho = 2785\text{kg/m}^3, \quad u = -40\text{m/s}, \quad p = 1.0 \times 10^2\text{Pa}, \quad s_{xx} = 0.0\text{Pa}. \end{cases} \tag{6.7}$$

The solutions of this test are shown in Fig.12. From this figure, we can find the exact solutions match numerical solutions very well.

Test 8

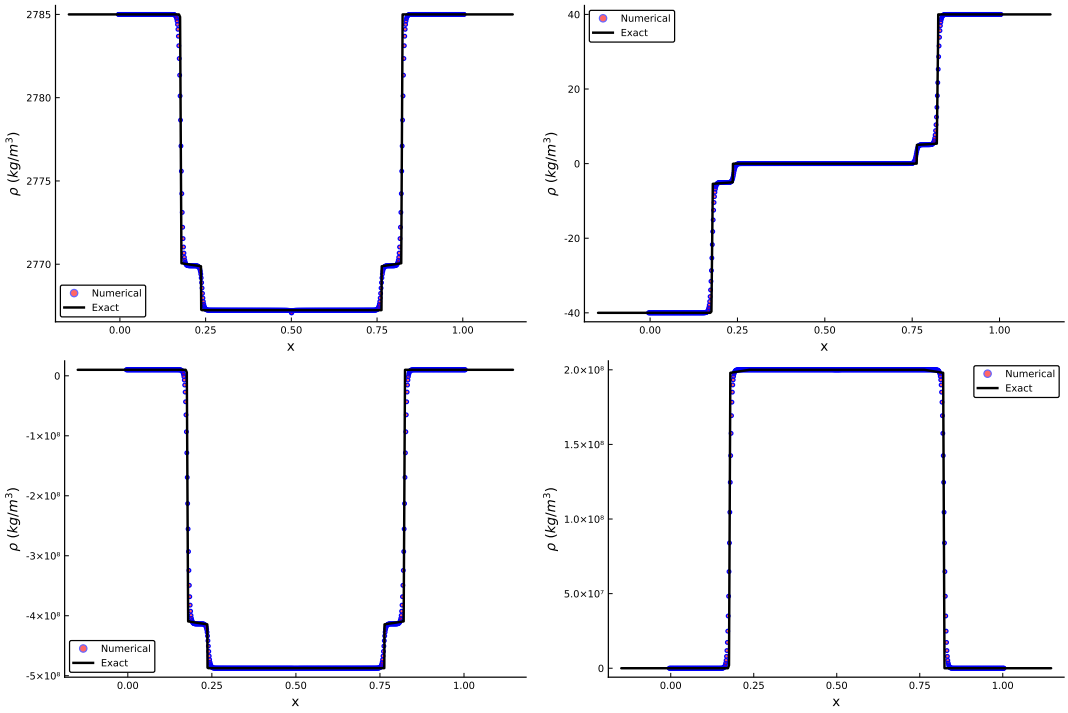

Figure 8: Comparison for Test 4 with the wave structure of $R^E R^P | R^P R^E$.

In this test, we consider an example with zero initial velocities on both sides, driving by the gradient of the pressure, there are rarefaction waves produced into the higher pressure side and shock waves generated into the lower pressure side. The initial condition is given as

$$\begin{cases} \text{L: Al}, \quad \rho = 2785\text{kg/m}^3, \quad u = 0.0\text{m/s}, \quad p = 1.0 \times 10^{10}\text{Pa}, \quad s_{xx} = 0.0\text{Pa}, \\ \text{R: Al}, \quad \rho = 2785\text{kg/m}^3, \quad u = 0.0\text{m/s}, \quad p = 1.0 \times 10^{2}\text{Pa}, \quad s_{xx} = 0.0\text{Pa}. \end{cases} \tag{6.8}$$

Shown in Fig.16, we can see there are two shocks in the right side and two rarefaction waves on the left side.

Test 9

Now we will consider two multi-material tests with different materials on both sides. In this test, on the left side, the lighter material of aluminum impacts the heavier material of Copper. The initial condition is given as

$$\begin{cases} \text{L: Al}, \quad \rho = 2785\text{kg/m}^3, \quad u = 40\text{m/s}, \quad p = 0.1\text{Pa}, \quad s_{xx} = 0.0\text{Pa}, \\ \text{R: Copper}, \quad \rho = 8930\text{kg/m}^3, \quad u = 0.0\text{m/s}, \quad p = 0.1\text{Pa}, \quad s_{xx} = 0.0\text{Pa}. \end{cases} \tag{6.9}$$

Shown in the Fig.14, there is a large jump of density at the material interface and both the elastic shock and the plastic shock exist in each side of the interface. Comparing with the numerical results of the scheme with MHLLCEP approximate solver, we can find that our exact Riemann solver can solve the Riemann problem with multi-materials very well.

Test 10

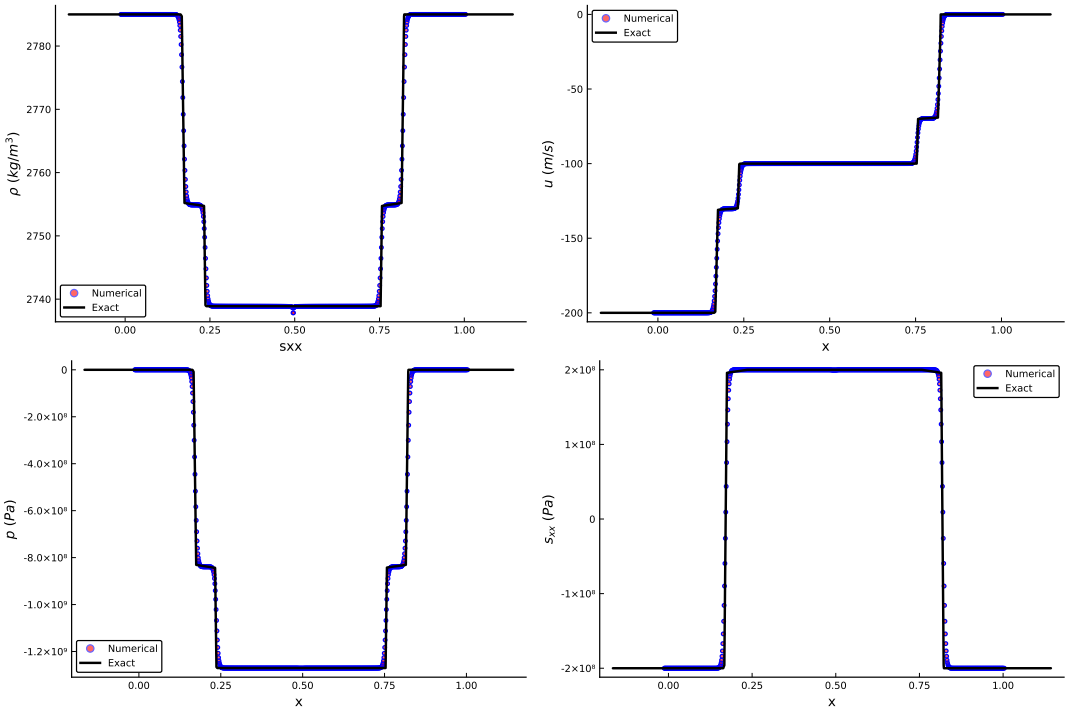

Figure 9: Comparison results for Test 5 with the structure of $R^E R^P | R^P R^E$.

Here we test another multi-materials case. In this test the initial condition is given as

$$\begin{cases} \text{L: Copper}, \quad \rho = 8930\text{kg/m}^3, \quad u = 0.0\text{m/s}, \quad p = 1.0 \times 10^{10}\text{Pa}, \quad s_{xx} = 0.0\text{Pa}, \\ \text{R: Al}, \quad \rho = 2785\text{kg/m}^3, \quad u = 0\text{m/s}, \quad p = 10.0\text{Pa}, \quad s_{xx} = 0.0\text{Pa}. \end{cases} \tag{6.10}$$

Shown in Fig.15, there are two rarefaction waves on the left side and two shocks on the right side. Moreover, we can find that there is the discontinuity of pressure on the interface, and the Cauchy stress is continuous, which satisfies the theoretical analysis.

Test 11

This test is the half Riemann problem with a given velocity $u^* = -20\text{m/s}$ on the left, and the right initial condition is

$$\text{Copper}, \quad \rho = 8930\text{kg/m}^3, \quad u = 0.0\text{m/s}, \quad p = 0.1\text{Pa}, \quad s_{xx} = 0.0\text{Pa}. \tag{6.11}$$

In Fig.16, comparison results are given by the exact half Riemann solver and the numerical method. We can see that the exact solver can resolve both the elastic shock and the plastic shock wave very well.

Test 12

The second half Riemann case is with a given Cauchy stress $\sigma^* = 0\text{Pa}$ on the left, and the right initial condition is

$$\text{Copper}, \quad \rho = 8930\text{kg/m}^3, \quad u = 0.0\text{m/s}, \quad p = 1.0 \times 10^9\text{Pa}, \quad s_{xx} = 0.0\text{Pa}. \tag{6.12}$$

In Fig.17, we give the results computed by the exact Riemann solver and the numerical simulation. From

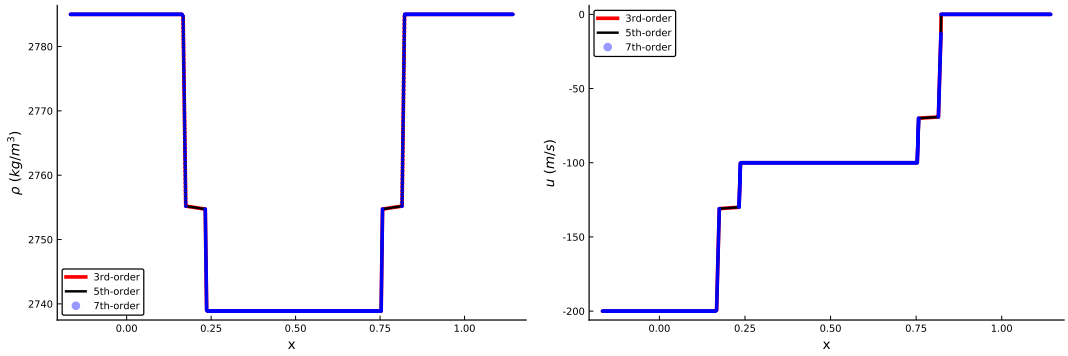

Figure 10: Comparison results for Test 5 with different orders of the Gaussian quadrature method.

this figure one can see, the exact solver can resolve the elastic and plastic rarefaction waves well.

7. Conclusions

In this paper, we have analyzed the Riemann problem in detailed for one-dimensional multi-material elastic-plastic flows with the Mie-Grüneisen EOS, hypo-elastic constitutive model and the von Mises' yielding condition and found

1. The sonic speed periods a significant jump when the material is yielding.
2. the plastic wave is always faster than the elastic wave for the reason of the sonic speed jump.
3. There are only thirty-six possible cases of the wave structure in the Riemann problem.
4. All the variables after the non-linear waves can be written as functions of the density theoretically.
5. If the initial material is in the negative plastic state, after being expanded, the material may be into the elastic state or the positive plastic state and vice versa.

Then, based on the above analysis, we have constructed exact Riemann solvers for both the Riemann problem and the half Riemann problem, separately.

Because of the iteration process, the CPU cost of the exact Riemann solver is of course more expensive than approximate ones. However, the main purpose of the exact Riemann solver is used to study the structures of the Riemann problem itself and give reference results to construct high performance approximate solvers. Tested by a large number of examples, the exact Riemann solver is reasonable and its solutions are matching well with the numerical results for both single material problems and multi-material Riemann problems.

Acknowledgement

We thank Professor Jiequan Li for many useful and insightful discussions. This work has been supported by Science Challenge Project (Grant No. TZ2016002) and NSFC (Grant No. 11672047).

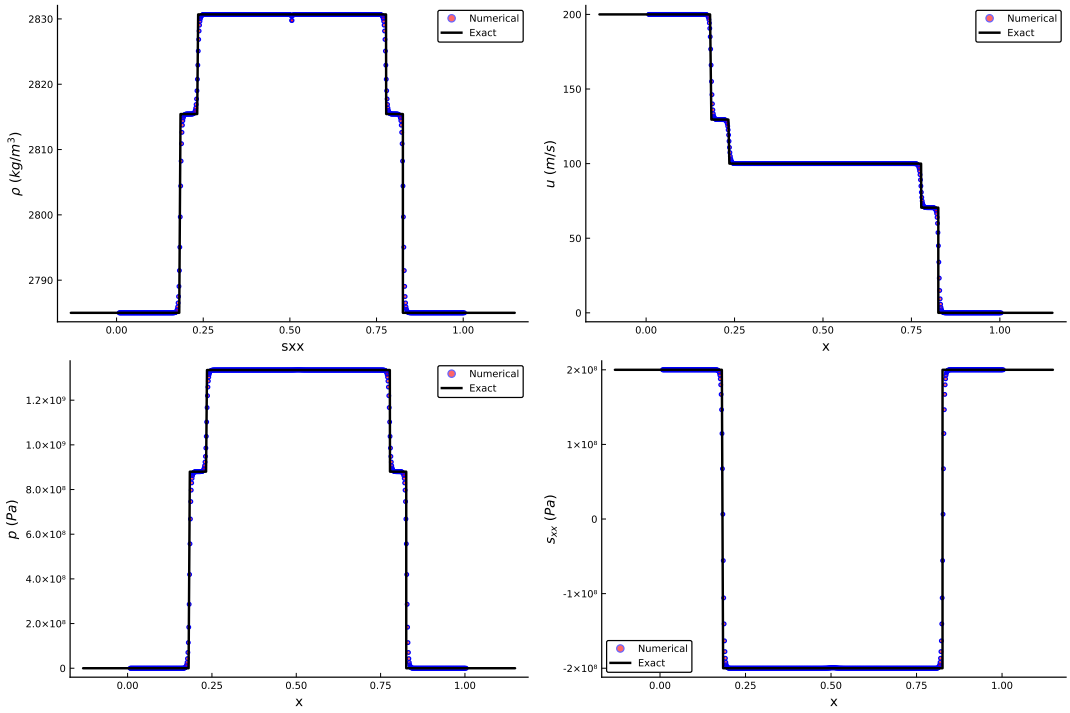

Figure 11: Comparison results for Test 6 with the structure of $S^E S^P | S^P S^E$.

References

[1] K. M. Shyue, A fluid-mixture type algorithm for compressible multicomponent flow with Mie-Grneisen equation of state, Journal of Computational Physics 171 (2) (2001) 678–707.

[2] S. B. Segletes, Thermodynamic stability of the Mie–grüneisen equation of state, and its relevance to hydrocode computations, Journal of applied physics 70 (5) (1991) 2489–2499.

[3] M. L. Wilkins, Calculation of elastic-plastic flow, Tech. rep., California Univ Livermore Radiation Lab (1963).

[4] P.-H. Maire, R. Abgrall, J. Breil, R. LoubèRe, B. Rebourcet, A nominally second-order cell-centered Lagrangian scheme for simulating elastic–plastic flows on two-dimensional unstructured grids, Journal of Computational Physics 235 (2013) 626–665.

[5] S. N. Atluri, On constitutive relations at finite strain: hypo-elasticity and elasto-plasticity with isotropic or kinematic hardening, Computer methods in applied mechanics and engineering 43 (2) (1984) 137–171.

[6] D. Steinberg, C. Lund, A constitutive model for strain rates from 10^{-4} to 10^{6} s^{-1}, Journal of Applied Physics 65 (4) (1989) 1528–1533.

[7] E. J. Lieberman, N. R. Morgan, D. J. Luscher, D. E. Burton, A higher-order Lagrangian discontinuous Galerkin hydrodynamic method for elastic-plastic flows, Computers & Mathematics with Applications 78 (2) (2019) 318–334.

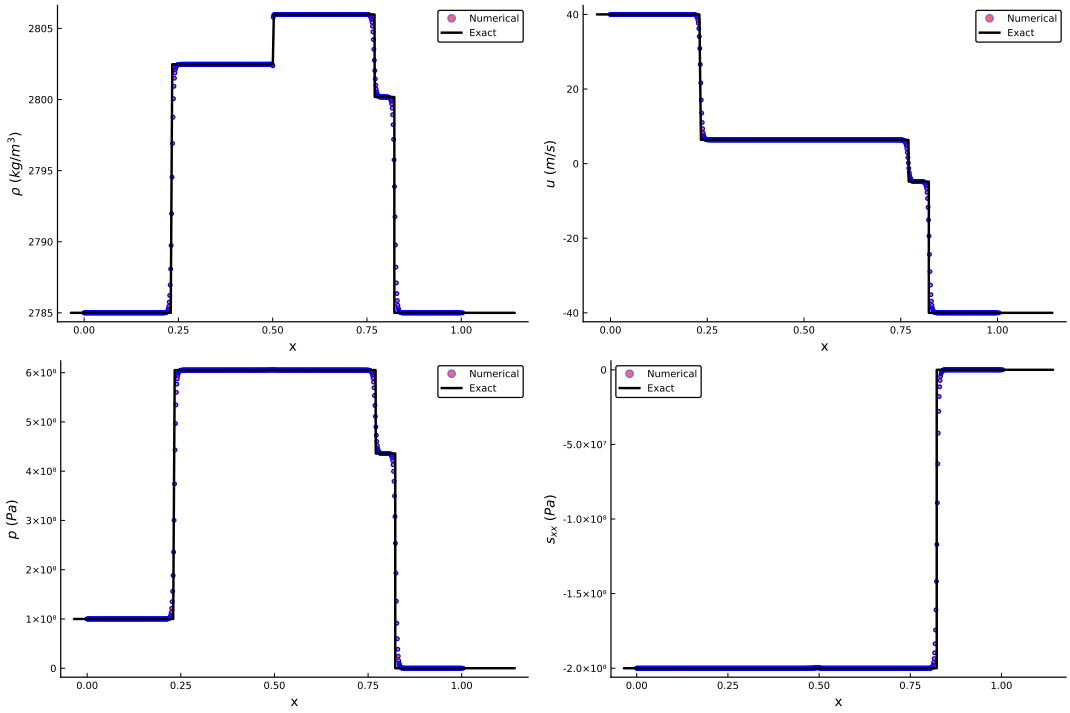

Figure 12: Comparison resutls for Test 7 with the structure of $R^P|R^P R^E$.

[8] J.-B. Cheng, W. Huang, S. Jiang, B. Tian, A third-order moving mesh cell-centered scheme for one-dimensional elastic-plastic flows, Journal of Computational Physics 349 (2017) 137–153.

[9] S. Thomson, Mathematical modelling of elastoplasticity at high stress, Ph.D. thesis, University of Oxford (2017).

[10] S. K. Godunov, A difference method for numerical calculation of discontinuous solutions of the equations of hydrodynamics, Matematicheskii Sbornik 89 (3) (1959) 271–306.

[11] B. Leer, Toward the ultimate ultimate conservative difference scheme. V. A second-order sequel to Godunov's method, Journal of Computational Physics 32 (101).

[12] P. L. Roe, Discrete models for the numerical analysis of time-dependent multidimensional gas dynamics, Journal of Computational Physics 63 (2) (1986) 458–476.

[13] A. Harten, P. D. Lax, B. Van Leer, On upstream differencing and Godunov-type schemes for hyperbolic conservation laws, Siam Review 25 (1) (1983) 53–79.

[14] E. F. Toro, M. Spruce, W. Speares, Restoration of the contact surface in the HLL-Riemann solver, Shock Waves 4 (1) (1994) 25–34.

[15] B. Einfeld, On Godunov-type methods for gas dynamics, SIAM Journal on Numerical Analysis 25 (2) (1988) 294–318.

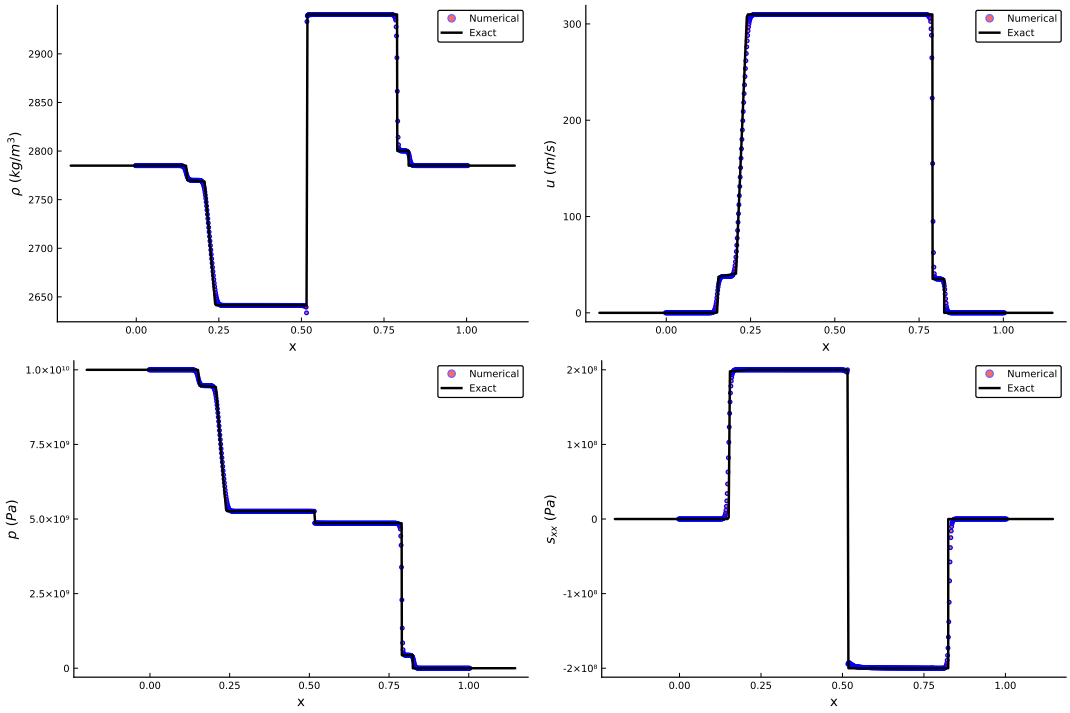

Figure 13: Comparison resutls for Test 8 with the structure of $R^E R^P | S^P S^E$.

[16] X. Deng, P. Boivin, F. Xiao, A new formulation for two-wave Riemann solver accurate at contact interfaces, Physics of Fluids 31 (4) (2019) 046102.

[17] S. Simon, J. C. Mandal, A simple cure for numerical shock instability in the HLLC Riemann solver, Journal of Computational Physics 378 (2019) 477–496.

[18] D. S. Balsara, A two-dimensional HLLC Riemann solver for conservation laws: Application to Euler and magnetohydrodynamic flows, Journal of Computational Physics 231 (22) (2012) 7476–7503.

[19] J. Vides, B. Nkonga, E. Audit, A simple two-dimensional extension of the HLL Riemann solver for hyperbolic systems of conservation laws, Journal of Computational Physics 280 (2015) 643675.

[20] J.-B. Cheng, L. Liu, S. Jiang, M. Yu, Z. Liu, A second-order cell-centered Lagrangian scheme with a HLLC Riemann solver of elastic and plastic waves for two-dimensional elastic-plastic flows, Journal of Computational Physics (2020) 109452.

[21] F. Bouchut, C. Klingenberg, K. Waagan, A multiwave approximate Riemann solver for ideal MHD based on relaxation II: numerical implementation with 3 and 5 waves, Numerische Mathematik 115 (4) (2010) p.647–679.

[22] S. L. Gavrilyuk, N. Favrie, R. Saurel, Modelling wave dynamics of compressible elastic materials, Journal of computational physics 227 (5) (2008) 2941–2969.

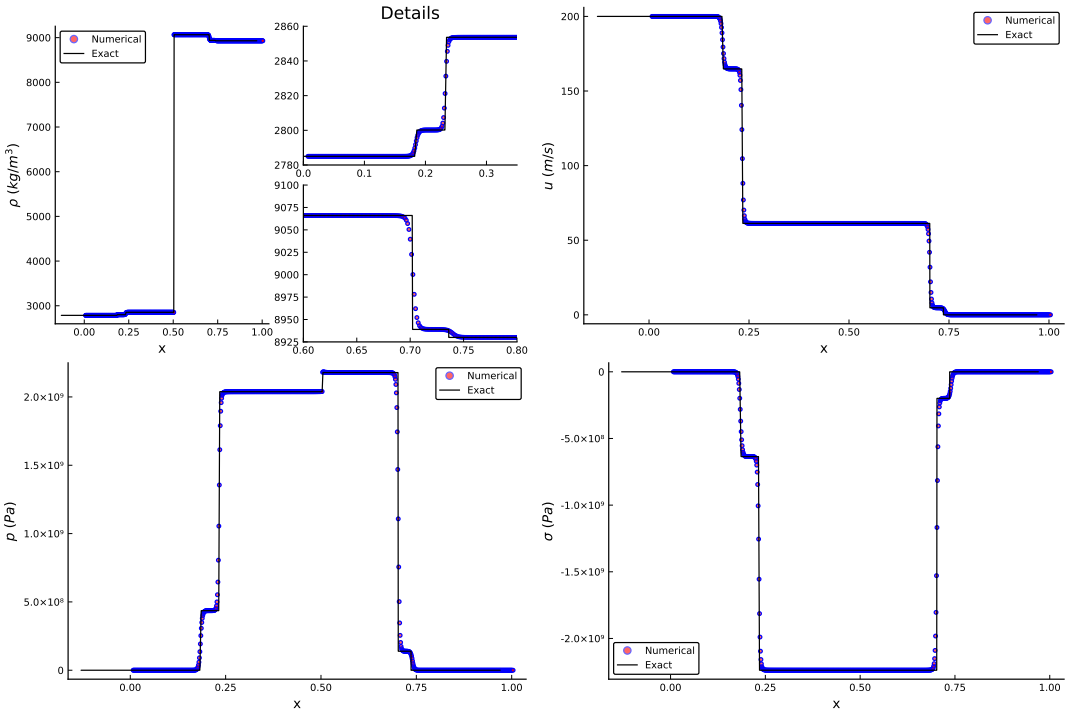

Figure 14: Comparison results for Test 9 with the structure of $R^E R^P | R^P R^E$.

[23] J.-B. Cheng, E. F. Toro, S. Jiang, M. Yu, W. Tang, A high-order cell-centered Lagrangian scheme for one-dimensional elastic–plastic problems, Computers & Fluids 122 (2015) 136–152.

[24] J. Cheng, Harten-Lax-van Leer-contact (HLLC) approximation Riemann solver with elastic waves for one-dimensional elastic-plastic problems, Applied Mathematics and Mechanics 37 (11) (2016) 1517–1538.

[25] L. Liu, J.-B. Cheng, Z. Liu, A multi-material HLLC Riemann solver with both elastic and plastic waves for 1D elastic-plastic flows, Computers & Fluids 192 (2019) 104265.

[26] F. Kerger, P. Archambeau, S. Erpicum, B. J. Dewals, M. Pirotton, An exact Riemann solver and a Godunov scheme for simulating highly transient mixed flows, Journal of Computational and Applied Mathematics 235 (8) (2011) 2030–2040.

[27] V. Deledicque, M. V. Papalexandris, An exact Riemann solver for compressible two-phase flow models containing non-conservative products, Journal of Computational Physics 222 (1) (2007) 217–245.

[28] R. Bernetti, V. A. Titarev, E. F. Toro, Exact solution of the riemann problem for the shallow water equations with discontinuous bottom geometry, Journal of Computational Physics 227 (6) (2008) 3212–3243.

[29] P. T. Barton, D. Drikakis, E. Romenski, V. A. Titarev, Exact and approximate solutions of Riemann problems in non-linear elasticity, Journal of Computational Physics 228 (18) (2009) 7046–7068.

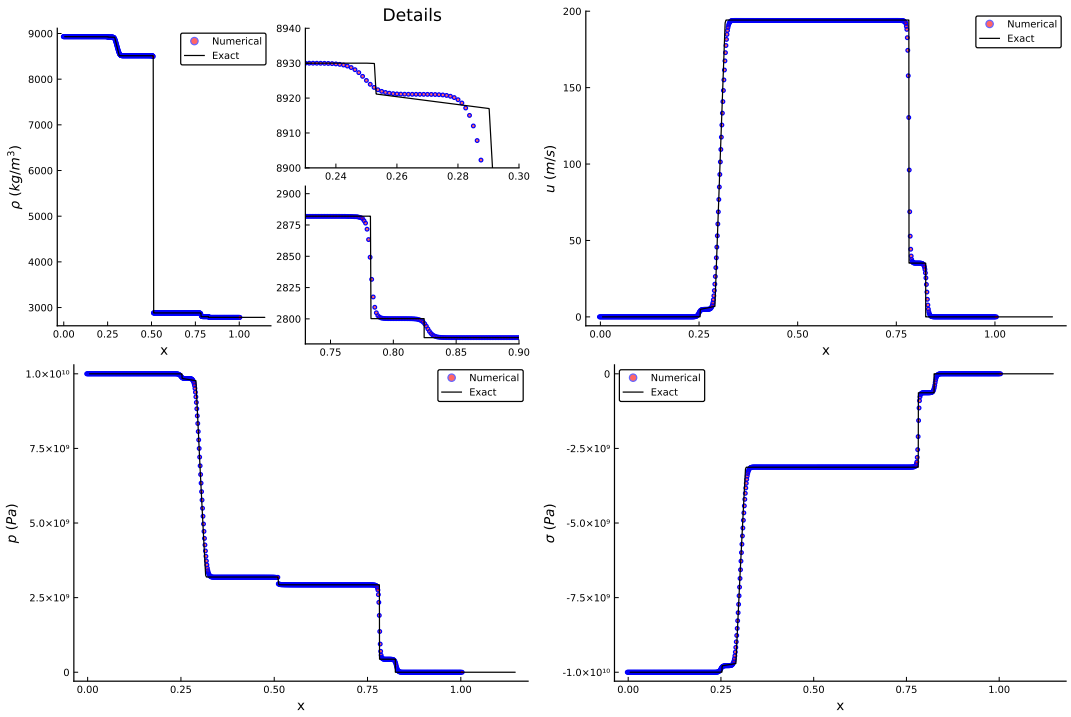

Figure 15: Comparison results for Test 10 with the structure of $R^E R^P | S^E S^P$.

[30] G. H. Miller, An iterative Riemann solver for systems of hyperbolic conservation laws, with application to hyperelastic solid mechanics, Journal of Computational Physics 193 (1) (2004) 198–225.

[31] Q. Zhan, Q. Ren, M. Zhuang, Q. Sun, Q. H. Liu, An exact Riemann solver for wave propagation in arbitrary anisotropic elastic media with fluid coupling, Computer Methods in Applied Mechanics and Engineering 329 (2018) 24–39.

[32] X. Garaizar, Solution of a Riemann problem for elasticity, Journal of elasticity 26 (1) (1991) 43–63.

[33] S. Gao, T. Liu, 1d exact elastic-perfectly plastic solid Riemann solver and its multi-material application, Advances in Applied Mathematics and Mechanics 9 (3) (2017) 621–650.

[34] S. Gao, T. Liu, C. Yao, A complete list of exact solutions for one-dimensional elastic-perfectly plastic solid Riemann problem without vacuum, Communications in Nonlinear Science and Numerical Simulation 63 (2018) 205–227.

[35] M. B. Tyndall, Numerical modelling of shocks in solids with elastic-plastic conditions, Shock Waves 3 (1) (1993) 55–66.

[36] J. Wang, K. Liu, D. Zhang, An improved CE/SE scheme for multi-material elasticplastic flows and its application, Computers and Fluids 38 (3) (2009) 544–551.

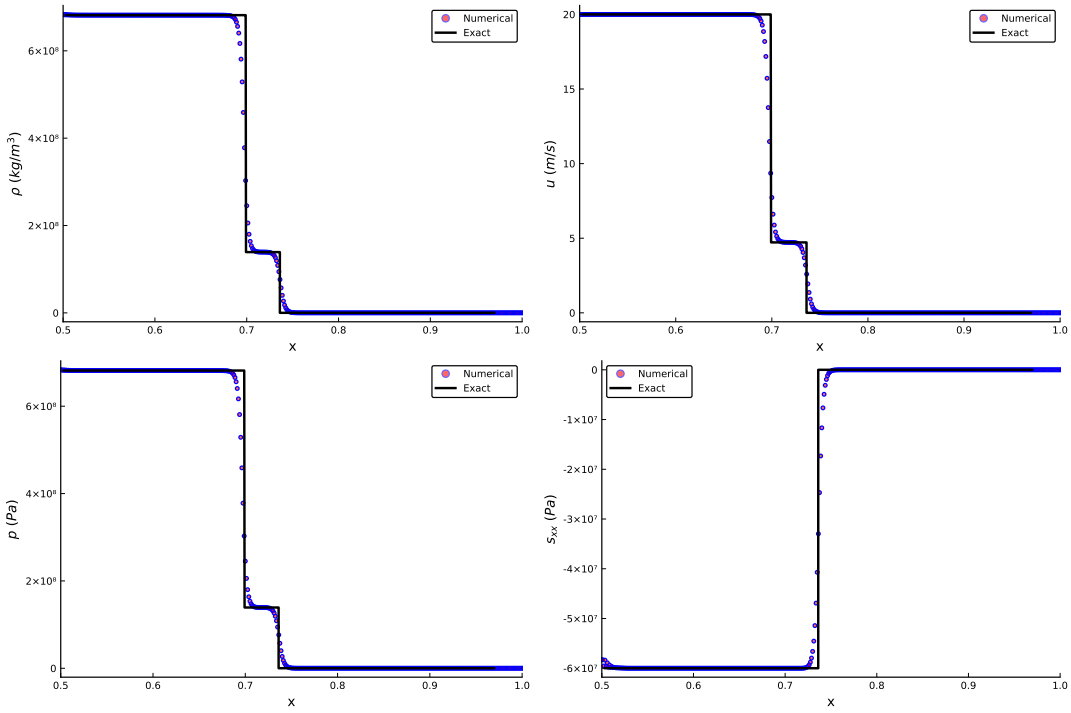

Figure 16: Comparison results for Test 11 with the structure of $S^E S^P$.

[37] A. L. Ortega, M. Lombardini, D. Pullin, D. I. Meiron, Numerical simulation of elastic–plastic solid mechanics using an Eulerian stretch tensor approach and HLLD Riemann solver, Journal of Computational Physics 257 (2014) 414–441.

[38] N. Favrie, S. Gavrilyuk, Dynamics of shock waves in elastic-plastic solids, in: ESAIM: Proceedings, Vol. 33, EDP Sciences, 2011, pp. 50–67.

[39] A. S. Khan, S. Huang, Continuum theory of plasticity, John Wiley & Sons, 1995.

[40] R. Batra, Linear constitutive relations in isotropic finite elasticity, Journal of Elasticity 51 (3) (1998) 243–245.

[41] E. F. Toro, Riemann solvers and numerical methods for fluid dynamics: a practical introduction, Springer Science & Business Media, 2013.

[42] A. G. Kulikovskii, N. V. Pogorelov, A. Y. Semenov, Mathematical aspects of numerical solution of hyperbolic systems, CRC Press, 2000.

[43] R. Saurel, R. Abgrall, A multiphase Godunov method for compressible multifluid and multiphase flows, Journal of Computational Physics 150 (2) (1999) 425–467.

[44] X. Deng, S. Inaba, B. Xie, K.-M. Shyue, F. Xiao, High fidelity discontinuity-resolving reconstruction for compressible multiphase flows with moving interfaces, Journal of Computational Physics 371 (2018) 945–966.

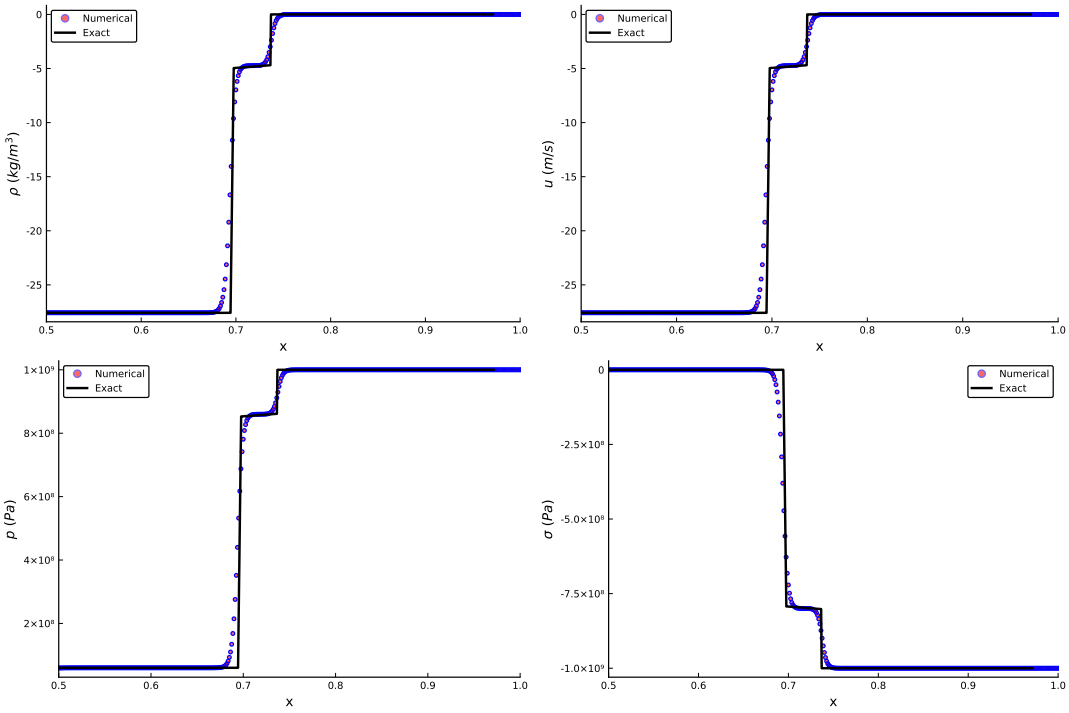

Figure 17: Comparison results for Test 11 with the structure of $R^E R^P$.

A. Numerical integration for the rarefaction wave

There are two integrations in functions $p(\rho)$ and $u(\rho)$ in the rarefaction wave, for example, in the equations (4.14) and (4.15). In this paper, we use a seventh-order (with 4 integrating points) Gaussian quadrature to make numerical integrations. For a function $g(x)$, the Gaussian integration from -1 to 1 is given as

$$\int_{-1}^{1} g(x)dx \approx \sum_{i=1}^{n} \omega_i g(x_i),$$

ω_i is the weight, and x_i is the integrating point, n is the number of the Gaussian quadrature points. Here $n = 4$. For the 7th-order Gaussian quadrature, integrating points and corresponding weights are

$$x_1,\ x_2 = \pm\sqrt{\frac{3}{7} - \frac{2}{7}\sqrt{\frac{6}{5}}} \quad \left(\omega_1,\ \omega_2 = \frac{18+\sqrt{30}}{36}\right),$$

$$x_3,\ x_4 = \pm\sqrt{\frac{3}{7} + \frac{2}{7}\sqrt{\frac{6}{5}}} \quad \left(\omega_3,\ \omega_4 = \frac{18-\sqrt{30}}{36}\right).$$

For the function $g(x)$ over $[\rho_0, \rho]$, this change of interval can be done in the following way:

$$\int_{\rho_0}^{\rho} g(x)dx = \frac{\rho-\rho_0}{2}\int_{-1}^{1} g\left(\frac{\rho-\rho_0}{2}x + \frac{\rho_0+\rho}{2}\right)dx.$$

At last, we can get

$$\int_{\rho_0}^{\rho} g(x)dx \approx \frac{\rho-\rho_0}{2}\sum_{i=1}^{n}\omega_i g\left(\frac{\rho-\rho_0}{2}x_i+\frac{\rho_0+\rho}{2}\right). \tag{A.1}$$

A.1. Integrating of $p(\rho)$

Taking Equation (4.14) as an example,

$$p(\rho) \approx p_{L(R)}e^{\frac{\lambda}{\rho_{L(R)}}-\frac{\lambda}{\rho}} + e^{-\frac{\lambda}{\rho}}\mathrm{Intg}_1, \tag{A.2}$$

where

$$\mathrm{Intg}_1 = \frac{\rho-\rho_{L(R)}}{2}\sum_{n=1}^{4}\omega_i f_2(\rho_i)e^{\lambda/\rho_i},$$

and $\rho_i = \frac{\rho-\rho_{L(R)}}{2}x_i + \frac{\rho_{L(R)}+\rho}{2}$.

Obviously, we can use (A.2) to evaluate all the values of $p(\rho_i)$ on all Gaussian quadrature points.

A.2. Integrating of $u(\rho)$

Taking Equation (4.15) as an example, if the wave is on the left side

$$u(\rho) = u_L - \int_{\rho_L}^{\rho}\frac{c_e(x)}{x}dx.$$

The numerical integration of $u(\rho)$ is given as

$$u(\rho) \approx u_L - \mathrm{Intg}_2 \tag{A.3}$$

where

$$\mathrm{Intg}_2 = \frac{\rho-\rho_{L(R)}}{2}\sum_{n=1}^{4}\omega_i\frac{c_e(\rho_i)}{\rho_i},$$

Different from (A.2), the sonic speed $c_e(\rho_i)$ is dependent on $p(\rho_i)$:

$$c_e(\rho_i) = \sqrt{a_0^2\frac{\partial f}{\partial\eta}\left(\frac{\rho_i}{\rho_0}\right) + \frac{p(\rho_i)}{\rho_i^2}\rho_0\Gamma_0 - \frac{\rho_0}{\rho_i^2}\Gamma_0 s_{xx}(\rho_i) + \frac{4}{3}\frac{\mu}{\rho_i}}. \tag{A.4}$$

After finishing the evaluation of $p(\rho_i)$, we can evaluate $c_e(\rho_i)$ by using the same process as (A.2).

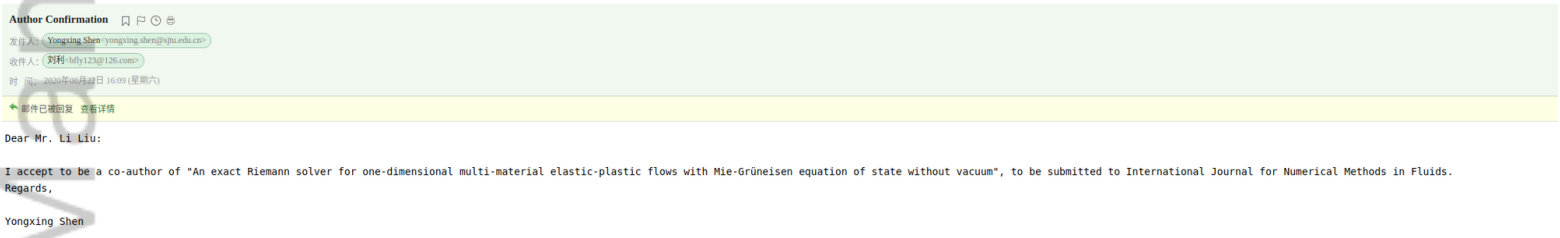

FLD_4917_Author_Confirmation.png

An exact Riemann solver for one-dimensional multi-material elastic-plastic flows with Mie-Grüneisen equation of state without vacuum

Li Liu, Jun-Bo Cheng*, Yongxing Shen

Based on the analysis of the Jacobian matrices in the elastic and plastic states in one-dimensional multi-material elastic-plastic flows with the Mie-Grüneisen equation of state(EOS), hypo-elastic constitutive model and the von Mises'yielding condition, relations are built for different variables across different type of waves. Then, exact Riemann solvers for the Riemann problem and the half Riemann problem are presented, respectively.

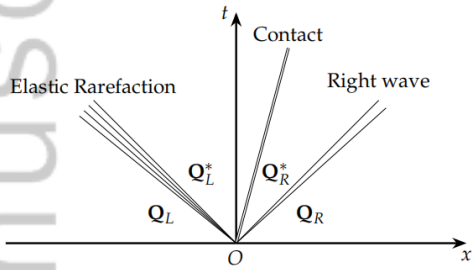

(a) Elastic rarefaction wave (R^E)

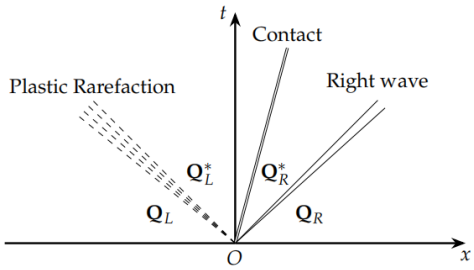

(b) Plastic rarefaction wave (R^P)

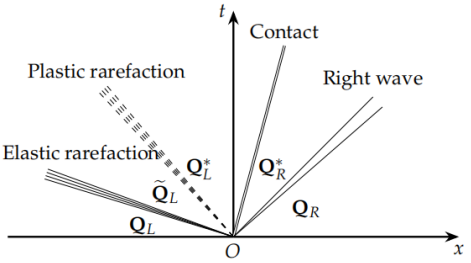

(c) Both elastic and plastic rarefaction waves ($R^E R^P$)

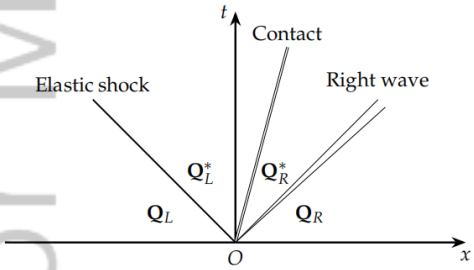

(d) Elastic shock wave (S^E)

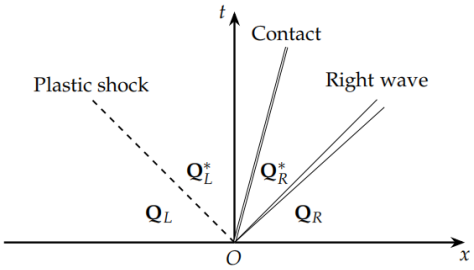

(e) Plastic shock wave (R^P)

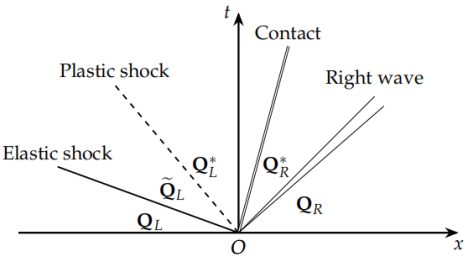

(f) Both elastic and plastic shock waves ($S^E S^P$)

FLD_4917_TOC.tiff

An exact Riemann solver for one-dimensional multi-material elastic-plastic flows with Mie-Grüneisen equation of state without vacuum

Li Liu [1], Jun-Bo Cheng [1,*], Yongxing Shen [2]

[1] *Laboratory of Computational Physics, Institute of Applied Physics and Computational Mathematics, Beijing 100094, China*

[2] *University of Michigan - Shanghai Jiao Tong University Joint Institute, Shanghai Jiao Tong University, Shanghai, 200240, China*

Abstract

In this paper, we present exact Riemann solvers for the Riemann problem and the half Riemann problem, respectively, for one-dimensional multi-material elastic-plastic flows with the Mie-Grüneisen equation of state(EOS), hypo-elastic constitutive model and the von Mises' yielding condition. We firstly analyze the Jacobian matrices in the elastic and plastic states, and then build the relations of different variables across different type of waves. Based on these formulations, an exact Riemann solver is constructed with totally thirty-six possible cases of wave structures. A large number of tests prove the rightness of the new exact Riemann solver. Moreover, an exact Riemann solver is also deduced for the half Riemann problem and its validity is tested by two examples.

Keywords: Elastic-plastic flows, Riemann problem, hypo-elastic model, exact Riemann solver, Mie-Grüneisen equation

1. Introduction

In this paper, an exact Riemann solver is built for one-dimensional multi-material elastic-plastic flows modeled by the Mie-Grüneisen equation of state (EOS) [1, 2], hypo-elastic constitutive model and the von Mises' yielding condition.

The elastic-plastic flow is used to describe the deformation process of solid materials, especially metals, under strong dynamics loading, such as explosive or high-speed impact. The simulation of elastic-plastic flows has important application backgrounds, especially in the Implosion Dynamics weapon and Inertial Confine Fusion (ICF). The first try of simulating the elastic-plastic flows was given by Wilkins [3] in 1960s. In his work, the hypo-elastic constitutive model with the von Mises' yielding condition (so-called the elastic-perfectly plastic model) is considered with a simple EOS that pressure only depends on density. Following [3], Maire et.al [4] developed a high-order cell-centered Lagrangian scheme with the same elastic-plastic constitutive model with the Mie-Grüneisen EOS which is widely used in charactering real materials [1]. Besides the elastic-perfectly plastic model, there are other more complex models for elastic-plastic deformations, such as the

*Correspondence to: Jun-Bo Cheng, Institute of Applied Physics and Computational Mathematics, Beijing 100094, China. E-mail: Cheng_junbo@iapcm.ac.cn

September 12, 2020

hypo-elastic constitutive model with strain hardening (HCMSH) [5] and Steinberg-Guinan (SG) constitutive model [6] and so on. In this paper, only the elastic-perfectly plastic model with the Mie-Grüneisen EOS is considered for its general applications in the numerical study of elastic-plastic flows [7, 8, 9].

Riemann problems and the corresponding solvers have been viewed as essential problems for the study of computational fluid dynamics (CFD) since the introduction of Godunov schemes [10] and their high-order extensions [11]. In the following two decades, a lot of famous and widely used approximate Riemann solvers are proposed, such as the Roe Riemann solver [12], the HLL [13], HLLC [14] and HLLE Riemann solvers[15]. Even recently, Riemann problems still attract much attention, especially in the following three aspects. The first is to reduce numerical dissipation and to approve the robustness of schemes [16, 17]; the second is to develop two-dimensional Riemann solvers [18, 19, 20]; and the third is to extend the existin approximate solvers to other systems, such as the magnetohydrodynamic (MHD) [21, 18] and elastic-plastic flows [22, 23, 24, 25]. In the study of Riemann problems, the exact Riemann solver has also played a very important role as it not only can give a guide and reference in constructing approximate Riemann solvers, but also can be used to determine the convergence and stability of numerical schemes. Besides the exact Riemann solver for Euler equations which is used in the first Godunov scheme given by Godunov [10], some exact Riemann solvers are also constructed for other systems, for example, for highly transient mixed flows [26], for two-phase flows containing non-conservative products [27] and for shallow water equations system [28]. In solving the Riemann problems of these systems, solving procedures are different. For example, for the shallow water equations with discontinuous bottom geometry [28], we only need to solve algebraic equations; but for general hyperbolic equations [10, 26, 27, 29, 30, 31], the iteration procedures are necessary. Recently, the exact Riemann solver for elastic-plastic flows also attracts much attention [29, 30, 31]. However, building the exact Riemann solver for elastic-plastic flows is not easy. Comparing with the governing equations of 1D pure fluids, for 1D elastic-plastic flows, there are two more equations, a non-conservative constitutive equation and the von Mises yielding condition, needed to be considered. The non-conservative character of the constitutive equation increases the difficulty in constructing Riemann solvers, while the von Mises yielding condition may lead to more non-linear waves in the wave structure of Riemann solvers. Moreover, in a general way, the equation of state(EOS) for solid materials is more complex than that for pure fluids, which directly increases the difficulty in solving the Riemann problem.

For the elastic-plastic flow with the hypo-elastic constitutive model and the von Mises' yielding condition, some approximate Riemann solvers[22, 23, 24, 25, 20] have been developed recently. However, for the exact Riemann solver, the research is relatively few, and focuses mainly on the problems with relatively simple constitutive models or relatively simple EOSs. For example, Garaizar [32] and Miller [30] introduced an exact Riemann solver for elastic or hyper-elastic materials, Gao and Liu [33, 34] firstly considered the yielding effect and developed an exact elastic-perfectly plastic solid Riemann solver. In Gao and Liu works [33, 34], a five-equation Eulerian governing system is constructed, and a complete list of sixty-four cases of wave type

is presented.

In this paper, we construct an exact Riemann solver for the system of 1D elastic-plastic flows with the Mie-Grüneisen EOS, the hypo-elastic constitutive model and the von Mises' yielding condition. Although Gao and Liu [33, 34] have developed a comprehensive exact Riemann solver for a five-equation system with 1D elastic-perfectly plastic solid, but their exact Riemann solver is not suitable for a general four-equation system because there are big differences between these two systems. In the four-equation system in Section 2.1, the elastic and plastic states are treated with same equations of mass, momentum, total energy and the same complex Mie-Grneisen EOS, but only different in deviatoric stress. While in the five-equation system, two states are separated and they have their own densities, velocities and EOSs. For example, in the elastic state, the pressure is only a function of density and the internal energy is not necessarily considered; in the plastic state, a linear stiffened-gas EOS is used, which is the simplified form of the Mie-Grneisen EOS. Moreover, the four-equation system is widely used in many engineering areas since the seminal work by Wilkins [3] and the following works [4, 35, 36, 23, 37, 38]. For these reasons, we want to construct an exact Riemann solver for the common used four-equation system and with a more general case of real materials characterized by the Mie-Grüneisen EOS [3].

This paper is organized as follows. In Section 2, we introduce the governing equations to be studied. In Section 3, the Riemann problem and the relations for every wave type (contact wave, shock wave and rarefaction wave) are derived. Then, the exact Riemann solver is given in Section 4. The half Riemann problem and its solver is introduced in Section 5. Some numerical examples are presented to validate our Riemann solvers in Section 6. Conclusions are shown in Section 7.

2. Governing equations

In this paper, the elastic energy is not included in the total energy. The exclusion of the elastic energy is usual for practical engineering problems [4] and is different from that in Ref.[22].

2.1. Motion equations

For a continuous one-dimensional homogeneous solid, the motion equations in the differential form are

$$\partial_t \mathbf{U} + \partial_x \boldsymbol{F}(\mathbf{U}) = 0,\ x \in\ \Omega \subset \mathbf{R},\ t > 0,$$

where

$$\mathbf{U} = \begin{bmatrix} \rho \\ \rho u \\ \rho E \end{bmatrix}, \quad \mathbf{F} = \begin{bmatrix} \rho u \\ \rho u^2 - \sigma \\ (\rho E - \sigma) u \end{bmatrix}, \tag{2.1}$$

ρ, u, σ and E are the density, velocity in $x-$direction, Cauchy stress and total energy per unit volume, respectively, E has the relation with the specific internal energy e as

$$E = e + \frac{1}{2}u^2, \tag{2.2}$$

$$\sigma = -p + s_{xx}, \tag{2.3}$$

where p and s_{xx} denote the hydrostatic pressure and the deviatoric stress in the $x-$ direction, respectively.

2.2. The equation of state (EOS)

The relation of the pressure with the density and the specific internal energy is gotten from the equation of state (EOS). In this paper, we consider the Mie-Grüneisen EOS,

$$p(\rho, e) = \rho_0 a_0^2 f(\eta) + \rho_0 \Gamma_0 e, \tag{2.4}$$

where $f(\eta) = \frac{(\eta-1)(\eta-\Gamma_0(\eta-1)/2)}{(\eta-s(\eta-1))^2}$, $\eta = \frac{\rho}{\rho_0}$, ρ_0, a_0, s and Γ_0 are the constant parameters of the Mie-Grüneisen EOS.

2.3. The constitutive relation

Hooke's law is used here to describe the relationship between the deviatoric stress and the strain [39, 40],

$$\dot{s}_{xx} = 2\mu\left(\dot{\varepsilon}_x - \frac{1}{3}\frac{\dot{V}}{V}\right), \tag{2.5}$$

where μ is the shear modulus, V is the volume, and the dot means the material time derivative,

$$\dot{()} = \frac{\partial()}{\partial t} + u\frac{\partial()}{\partial t}, \tag{2.6}$$

and

$$\dot{\varepsilon}_x = \frac{\partial u}{\partial x}, \quad \frac{\dot{V}}{V} = \frac{\partial u}{\partial x}. \tag{2.7}$$

By using Eq.(2.7), Eq.(2.5) can be rewritten as

$$\frac{\partial s_{xx}}{\partial t} + u\frac{\partial s_{xx}}{\partial t} = \frac{4}{3}\mu\frac{\partial u}{\partial x}. \tag{2.8}$$

2.4. The yielding condition

The Von Mises' yielding condition is used here to describe the elastic limit. In one spatial dimension, the von Mises' yielding criterion is given by

$$|s_{xx}| \leq \frac{2}{3}Y_0, \tag{2.9}$$

where Y_0 is the yield strength of the material in simple tensions.

3. The Riemann problem

The Riemann problem for 1D time dependent elastic-plastic equations is given as follows:

$$\begin{cases} \partial_t \rho + \partial_x(\rho u) = 0, \\ \partial_t(\rho u) + \partial_x(\rho u^2 + p - s_{xx}) = 0, \\ \partial_t(\rho E) + \partial_x\left[(\rho E + p - s_{xx})u\right] = 0, \\ \begin{cases} \partial_t s_{xx} + u\partial_x s_{xx} - \frac{4}{3}\partial_x u = 0, \\ |s_{xx}| \le \frac{2}{3}Y_0, \end{cases} \\ Q(x, t=0) = \begin{cases} Q_L, \text{ if } x < 0, \\ Q_R, \text{ if } x > 0, \end{cases} \end{cases} \tag{3.1}$$

where $Q = (\rho, \rho u, \rho E, s_{xx})^T$.

Firstly, we assume that the wave structure of this Riemann problem is self-similar [20, 41].

If the material is in the plastic state, the above forth equation can be simplified. Correspondingly, sonic velocity is different from that in the elastic state, which will be discussed in the following.

3.1. Elastic state

3.1.1. Jacobian matrix in elastic regions

For the Mie-Grüneisen EOS, if the material is not yielding,

$$|s_{xx}| < \frac{2}{3}Y_0,$$

the system (3.1) can be written as

$$\partial_t \mathbf{Q} + \mathbf{J}_e(\mathbf{Q})\partial_x \mathbf{Q} = 0,$$

where $Q = (\rho, \rho u, \rho E, s_{xx})$, and the Jacobian matrix is

$$\mathbf{J}_e(Q) = \begin{bmatrix} 0 & 1 & 0 & 0 \\ -u^2 + \frac{\partial p}{\partial \rho} + \Gamma(\frac{u^2}{2} - e) & u(2-\Gamma) & \Gamma & -1 \\ (\Gamma(\frac{u^2}{2} - e) - e - \frac{u^2}{2} + \frac{\sigma}{\rho} + \frac{\partial p}{\partial \rho})u & -\Gamma u^2 - \frac{\sigma}{\rho} + \frac{u^2}{2} + e & (1+\Gamma)u & -u \\ \frac{4}{3}\mu\frac{u}{\rho} & -\frac{4}{3}\mu\frac{1}{\rho} & 0 & u \end{bmatrix}, \tag{3.2}$$

where $\Gamma = \frac{\Gamma_0 \rho_0}{\rho}$.

The eigenvalues of $\mathbf{J}_e(\mathbf{Q})$ are given as

$$\lambda_1 = \lambda_2 = u, \quad \lambda_3 = u - c_e, \quad \lambda_4 = u + c_e,$$

where c_e means the sonic speed of the solid in the elastic state,

$$\begin{cases} c_e = \sqrt{a^2 - \dfrac{\rho_0}{\rho^2}\Gamma_0 s_{xx} + \dfrac{4}{3}\dfrac{\mu}{\rho}}, \\ a^2 = \dfrac{\partial p}{\partial \rho} + \dfrac{p}{\rho^2}\dfrac{\partial p}{\partial e} = a_0^2\dfrac{\partial f}{\partial \eta} + \dfrac{p}{\rho^2}\rho_0\Gamma_0. \end{cases} \tag{3.3}$$

Corresponding right eigenvectors are

$$r_1 = \begin{bmatrix} \frac{1}{b_1} \\ \frac{u}{b_1} \\ 0 \\ 1 \end{bmatrix}, \quad r_2 = \begin{bmatrix} -\frac{\Gamma}{b_1} \\ -\frac{\Gamma u}{b_1} \\ 1 \\ 0 \end{bmatrix}, \quad r_3 = \frac{1}{\phi^2}\begin{bmatrix} 1 \\ u - c_e \\ h - uc_e \\ \phi^2 \end{bmatrix}, \quad r_4 = \frac{1}{\phi^2}\begin{bmatrix} 1 \\ u + c_e \\ h + uc_e \\ \phi^2 \end{bmatrix}, \tag{3.4}$$

where

$$b_1 = \frac{\partial p}{\partial \rho} - \Gamma E, \quad h = E + \frac{p - s_{xx}}{\rho},$$

and

$$\phi^2 = a^2 - \frac{\rho_0}{\rho^2}\Gamma_0 s_{xx} - c_e^2 = -\frac{4\mu}{3}\frac{1}{\rho}.$$

3.1.2. Relations across the contact wave

For a system without molecular diffusion, there is no materials convecting across the contact wave or interface, so the velocities on two sides of the discontinuity are always equal. This can also be verified by eigenvectors in Eq.(3.4) and Eq.(3.51).

Use $\mathbf{Q}_L^*$ and $\mathbf{Q}_R^*$ to denote the two states connected by the contact wave in the solution, where $\mathbf{Q} = (\rho, u, p, s_{xx})$.

Thanks to Eq.(3.4), based on the theory of Generalised Riemann Invariants introduced by [41, 42], for the λ_1-wave we have

$$\frac{d\rho}{\frac{1}{b_1}} = \frac{d\rho u}{\frac{u}{b_1}} = \frac{d\rho E}{0} = \frac{ds_{xx}}{1}. \tag{3.5}$$

From above equations, we can easily deduce that

$$du = 0, \quad d(s_{xx} - p) = 0, \tag{3.6}$$

which means

$$u_L^* = u_R^*, \tag{3.7}$$

and

$$\sigma_{x,L}^* = \sigma_{x,R}^*, \tag{3.8}$$

where $()_L^*$ and $()_R^*$ denote $()$ in the regions of $\mathbf{Q}_L^*$ and $\mathbf{Q}_R^*$, respectively. Here we do not show the details of the derivation for a simple presentation.

Similarly, for the λ_2-wave one has

$$\frac{d\rho}{\frac{-\Gamma}{b_1}} = \frac{d\rho u}{\frac{-u\Gamma}{b_1}} = \frac{d\rho E}{1} = \frac{ds_{xx}}{0}. \tag{3.9}$$

From the above equations, we can easily deduce that

$$du = 0, \quad dp = 0, \quad ds_{xx} = 0, \tag{3.10}$$

which means

$$u_L^* = u_R^*, \tag{3.11}$$

$$p_L^* = p_R^*, \quad s_{xx,L}^* = s_{xx,R}^*. \tag{3.12}$$

From Eq.(3.12), we get that

$$\sigma_{x,L}^* = \sigma_{x,R}^*. \tag{3.13}$$

At last, for the λ_1 and λ_2 waves, one can find that the following two relations always hold:

$$u_L^* = u_R^*, \quad \sigma_{x,L}^* = \sigma_{x,R}^*. \tag{3.14}$$

For convenience, we define

$$s^* = u_L^* = u_R^*. \tag{3.15}$$

where s^* denotes the velocity of the contact wave.

3.1.3. Relations across rarefaction waves

Left-going rarefaction wave

Across the left wave associated with λ_3-wave, ($\lambda_3 = u - c_e$), we have

$$\frac{d\rho}{1} = \frac{d(\rho u)}{u - c_e} = \frac{d(\rho E)}{h - uc_e} = \frac{ds_{xx}}{-\frac{4\mu}{3}\frac{1}{\rho}}. \tag{3.16}$$

which leads to

$$\mathrm{d}u = -\frac{c_e}{\rho}\mathrm{d}\rho, \tag{3.17}$$

$$\mathrm{d}E = -\frac{\sigma + \rho u c_e}{\rho^2}d\rho, \tag{3.18}$$

$$\mathrm{d}s_{xx} = -\frac{4}{3}\frac{\mu}{\rho}d\rho. \tag{3.19}$$

Using (2.4), one can get

$$dE = de + udu. \tag{3.20}$$

Substituting (3.17) and (3.18) into the above equation yields

$$de = -\frac{\sigma}{\rho^2}d\rho = \frac{p - s_{xx}}{\rho^2}d\rho. \tag{3.21}$$

Thanks to (2.4), one can get

$$dp = \frac{\partial p}{\partial \rho}d\rho + \frac{\partial p}{\partial e}de = a_0^2\frac{\partial f}{\partial \eta}d\rho + \rho_0\Gamma_0 de, \tag{3.22}$$

Substituting (3.21) into the above equation yields

$$dp = \left(a_0^2\frac{\partial f}{\partial \eta} + \frac{p}{\rho^2}\rho_0\Gamma_0 - \frac{\rho_0}{\rho^2}\Gamma_0 s_{xx}\right)d\rho. \tag{3.23}$$

The above equation can be rewritten as a differential equation of $p(\rho)$

$$p'(\rho) - \lambda\frac{p}{\rho^2} = f_2(\rho), \tag{3.24}$$

where

$$\lambda = \rho_0\Gamma_0 \quad f_2(\rho) = a_0^2\frac{\partial f}{\partial \eta} - \lambda\frac{s_{xx}(\rho)}{\rho^2}. \tag{3.25}$$

By integrating (3.24) across the left rarefaction wave, the pressure can be solved out as

$$pe^{\frac{\lambda}{\rho}} - \int f_2(\rho)e^{\frac{\lambda}{\rho}}d\rho = \text{constant}. \tag{3.26}$$

Integrating (3.17) across the left rarefaction wave yields

$$u + \int \frac{c_e}{\rho}d\rho = \text{constant}. \tag{3.27}$$

Right-going rarefaction wave

Across the right wave associated with λ_4-wave, ($\lambda_3 = u + c_e$), we have

$$\frac{d\rho}{1} = \frac{d(\rho u)}{u + c_e} = \frac{d(\rho E)}{h + uc_e} = \frac{ds_{xx}}{-\frac{4\mu}{3}\frac{1}{\rho}}. \tag{3.28}$$

which leads to

$$\mathrm{d}u = \frac{c_e}{\rho}\mathrm{d}\rho, \tag{3.29}$$

$$\mathrm{d}E = -\frac{\sigma + \rho u c_e}{\rho^2}d\rho, \tag{3.30}$$

$$\mathrm{d}s_{xx} = -\frac{4}{3}\frac{\mu}{\rho}d\rho. \tag{3.31}$$

By using the same method as the left wave, one can get

$$pe^{\frac{\lambda}{\rho}} - \int f_2(\rho)e^{\frac{\lambda}{\rho}}d\rho = \text{constant}. \tag{3.32}$$

$$u - \int \frac{c_e}{\rho}d\rho = \text{constant}. \tag{3.33}$$

3.1.4. Relations across shock waves

Now we consider a shock wave moving with the speed of s. The data in front of the shock is $(\rho_1, u_1, p_1, s_{xx1})$ and that after the shock is $(\rho_2, u_2, p_2, s_{xx2})$.

We transform the equations to a frame of reference moving with the shock. The Rankine-Hugoniot conditions are given as

$$\rho_2(u_2 - s) = \rho_1(u_1 - s), \tag{3.34}$$

$$\rho_2 u_2(u_2 - s) = \rho_1 u_1(u_1 - s) + \sigma_2 - \sigma_1, \tag{3.35}$$

$$\rho_2 E_2(u_2 - s) = \rho_1 E_1(u_1 - s) + \sigma_2 u_2 - \sigma_1 u_1. \tag{3.36}$$

Substituting (3.34) into (3.35) yields

$$\rho_1(u_2 - u_1)(u_1 - s) = \sigma_2 - \sigma_1. \tag{3.37}$$

From (3.34), one has

$$u_1 - s = \frac{(u_1 - u_2)\rho_2}{\rho_2 - \rho_1}, \tag{3.38}$$

then substituting it into (3.37) yields

$$-t(u_2 - u_1)^2 = \sigma_2 - \sigma_1, \tag{3.39}$$

where $t = \frac{\rho_1\rho_2}{\rho_2 - \rho_1}$.

By using the same methods for (3.39), (3.36) can be written as

$$t(u_1 - u_2)(E_2 - E_1) = \sigma_2 u_2 - \sigma_1 u_1. \tag{3.40}$$

Because of $E = e + \frac{1}{2}u^2$, we can get

$$e_2 - e_1 = -\frac{\sigma_1 + \sigma_2}{2t}. \tag{3.41}$$

Using the EOS of Mie-Grüneisen (2.4), can get

$$e = c_0 p - c_1 f(\rho/\rho_0), \tag{3.42}$$

where $c_0 = \frac{1}{\rho_0 \Gamma_0}$ and $c_1 = \frac{a_0^2}{\Gamma_0}$. Put the above equation into (3.41), we can formulate the pressure p_2 in terms of ρ_2.

$$p_2 = \frac{2t(c_1 f(\rho_2/\rho_0) + e_1) - (\sigma_1 + s_{xx2})}{2tc_0 - 1}. \tag{3.43}$$

Thanks to (3.66), s_{xx2} can be written as

$$s_{xx2} = s_{xx1} - \frac{4}{3}\mu \ln(\frac{\rho_2}{\rho_1}). \tag{3.44}$$

Then, the Cauchy stress can be written as

$$\sigma_2 = -p_2 + s_{xx2}. \tag{3.45}$$

We can use (3.39) to solve the velocity after the shock

$$u_2 = \begin{cases} u_1 - \sqrt{\dfrac{\sigma_1 - \sigma_2}{t}} & \text{Left-going,} \\ u_1 + \sqrt{\dfrac{\sigma_1 - \sigma_2}{t}} & \text{Right-going.} \end{cases} \tag{3.46}$$

And the shock speed is given as

$$s = \frac{\rho_2 u_2 - \rho_1 u_1}{\rho_2 - \rho_1}. \tag{3.47}$$

3.2. Plastic state

When the material is yielding,

$$|s_{xx}| = \frac{2}{3} Y_0, \tag{3.48}$$

the equations of Riemann problem can be simplified as

$$\begin{cases} \partial_t \rho + \partial_x(\rho u) = 0, \\ \partial_t(\rho u) + \partial_x(\rho u^2 + p - s_{xx}) = 0, \\ \partial_t(\rho E) + \partial_x\left[(\rho E + p - s_{xx})u\right] = 0, \\ |s_{xx}| = \dfrac{2}{3} Y_0, \\ U(x, t=0) = \begin{cases} U_L, \text{ if } x < 0, \\ U_R, \text{ if } x > 0, \end{cases} \end{cases} \tag{3.49}$$

where $\mathbf{U} = (\rho, \rho u, \rho E)$.

3.2.1. Jacobian matrix in plastic regions

Motion equations of (3.49) can be written as

$$\partial_t \mathbf{U} + \mathbf{J}_p(\mathbf{U})\partial_x \mathbf{U} = 0,$$

where the Jacobian matrix is

$$\mathbf{J}_p(\mathbf{U}) = \begin{bmatrix} 0 & 1 & 0 \\ -u^2 + \frac{\partial p}{\partial \rho} + \Gamma(\frac{u^2}{2} - e) & u(2-\Gamma) & \Gamma \\ (\Gamma(\frac{u^2}{2} - e) - e - \frac{u^2}{2} + \frac{\sigma}{\rho} + \frac{\partial p}{\partial \rho})u + \frac{u^2}{2} & -\Gamma u^2 - \frac{\sigma}{\rho} + e & (1+\Gamma)u \end{bmatrix}.$$

Eigenvalues of $\mathbf{J}_p(\mathbf{Q})$ are given as

$$\lambda_1 = u, \quad \lambda_2 = u - c_p, \quad \lambda_3 = u + c_p,$$

where c_p shows the sonic speed in the plastic state,

$$c_p = \sqrt{a^2 - \frac{\rho_0}{\rho^2}\Gamma_0 s_{xx}}. \tag{3.50}$$

The corresponding right eigenvectors are

$$r_1 = \begin{bmatrix} -\frac{\Gamma}{b_1} \\ -\frac{\Gamma u}{b_1} \\ 1 \end{bmatrix}, \quad r_2 = \frac{1}{h - uc_p}\begin{bmatrix} 1 \\ u - c_p \\ h - uc_p \end{bmatrix}, \quad r_3 = \frac{1}{h + uc_p}\begin{bmatrix} 1 \\ u + c_p \\ h + uc_p \end{bmatrix}. \tag{3.51}$$

Comparing Eq.(3.3) with Eq.(3.50), we notice that the sonic speed is not continuous between the elastic state and plastic state. As the shear modulus μ is always positive, the elastic wave runs always faster than the plastic wave.

3.2.2. Relations across the contact wave

According to the eigenvectors in Eq.(3.51), for the λ_1-wave ($\lambda_1 = u$), we have

$$\frac{d\rho}{\frac{-\Gamma}{b_1}} = \frac{d(\rho u)}{\frac{-u\Gamma}{b_1}} = \frac{d(\rho E)}{1}. \tag{3.52}$$

From the above equations, we can easily deduce that

$$du = 0, \quad dp = 0,$$

which means that

$$u_L^* = u_R^*, \quad p_L^* = p_R^*.$$

Because $s^*_{xxL} = s^*_{xxR}$, thanks to (2.3), one can get

$$\sigma^*_L = \sigma^*_R.$$

For convenience, we define

$$s^* = u^*_L = u^*_R.$$

3.2.3. Relations across rarefaction waves

Left-going rarefaction wave

Across the left wave associated with λ_2-wave, ($\lambda_2 = u - c_p$), we have

$$\frac{d\rho}{1} = \frac{d(\rho u)}{u - c_p} = \frac{d(\rho E)}{h - uc_p}. \tag{3.53}$$

Similar to Section 3.1.3, we can get the relations

$$pe^{\frac{\lambda}{\rho}} - \int f_2(\rho) e^{\frac{\lambda}{\rho}} d\rho = \text{constant}. \tag{3.54}$$

and

$$u + \int \frac{c_p}{\rho} d\rho = \text{constant}. \tag{3.55}$$

Right-going rarefaction wave

Across the right wave associated with λ_3-wave, ($\lambda_3 = u + c_p$), we have

$$\frac{d\rho}{1} = \frac{d(\rho u)}{u + c_p} = \frac{d(\rho E)}{h + uc_p}. \tag{3.56}$$

Similarly, we can get

$$pe^{\frac{\lambda}{\rho}} - \int f_2(\rho) e^{\frac{\lambda}{\rho}} d\rho = \text{constant}. \tag{3.57}$$

$$u - \int \frac{c_p}{\rho} d\rho = \text{constant}. \tag{3.58}$$

3.2.4. Relations across a shock wave

By using the same deducing process as Section 3.1.4, we can get the state after the shock wave:

$$s_{xx2} = s_{xx1}, \tag{3.59}$$

$$p_2 = \frac{2t(c_1 f(\rho_2/\rho_0) + e_1) - (\sigma_1 + s_{xx2})}{2tc_0 - 1}, \tag{3.60}$$

where $c_0 = \frac{1}{\rho_0 \Gamma_0}$, $c_1 = \frac{a_0^2}{\Gamma_0}$, $\sigma_2 = -p_2 + s_{xx2}$,

$$u_2 = \begin{cases} u_1 - \sqrt{\dfrac{\sigma_1 - \sigma_2}{t}} & \text{Left-going,} \\ u_1 + \sqrt{\dfrac{\sigma_1 - \sigma_2}{t}} & \text{Right-going.} \end{cases} \tag{3.61}$$

And the shock speed is given as

$$s = \frac{\rho_2 u_2 - \rho_1 u_1}{\rho_2 - \rho_1}. \tag{3.62}$$

3.3. A relation between ρ and s_{xx}

Thanks to (2.6), the equations of the density and the deviatoric stress in Eq.(3.1) can be written as

$$\frac{\partial u}{\partial x} = -\frac{1}{\rho}\frac{d\rho}{dt}, \tag{3.63}$$

and

$$\frac{ds_{xx}}{dt} = \frac{4}{3}\mu\frac{\partial u}{\partial x}. \tag{3.64}$$

Substituting (3.63) into (3.64) yields

$$\frac{ds_{xx}}{dt} = -\frac{4}{3}\mu\frac{1}{\rho}\frac{d\rho}{dt}. \tag{3.65}$$

Integrate the above equation from the data in front of a wave to the data behind the wave and perform some simple algebraic manipulations, one can get

$$s_{xx} + \frac{4}{3}\mu\ln(\rho) = \text{constant}. \tag{3.66}$$

Analyzing (3.66), one can find, $\frac{\partial s_{xx}}{\partial \rho} < 0$. So, if the material is compressed and ρ increases, s_{xx} will decrease; if the material is expanded and ρ decreases, s_{xx} will increase. According to the compressed or expanded process of the material, even if the initial material is in the plastic state, the material can be into a different state. With considering of the von Mises yielding condition, all cases are shown as follows:

1. If $s_{xx} = \frac{2}{3}Y^0$, initial material reaches the elastic limit. If the material is compressed so that $\rho_{plastic} > \rho^* > \rho$, one can get $|s_{xx}^*| < \frac{2}{3}Y^0$, the compressed material jumps from the plastic state to the elastic state. Here ρ and s_{xx} mean the initial density and deviatoric stress, respectively, $\rho_{plastic} = \rho e^{\left(-\frac{Y_0}{2\mu} + \frac{3s_{xx}}{4\mu}\right)}$, $()^*$ denotes the variable () of the compressed or expanded material.

2. If $s_{xx} = \frac{2}{3}Y^0$ and the material is compressed greatly so that $\rho_{plastic} < \rho^*$, $s_{xx}^* \leq -\frac{2}{3}Y^0$, the compressed material will jump from the positive plastic state to the negative plastic state. Here the positive or negative plastic state means $s_{xx} = \frac{2}{3}Y^0$ or $s_{xx} = -\frac{2}{3}Y^0$, respectively.

3. If $s_{xx} = \frac{2}{3}Y^0$ and the material is expanded, $s_{xx}^* > \frac{2}{3}Y^0$, the material is still in the positive plastic state.

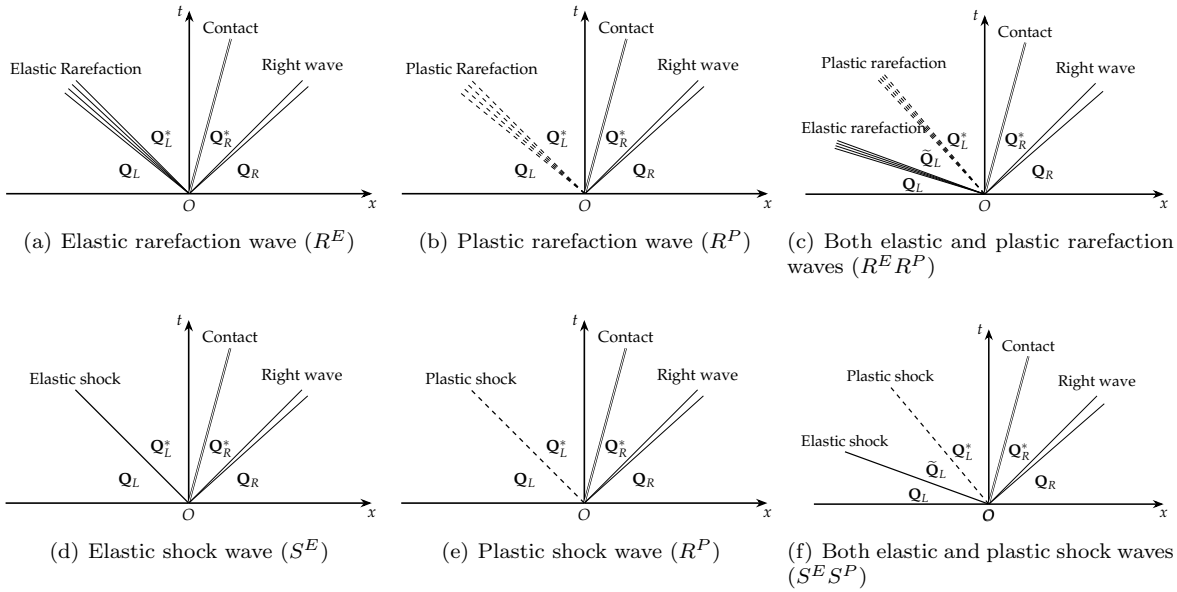

(a) Elastic rarefaction wave (R^E)

(b) Plastic rarefaction wave (R^P)

(c) Both elastic and plastic rarefaction waves ($R^E R^P$)

(d) Elastic shock wave (S^E)

(e) Plastic shock wave (R^P)

(f) Both elastic and plastic shock waves ($S^E S^P$)

Figure 1: The possible cases of Riemann solution structures in the left side.

4. If $s_{xx} = -\frac{2}{3}Y^0$ and the material is expanded so that $\rho_{plastic} < \rho^* < \rho$, one can get $|s^*_{xx}| < \frac{2}{3}Y^0$, the expanded material jumps from the plastic state to the elastic state.

5. If $s_{xx} = -\frac{2}{3}Y^0$ and the material is expanded greatly so that $\rho_{plastic} > \rho^*$, $s^*_{xx} \geq \frac{2}{3}Y^0$, the expanded material will jump from the negative plastic state to the positive plastic state.

6. If $s_{xx} = -\frac{2}{3}Y^0$ and the material is compressed, $s^*_{xx} < -\frac{2}{3}Y^0$, the material is still in the negative plastic state.

4. Exact Riemann solver

Now we consider the constructing details of the exact Riemann solver. For the Riemann problem in Section 3, there are 6×6 possible cases in the Riemann solution with different wave structures. The left six cases are shown in Fig.1. Here we remark that *we do not consider vacuum in building our exact Riemann solver*, for the reason that vacuum hardly ever appears in the elastic-plastic deformation of solid materials that we have studied.

4.1. The solving process

From Section 3, we can find that all variables can be formulated in terms of the density. So we define functions f_u and f_σ:

$$\begin{cases} f_u(\rho_L^*, \rho_R^*, \mathbf{Q}_L, \mathbf{Q}_R) = u_L^*(\rho_L^*, \mathbf{Q}_L) - u_R^*(\rho_R^*, \mathbf{Q}_R), \\ f_\sigma(\rho_L^*, \rho_R^*, \mathbf{Q}_L, \mathbf{Q}_R) = \sigma_L^*(\rho_L^*, \mathbf{Q}_L) - \sigma_R^*(\rho_R^*, \mathbf{Q}_R). \end{cases} \tag{4.1}$$

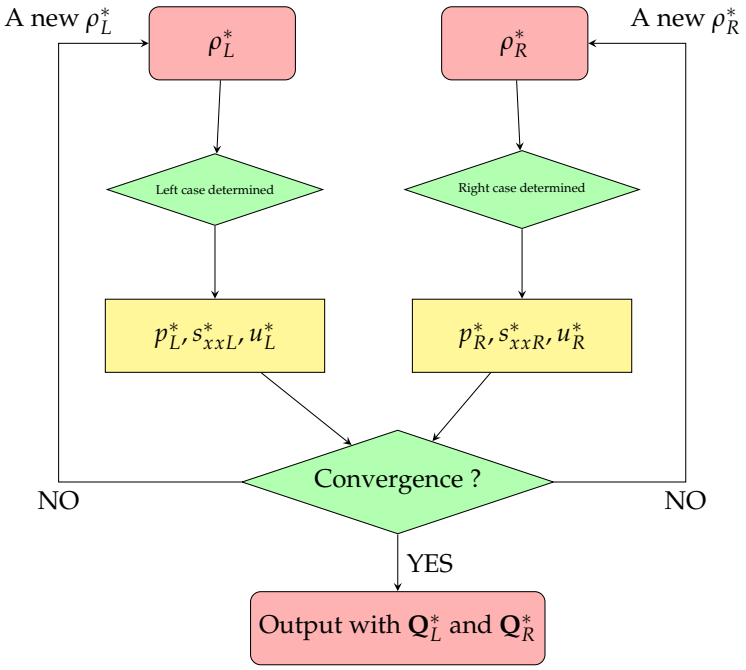

Figure 2: A flow chat of the Newton iteration process.

By using the relations across the contact wave in Section 3.1.2 and Section 3.2.2, we can get

$$\begin{cases} f_u(\rho_L^*, \rho_R^*, \mathbf{Q}_L, \mathbf{Q}_R) = u_L^*(\rho_L^*, \mathbf{Q}_L) - u_R^*(\rho_R^*, \mathbf{Q}_R) = 0, \\ f_\sigma(\rho_L^*, \rho_R^*, \mathbf{Q}_L, \mathbf{Q}_R) = \sigma_L^*(\rho_L^*, \mathbf{Q}_L) - \sigma_R^*(\rho_R^*, \mathbf{Q}_R) = 0. \end{cases} \tag{4.2}$$

Obviously, this system is uniquely solvable, but we can not get the analytical solution of (4.2). We have to use an iteration procedure to solve (4.2) and the solving process is shown in Fig.2. The details are introduced in the following.

Initial:

The initial densities are given as

$$\rho_{L(1)}^* = \frac{\rho_L + \rho_R}{2} \quad \rho_{R(1)}^* = \frac{\rho_L + \rho_R}{2}. \tag{4.3}$$

Iterations begin:

Step 1 Determining the case of the wave structure:

Given $\rho_{L(k)}^*$ and $\rho_{R(k)}^*$ in the k-th iteration step, we can use the method introduced in Section 4.2 to determine the case of wave structure of this Riemann problem. In the procedure for solving the Riemann problem, the subscript (k) means the variable in the k-th iteration step.

Step 2 Evaluating $f_{u(k)}$ and $f_{\sigma(k)}$:

After determining the structures case, we need to solve Cauchy stresses and velocities in regions $\mathbf{Q}_L^*$

and $\mathbf{Q}_R^*$ and the details are given in Section 4.4.

Step 3 Evaluating the derivatives of $f_{u(k)}$ and $f_{\sigma(k)}$.

The derivatives of $f_{u(k)}$ and $f_{\sigma(k)}$ are given as

$$\frac{\partial f_{u(k)}}{\partial \rho^*_{L(R)}} = \frac{f_{u(k)} - f_{u(k-1)}}{\rho^*_{L(R)(k)} - \rho_{L(R)(k-1)}}, \quad \frac{\partial f_{\sigma(k)}}{\partial \rho^*_{L(R)}} = \frac{f_{\sigma(k)} - f_{\sigma(k-1)}}{\rho^*_{L(R)(k)} - \rho_{L(R)(k-1)}}. \tag{4.4}$$

At the first step, we use a simple numerical difference method to evaluate

$$\frac{\partial f_{u(1)}}{\partial \rho^*_{L(R)}} = \frac{f_u(\rho^*_{L(R)(1)} + \Delta\rho) - f_u(\rho^*_{L(R)(1)})}{\Delta\rho_{L(R)(1)}}, \quad \frac{\partial f_{u(1)}}{\partial \rho^*_{L(R)}} = \frac{f_u(\rho^*_{L(R)(1)} + \Delta\rho) - f_u(\rho^*_{L(R)(1)})}{\Delta\rho_{L(R)(1)}}, \tag{4.5}$$

where $\Delta\rho$ is a small quantity, here we define it as

$$\Delta\rho = \frac{\rho^*_{L(R)(1)}}{100}. \tag{4.6}$$

Step 4 Evaluating $\rho^*_{L(k+1)}$ and $\rho^*_{R(k+1)}$:

$$\begin{bmatrix} \rho^*_{L(k+1)} \\ \rho^*_{R(k+1)} \end{bmatrix} = \begin{bmatrix} \rho^*_{L(k)} \\ \rho^*_{R(k)} \end{bmatrix} - \begin{bmatrix} \frac{\partial f_{u(k)}}{\partial \rho^*_L} & \frac{\partial f_{u(k)}}{\partial \rho^*_R} \\ \frac{\partial f_{\sigma(k)}}{\partial \rho^*_L} & \frac{\partial f_{\sigma(k)}}{\partial \rho^*_R} \end{bmatrix}^{-1} \begin{bmatrix} f_{u(k)} \\ f_{\sigma(k)} \end{bmatrix} \tag{4.7}$$

Step 5 Convergence test:

The iteration is convergent if

$$\mathrm{CHA} \le \mathrm{TOL}, \tag{4.8}$$

where

$$\mathrm{CHA} = \max\left[\frac{|\rho^*_{L(k+1)} - \rho^*_{L,(k)}|}{\frac{1}{2}|\rho^*_{L(k+1)} + \rho^*_{L(k)}|}, \frac{|\rho^*_{R(k+1)} - \rho^*_{R,(k)}|}{\frac{1}{2}|\rho^*_{R(k+1)} + \rho^*_{R(k)}|}, |f_u|, |f_\sigma| \right], \tag{4.9}$$

$$\mathrm{TOL} = 10^{-4}.$$

If not, go to Step 1 and continue the iteration procedure until convergent. Numerical examples show, after 2-4 iterations, the condition (4.8) is satisfied.

Iterations end

4.2. Determining the case of structures

Given the value of density $\rho^*_{L(R)}$, we can distinguish the non-linear wave is a shock or rarefaction wave. This is done easily by comparing $\rho^*_{L(R)}$ with $\rho_{L(R)}$, the subscript $_{L(R)}$ means in the left(right) side of the contact wave.

$$\begin{cases} \text{a rarefaction wave:} & \text{if } \rho_{L(R)} > \rho^*_{L(R)}, \\ \text{a shock wave:} & \text{if } \rho_{L(R)} < \rho^*_{L(R)}. \end{cases} \tag{4.10}$$

Table 4.1: The condition of cases classification.

$\hat{\rho^*} < \rho$	$\hat{s}_{xx} < \frac{2}{3}Y_0$	$s_{xx} = \frac{2}{3}Y_0$ and $\hat{s}_{xx} \geq \frac{2}{3}Y_0$	other
	Case a: R^E	Case b: R^P	Case c: $R^E R^P$
$\hat{\rho^*} > \rho$	$\hat{s}_{xx} > -\frac{2}{3}Y_0$	$s_{xx} = -\frac{2}{3}Y_0$ and $\hat{s}_{xx} \leq -\frac{2}{3}Y_0$	other
	Case d: S^E	Case e: S^P	Case f: $S^E S^P$

Thanks to (3.66), the deviatoric stress can be evaluated as

$$\hat{s}_{xxL(R)} = -\frac{4}{3}\mu \ln\left(\frac{\rho^*_{L(R)}}{\rho_{L(R)}}\right) + s_{xxL(R)}. \tag{4.11}$$

According to the values of initial and evaluated deviatoric stresses in (4.11) in one side of the contact wave, the non-linear wave in this side may be:

$$\begin{cases} \text{an elastic rarefaction} & \text{if } \hat{s}_{xxL(R)} < \frac{2}{3}Y^0, \\ \text{a plastic rarefaction} & \text{if } s_{xxL(R)} = \frac{2}{3}Y^0 \text{ and } \hat{s}_{xxL(R)} \geq \frac{2}{3}Y_0, \\ \text{an elastic rarefaction and a following plastic rarefaction} & \text{if } s_{xxL(R)} < \frac{2}{3}Y_0 \text{ and } \hat{s}_{xxL(R)} \geq \frac{2}{3}Y_0, \\ \text{an elastic shock} & \text{if } \hat{s}_{xxL(R)} > -\frac{2}{3}Y_0, \\ \text{a plastic shock} & \text{if } s_{xxL(R)} = -\frac{2}{3}Y_0 \text{ and } \hat{s}_{xxL(R)} \leq -\frac{2}{3}Y_0, \\ \text{an elastic shock and a following plastic shock} & \text{if } s_{xxL(R)} > -\frac{2}{3}Y_0 \text{ and } \hat{s}_{xxL(R)} \leq -\frac{2}{3}Y_0. \end{cases} \tag{4.12}$$

Combining (4.10) and (4.12), we can find, in any side of the wave structures of this Riemann problem, there are six cases showed in Table 4.1, where capital letters "S" and "R" mean the shock and rarefaction wave, respectively; superscript letters "E" and "P" indicate the elastic and plastic state of a wave, respectively. Otherwise, the subscript L or R are omitted for simplification.

4.3. Evaluating states in middle regions ($\tilde{\mathbf{Q}}_L$ and $\tilde{\mathbf{Q}}_R$)

Cases (R^E, R^P, S^E and S^P)

For cases (R^E, R^P, S^E and S^P) in Fig.1, the material is totally yielding or totally not yielding, there is no midlle state $\tilde{\mathbf{Q}}_{L(R)}$. For expression convenience, we let

$$(\tilde{\rho}_{L(R)}, \tilde{u}_{L(R)}, \tilde{p}_{L(R)}, \tilde{s}_{xx}) = (\rho_{L(R)}, u_{L(R)}, p_{L(R)}, s_{xxL(R)}), \tag{4.13}$$

Case ($R^E R^P$)

Using the methods introduced in the Section (3.1.3), we can easily deduce the formulation of all unknown variables after the rarefaction wave. Here we do not show the details of the deduction.

For the case ($R^E R^P$), after the elastic rarefaction wave, the deviatoric stress achieves the elastic limit. Thanks to (4.10) and (4.12), one can easily deduce that

$$\tilde{s}_{xxL(R)} = \frac{2}{3}Y_0.$$

By using (3.66), the density in $\tilde{\mathbf{Q}}_{L(R)}$ is given as

$$\tilde{\rho}_{L(R)} = \rho_{L(R)}\exp\left(-\frac{Y_0}{2\mu} + \frac{3s_{xxL(R)}}{4\mu}\right).$$

From (3.26) and (3.32), for the case ($R^E R^P$), the pressure is rearranged as

$$\tilde{p}_{L(R)} = p_{L(R)}e^{\frac{\lambda}{\rho_{L(R)}} - \frac{\lambda}{\tilde{\rho}_{L(R)}}} + e^{-\frac{\lambda}{\tilde{\rho}_{L(R)}}}\int_{\rho_{L(R)}}^{\tilde{\rho}_{L(R)}} f_2(x)e^{\frac{\lambda}{x}}dx, \tag{4.14}$$

where

$$\lambda = \rho_0\Gamma_0 \quad f_2(\rho) = a_0^2\frac{\partial f}{\partial \eta} - \lambda\frac{s_{xx}(\rho)}{\rho^2},\ s_{xx}(\rho) = -\frac{4}{3}\mu\ln\left(\frac{\rho}{\rho_{L(R)}}\right) + s_{xxL(R)}.$$

Thanks to (3.27) and (3.33), for the rarefaction wave case ($R^E R^P$), the velocity is given as

$$\tilde{u}_{L(R)} = \begin{cases} u_L - \displaystyle\int_{\rho_L}^{\tilde{\rho}_{L(R)}} \frac{c_e(x)}{x}dx & \text{for the left-going rarefaction wave,} \\ u_R + \displaystyle\int_{\rho_R}^{\tilde{\rho}_{L(R)}} \frac{c_e(x)}{x}dx & \text{for the right-going rarefaction wave,} \end{cases} \tag{4.15}$$

where the sonic speed is given as

$$c_e(\rho) = \sqrt{a_0^2\frac{\partial f}{\partial \eta} + \frac{p(\rho)}{\rho^2}\rho_0\Gamma_0 - \frac{\rho_0}{\rho^2}\Gamma_0 s_{xx}(\rho) + \frac{4}{3}\frac{\mu}{\rho}}.$$

Remark 1: In (4.14) and (4.15), there are two integral terms. Obviously, because of the complexity of the EOS, we can not get the exact integral values. We have to use the numerical methods to approximate the two integral terms with high order accuracy. The approximation methods are introduced in the Appendix A.

Case ***($S^E S^P$)***

Using the methods introduced in the Section (3.1.4), we can easily deduce the formulation of all unknown variables in $\tilde{\mathbf{Q}}_{L(R)}$. In order to shorten the length of our paper, we do not show the details of the deduction.

For the case ($S^E S^P$), after the elastic shock wave, the deviatoric stress achieves the elastic limit. So, by using (4.10) and (4.12), one can easily deduce that

$$\tilde{s}_{xxL(R)} = -\frac{2}{3}Y_0.$$

From (3.66), after the elastic shock wave, the density in $\tilde{\mathbf{Q}}_{L(R)}$ is given as

$$\tilde{\rho}_{L(R)} = \rho_{L(R)} \exp\left(\frac{Y_0}{2\mu} + \frac{3s_{xxL(R)}}{4\mu}\right).$$

By using (3.43), the pressure can be solved as

$$\tilde{p}_{L(R)} = \frac{2t(c_1 f(\tilde{\rho}_{L(R)}/\rho_0) + e_{L(R)}) - (\sigma_{L(R)} + \tilde{s}_{xxL(R)})}{2tc_0 - 1}, \tag{4.16}$$

where $c_0 = \frac{1}{\rho_0 \Gamma_0}$, $c_1 = \frac{a_0^2}{\Gamma_0}$ and $t = \frac{\rho_{L(R)}\tilde{\rho}_{L(R)}}{\tilde{\rho}_{L(R)} - \rho_{L(R)}}$.

Thanks to (3.46), the velocity can be written as

$$\begin{cases} \tilde{u}_L = u_L - \sqrt{\frac{\sigma_L - \tilde{\sigma}_L}{t}}, \\ \tilde{u}_R = u_R + \sqrt{\frac{\sigma_R - \tilde{\sigma}_R}{t}}, \end{cases} \tag{4.17}$$

where

$$\tilde{\sigma}_{L(R)} = -\tilde{p}_{L(R)} + \tilde{s}_{xxL(R)}. \tag{4.18}$$

4.4. Evaluating states in regions $\mathbf{Q}_L^*$ and $\mathbf{Q}_R^*$

Rarefaction wave cases (R^E, R^P and $R^E R^P$)

For the three rarefaction wave cases, thanks to (3.66) and (3.48), s_{xx} in $\mathbf{Q}_L^*$ and $\mathbf{Q}_R^*$ are

$$s^*_{xxL(R)} = \begin{cases} -\frac{4}{3}\mu \ln\left(\frac{\rho^*_{L(R)}}{\tilde{\rho}_{L(R)}}\right) + s_{xxL(R)} & \text{for case } (R^E), \\ \frac{2}{3}Y_0 & \text{for cases } (R^P \text{ and } R^E R^P). \end{cases}$$

From (4.14), the pressure in the star region is

$$p^*_{L(R)} = \tilde{p}_{L(R)} e^{\frac{\lambda}{\rho_{L(R)}} - \frac{\lambda}{\rho}} + e^{-\frac{\lambda}{\rho^*_{L(R)}}} \int_{\tilde{\rho}_{L(R)}}^{\rho^*_{L(R)}} f_2(x) e^{\frac{\lambda}{x}} dx, \tag{4.19}$$

where

$$\lambda = \rho_0 \Gamma_0 \quad f_2(\rho) = a_0^2 \frac{\partial f}{\partial \eta} - \lambda \frac{s_{xx}(\rho)}{\rho^2}, \ s_{xx}(\rho) = -\frac{4}{3}\mu \ln\left(\frac{\rho}{\rho_{L(R)}}\right) + s_{xxL(R)}.$$

By Equations (3.27) and (3.33) the velocity in regions $\mathbf{Q}_L^*$ and $\mathbf{Q}_R^*$ can be written as

$$u^*_{L(R)} = \begin{cases} \tilde{u}_L - \int_{\rho_L}^{\rho^*_{L(R)}} \frac{c(x)}{x} dx, \\ \tilde{u}_R + \int_{\rho_R}^{\rho^*_{L(R)}} \frac{c(x)}{x} dx, \end{cases} \tag{4.20}$$

where

$$c(\rho)=\begin{cases}\sqrt{a_0^2\dfrac{\partial f}{\partial \eta}+\dfrac{p(\rho)}{\rho^2}\rho_0\Gamma_0-\dfrac{\rho_0}{\rho^2}\Gamma_0 s_{xx}(\rho)+\dfrac{4}{3}\dfrac{\mu}{\rho}} & \text{for case } (R^E),\\ \sqrt{a_0^2\dfrac{\partial f}{\partial \eta}+\dfrac{p(\rho)}{\rho^2}\rho_0\Gamma_0-\dfrac{\rho_0}{\rho^2}\Gamma_0 s_{xx}(\rho)} & \text{for cases } (R^P \text{ and } R^E R^P).\end{cases}$$

Remark 2: Just like **Remark 1**, we have to use numerical integral methods introduced in the Appendix A to evaluate the integral terms in (4.19) and (4.20).

Shock wave cases (S^E, S^P and $S^E S^P$)

For shock wave cases, the deviatoric stresses in $\mathbf{Q}_L^*$ and $\mathbf{Q}_R^*$ are given as

$$s_{xx}(\rho)=\begin{cases}-\dfrac{4}{3}\mu\ln\left(\dfrac{\rho}{\tilde{\rho}_{L(R)}}\right)+\tilde{s}_{xxL(R)}, & \text{for case } (S^E),\\ -\dfrac{2}{3}Y_0, & \text{for cases (} S^P \text{ and } S^E S^P).\end{cases}$$

(3.43) gives direct expression for the the pressure in the star region as

$$p^*_{L(R)}=\frac{2t\left(c_1 f(\rho^*_{L(R)}/\rho_0)+\tilde{e}_{L(R)}\right)-\left(\tilde{\sigma}_{L(R)}+s_{xx}(\rho^*_{L(R)})\right)}{2tc_0-1},$$

where $c_0=\frac{1}{\rho_0\Gamma_0}$, $c_1=\frac{a_0^2}{\Gamma_0}$ and $t=\frac{\rho^*_{L(R)}\tilde{\rho}_{L(R)}}{\rho^*_{L(R)}-\tilde{\rho}_{L(R)}}$.

Thanks to (3.46), the velocities in $\mathbf{Q}_L^*$ and $\mathbf{Q}_R^*$ are

$$u^*_{L(R)}=\begin{cases}\tilde{u}_L-\sqrt{\dfrac{\tilde{\sigma}_L-\sigma^*_{L(R)}}{t}} & \text{for the left-going shock wave,}\\ \tilde{u}_R+\sqrt{\dfrac{\tilde{\sigma}_R-\sigma^*_{L(R)}}{t}} & \text{for the right-going shock wave,}\end{cases}$$

where $\sigma^*_{L(R)}=-p^*_{L(R)}+s^*_{xxL(R)}$.

5. Half Riemann problem and its solver

Sometimes we need to analyse a half Riemann problem with a given velocity or Cauchy stress. Shown in Fig.3, in these cases, we only need to solve states in one side. There are six possible cases which are introduced in Section 3. Here we will use the example shown in Fig.3 to show how to solve the half Riemann problem.

As we know the velocity u^* or the Cauchy stress σ^* on one side, for example , the left side, there is only one equation need to be solved:

$$f(\rho^*,\mathbf{Q}_R)=u(\rho^*,\mathbf{Q}_R)-u^*=0, \tag{5.1}$$

or

$$f(\rho^*,\mathbf{Q}_R)=\sigma(\rho^*,\mathbf{Q}_R)-\sigma^*=0. \tag{5.2}$$

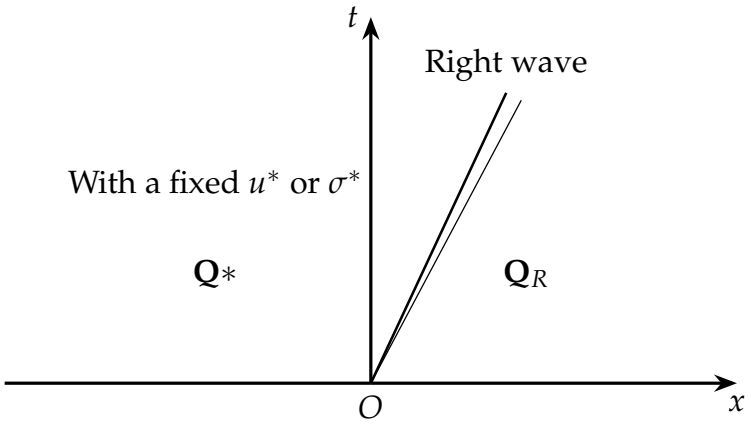

Figure 3: Half Riemann problem with a given left velocity or Cauchy stress.

Similar to the process in Section (4.1), we have to use an iteration procedure to solve (5.1) or (5.2) and the solving process is list in the following.

Initial:

The initial density is given as

$$\rho^*_{(1)} = \rho_R. \tag{5.3}$$

Iterations begin:

Step 1 Determine the case of the wave structures:

Given the value of $\rho^*_{(k)}$ in the k-th iteration step, use the methods introduced in Section 4.2 to determine the case of wave structure of this Riemann problem. Here the subscript (k) means the variable in the k-th iteration step.

Step 2 Elevate $f(\rho^*, \mathbf{Q}_R)$:

After determining the structure case, evaluate the velocity (or the Cauchy stress) in the region $\mathbf{Q}^*$ and the details are given in Section 4.4.

Step 3 Evaluate the derivative of $f(\rho^*, \mathbf{Q}_R)$:

The derivative of f is given by

$$\frac{\partial f_{(k)}}{\partial \rho^*} = \frac{f_{(k)} - f_{(k-1)}}{\rho^*_{(k)} - \rho^*_{(k-1)}}, \text{ for } k > 1$$

At the first step,

$$\frac{\partial f_{(1)}}{\partial \rho^*} = \frac{f(\rho^* + \Delta\rho) - f(\rho^*)}{\Delta\rho},$$

where $\Delta\rho$ is a small quantity, here we set $\Delta\rho = \frac{\rho^*_{(1)}}{100}$.

Step 4 Evaluate $\rho^*_{(k+1)}$:

A new density can be updated by

$$\rho^*_{(k+1)} = \rho^*_{(k)} - f/\frac{\partial f_{(k)}}{\partial \rho}.$$

Step 5 Convergence test:

The iteration is convergent if

$$\text{CHA} \leq \text{TOL}, \tag{5.4}$$

where

$$\text{CHA} = \max\left[\frac{|\rho^*_{(k+1)} - \rho^*_{(k)}|}{\frac{1}{2}|\rho^*_{(k+1)} + \rho^*_{(k)}|}, |f|\right], \quad \text{TOL} = 10^{-4}.$$

If not, go to Step 1 and continue the iteration procedure until convergent. Numerical examples show, after 2-4 iterations, the condition (5.4) is satisfied.

Iterations end.

6. Numerical tests

In this section, we will solve different elastic-plastic Riemann problems with several different wave structures in the Riemann solutions. In order to verify the correctness of our exact Riemann solver, we use a third-order numerical scheme for 1D elastic-plastic flows to evaluate these Riemann problems and compare numerical results with our exact solution. Before considering elastic-plastic Riemann problems, a two-phase impact benchmark problem [43, 1, 44] is firstly taken in to test the correctness of the numerical method [25].

6.1. Two-phase impact benchmark problem

At the beginning of this problem, there is a right-moving copper with the speed $u_1 = 1500$m/s interacting with a solid explosive at the rest on the right of the plate under the uniform atmospheric condition which has pressure $p_0 = 10^5$Pa and temperature $T_0 = 300$K throughout the domain. Cochran-Chan equation of state which is in the form of Mie-Grüneisen form [1] is used but derivative stress is not considered in this problem. The Cochran-Chan EOS is

$$p(\rho, e) = p_{\text{ref}}(\rho) + \Gamma(\rho)[e - e_{\text{ref}}(\rho)].$$

where

$$\begin{aligned}
&\Gamma = \Gamma_0 \\
&p_{\text{ref}}(\rho) = \beta_1 \left(\frac{\rho_0}{\rho}\right)^{-\varepsilon_1} - \beta_2 \left(\frac{\rho_0}{\rho}\right)^{\varepsilon_2}, \\
&e_{\text{ref}}(\rho) = -\frac{\beta_1}{\rho_0(1-\varepsilon_1)}\left[\left(\frac{\rho_0}{\rho}\right)^{1-\varepsilon_1} - 1\right] + \frac{\beta_1}{\rho_0(1-\varepsilon_2)}\left[\left(\frac{\rho_0}{\rho}\right)^{1-\varepsilon_2} - 1\right] - C_\nu T_0
\end{aligned}$$

For the copper and solid explosive, the parameters are given as

$$\begin{cases} (\rho_0, \beta_1, \beta_2, \varepsilon_1, \varepsilon_2, \Gamma_0, C_\nu)_{\text{Copper}} = (8900\text{kg/m}^3, 145.67\text{GPa}, 147.75\text{GPa}, 2.99, 1.99, 2, 393\text{J/kg}\cdot\text{K}) \\ (\rho_0, \beta_1, \beta_2, \varepsilon_1, \varepsilon_2, \Gamma_0, C_\nu)_{\text{Explosive}} = (1840\text{kg/m}^3, 12.87\text{GPa}, 13.42\text{GPa}, 4.1, 3.1, 0.93, 1087\text{J/kg}\cdot\text{K}) \end{cases}$$

In this problem, the yielding strength is set to zero and the 3rd-order cell-centered Lagrangian scheme [25] is used. We solve this problem with 200 grids and CFL number is set as 0.5. The final time is $t = 85\mu$s. Results of density and velocity shown in Fig.4 are compared the exact solution and numerical solution in [16]. This comparison verifies the correctness of our numerical scheme.

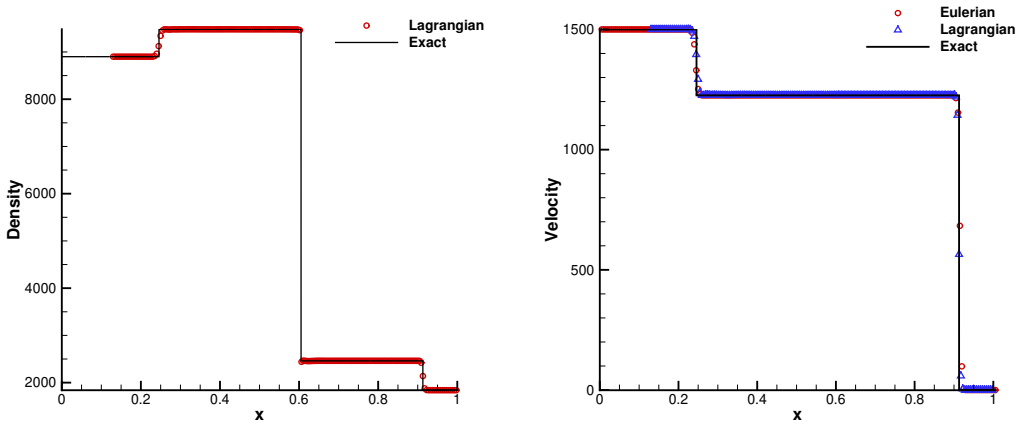

Figure 4: Numerical results for the two-phase impact benchmark [43, 1, 44].(The "Eulerian" and the "Exact" results are extracted from [44] and the "Lagrangian" result are computed by the method in [25])

6.2. Elastic-plastic Riemann problems

By choosing different initial conditions, different Riemann problems are tested in following with several different wave structures in the solutions. Two materials, copper and aluminum are considered with the parameters $(\rho_0, a_0, \Gamma_0, s, \mu)_{\text{Copper}} = (8930\text{kg/m}^3, 3940\text{m/s}, 2, 1.49, 2.76, 2.76\times10^{10}\text{Pa})$ and $(\rho_0, a_0, \Gamma_0, s, \mu)_{\text{Al}} = (2785\text{kg/m}^3, 5328\text{m/s}, 2, 1.338, 4.5\times10^{10}\text{Pa})$, respectively. The yielding strengths of the two materials are $Y_{0,\text{Al}} = 3\times10^8$Pa and $Y_{0,\text{Copper}} = 9\times10^7$Pa, respectively. The computational domain is setted as $[0, 1m]$ with 800 cell points and the initial interface is located at $0.5m$, the terminal time is $t = 5\times10^{-5}s$. Otherwise, in the initial condition, "L" and "R" mean $x < 0.5m$ and $x > 0.5m$, respectively.

Test 1

In this case, the material is yielding at both sides, so there are three waves with two plastic shock waves and one contact. The initial condition is

$$\begin{cases} \text{L: Al}, \quad \rho = 2785\text{kg/m}^3, \quad u = 20\text{m/s}, \quad p = 1.0\text{Pa}, \quad s_{xx} = -2.0\times10^8\text{Pa}, \\ \text{R: Al}, \quad \rho = 2785\text{kg/m}^3, \quad u = 0\text{m/s}, \quad p = 1.0\text{Pa}, \quad s_{xx} = -2.0\times10^8\text{Pa}, \end{cases} \tag{6.1}$$

It can be seen that the exact solution matches the numerical results very well in Fig.5.

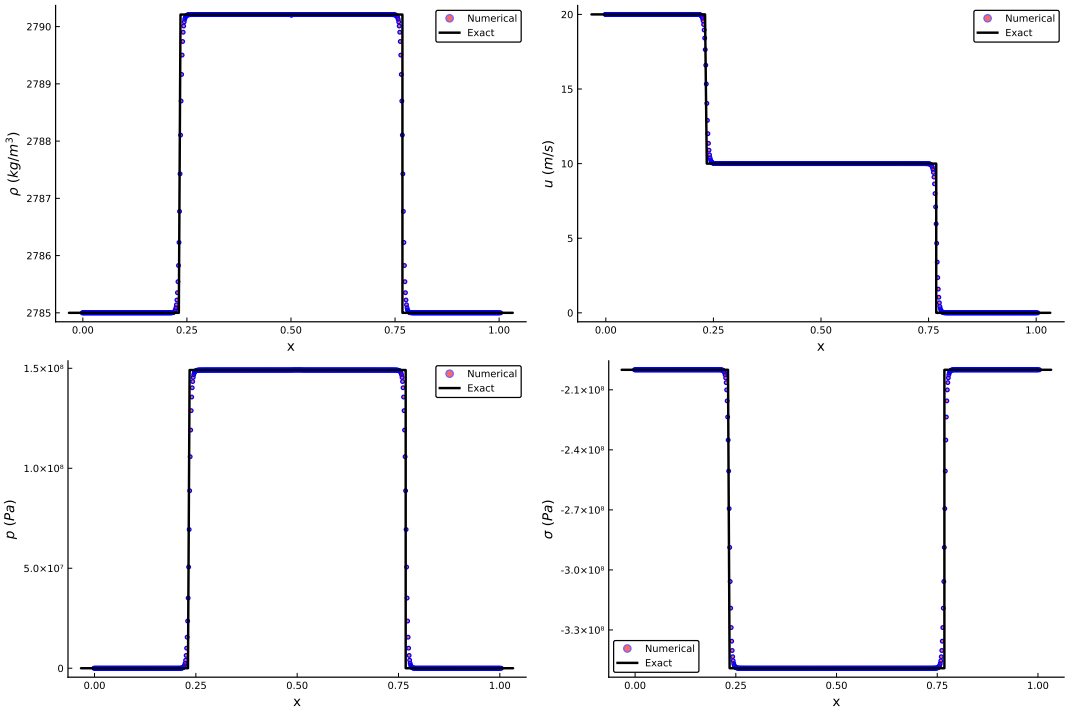

Figure 5: Comparison for Test 1 with the structure of $S^P|S^P$.

Test 2

Here we consider a case with yielding process at both sides, so there are five waves in the wave structure of this Riemann problem. The initial condition is

$$\begin{cases} \text{L: Al}, \quad \rho = 2785\text{kg/m}^3, \quad u = 800\text{m/s}, \quad p = 1.0\text{Pa}, \quad s_{xx} = 0.0\text{Pa}, \\ \text{R: Al}, \quad \rho = 2785\text{kg/m}^3, \quad u = 0\text{m/s}, \quad p = 1.0\text{Pa}, \quad s_{xx} = 0.0\text{Pa}, \end{cases} \tag{6.2}$$

Shown in Fig.6, the exact solution matches the numerical results well generally, except the under-cooling effect performed in the numerical results, but it is not considered in the designing of the exact Riemann solver.

Test 3

In this example, we test the case with two elastic rarefaction waves. In the wave structure there is one elastic rarefaction wave on each side of the contact wave. The initial condition is given as

$$\begin{cases} \text{L: Al}, \quad \rho = 2785\text{kg/m}^3, \quad u = -2.0\text{m/s}, \quad p = 1.0^7\text{Pa}, \quad s_{xx} = 0.0\text{Pa}, \\ \text{R: Al}, \quad \rho = 2785\text{kg/m}^3, \quad u = 2.0\text{m/s}, \quad p = 1.0 \times 10^7\text{Pa}, \quad s_{xx} = 0.0\text{Pa}, \end{cases} \tag{6.3}$$

We can see that the results of the exact solution match the numerical results very well.

Test 4

In this test we test the example with both elastic and plastic rarefaction waves on both sides of contact

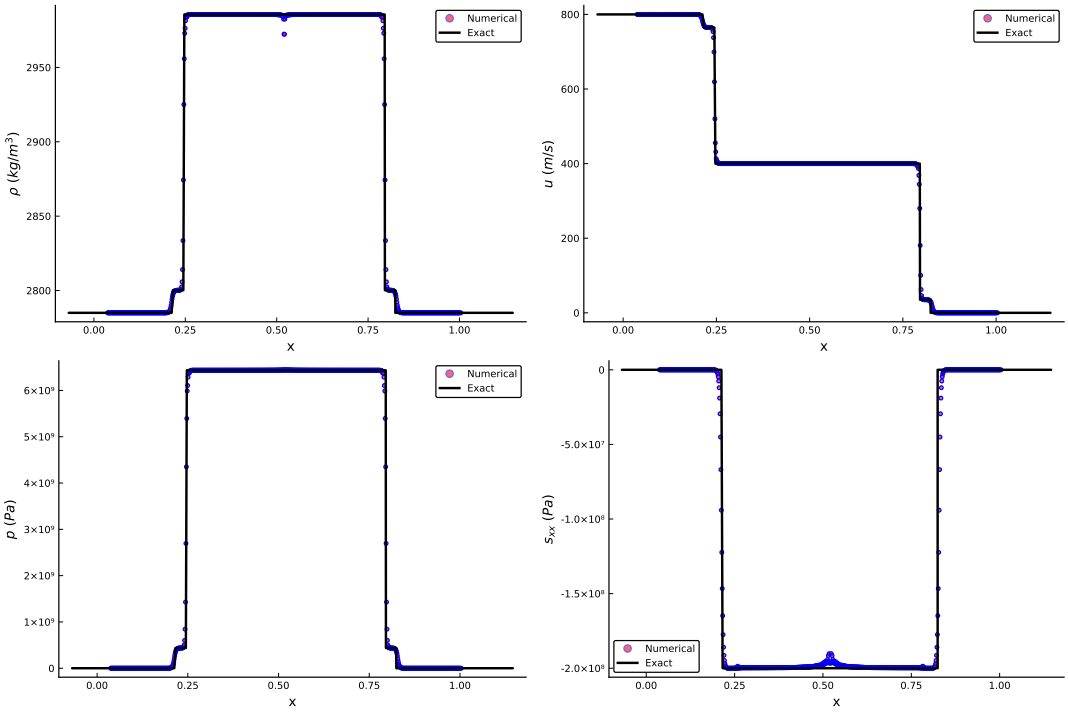

Figure 6: Comparison for Test 2 with the structure of $S^E S^P | S^P S^E$.

wave. The initial condition is

$$\begin{cases} \text{L: Al}, \quad \rho = 2785\text{kg/m}^3, \quad u = -40\text{m/s}, \quad p = 1.0 \times 10^7\text{Pa}, \quad s_{xx} = 0.0\text{Pa}, \\ \text{R: Al}, \quad \rho = 2785\text{kg/m}^3, \quad u = 40\text{m/s}, \quad p = 1.0 \times 10^7\text{Pa}, \quad s_{xx} = 0.0\text{Pa}. \end{cases} \tag{6.4}$$

Results are shown in Fig.8, the results of the exact solver match the numerical results very well.

Test 5

The initial condition of this Riemann problem is

$$\begin{cases} \text{L: Al}, \quad \rho = 2785\text{kg/m}^3, \quad u = -200\text{m/s}, \quad p = 1.0\text{Pa}, \quad s_{xx} = -2.0^8\text{Pa}, \\ \text{R: Al}, \quad \rho = 2785\text{kg/m}^3, \quad u = 0\text{m/s}, \quad p = 1.0\text{Pa}, \quad s_{xx} = -2.0^8\text{Pa}. \end{cases} \tag{6.5}$$

Obviously, at the beginning, the material is in the negative plastic state (i.e. $s_{xxL(R)} = -\frac{2}{3}Y^0$). According to the analysis introduced in Section 3.3, after an expanding process the material will turn back into an elastic state and will yield again into a positive plastic state. Our exact solution in Fig.9 are consistent with the analysis in Section 3.3. Of course, our exact solution matches the numerical solutions very well.

In this case, we also compared the results given with different orders of the Gaussian quadrature method in Fig.10, from which we can see that there is nearly no difference between the results, so the Riemann solver is not sensitive to the accuracy of the Gaussian quadrature method.

Test 6

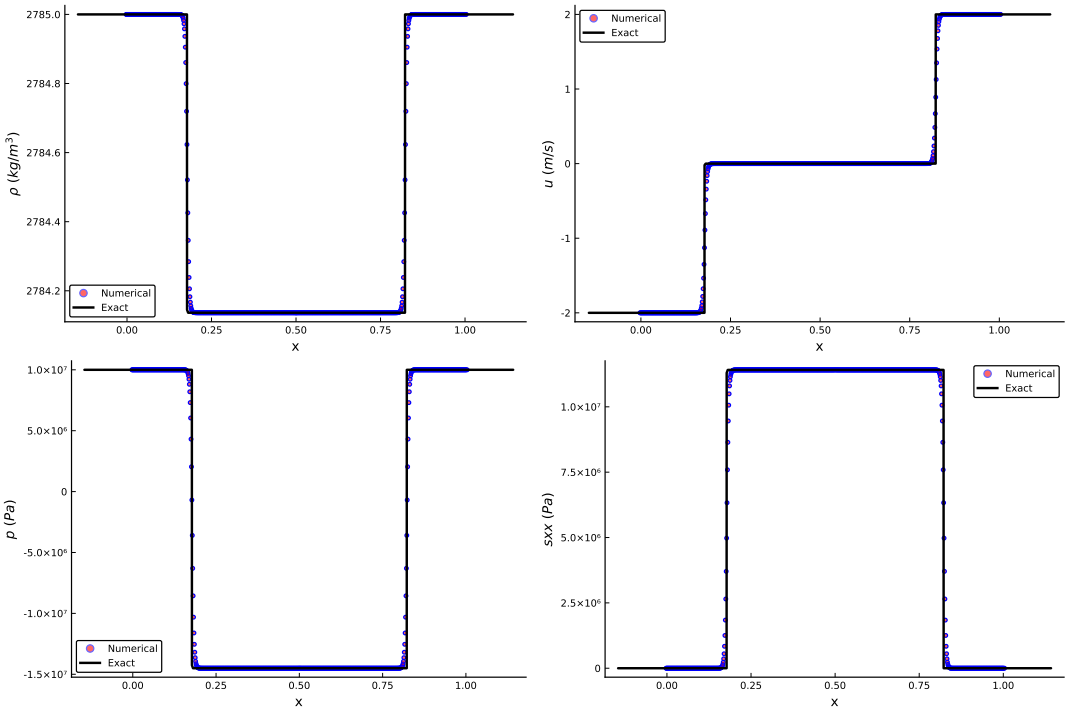

Figure 7: Comparison results for Test 3 with the wave structures of $R^E|R^E$.

The initial condition of this Riemann problem is

$$\begin{cases} \text{L: Al}, \quad \rho = 2785\text{kg/m}^3, \quad u = 200\text{m/s}, \quad p = 1.0\text{Pa}, \quad s_{xx} = 2.0^8\text{Pa}, \\ \text{R: Al}, \quad \rho = 2785\text{kg/m}^3, \quad u = 0\text{m/s}, \quad p = 1.0\text{Pa}, \quad s_{xx} = 2.0^8\text{Pa}. \end{cases} \tag{6.6}$$

Different from Test 5, at the beginning, the material is in the positive plastic state (i.e. $s_{xxL(R)} = \frac{2}{3}Y^0$). According to the analysis introduced in Section 3.3, after an compressing process the material will turn back into an elastic state and will yield again into a negative plastic state. We can get the exact solutions which match the numerical solutions very well in Fig.11.

Test 7

All the above five tests have symmetrical wave structures. Here we will test an example with different structures on two sides: one plastic shock on the left side and both the elastic shock and plastic shock on the right side of one contact wave. The initial condition is given as

$$\begin{cases} \text{L: Al}, \quad \rho = 2785\text{kg/m}^3, \quad u = 40\text{m/s}, \quad p = 1.0 \times 10^8\text{Pa}, \quad s_{xx} = -2.0 \times 10^8\text{Pa}, \\ \text{R: Al}, \quad \rho = 2785\text{kg/m}^3, \quad u = -40\text{m/s}, \quad p = 1.0 \times 10^2\text{Pa}, \quad s_{xx} = 0.0\text{Pa}. \end{cases} \tag{6.7}$$

The solutions of this test are shown in Fig.12. From this figure, we can find the exact solutions match numerical solutions very well.

Test 8

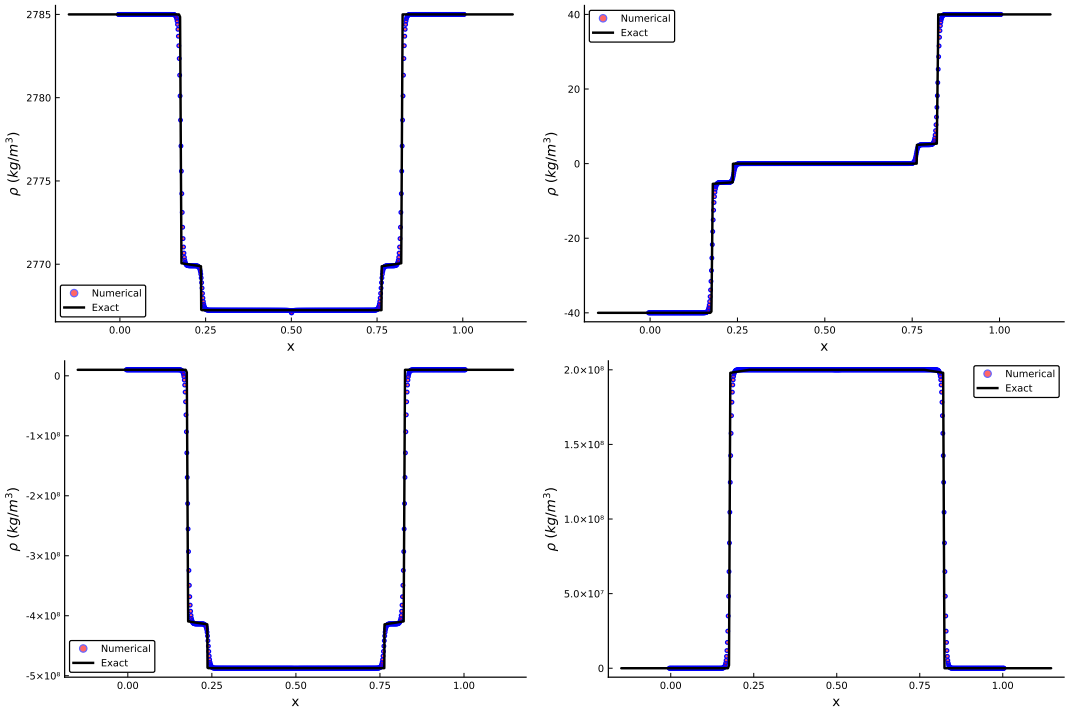

Figure 8: Comparison for Test 4 with the wave structure of $R^E R^P | R^P R^E$.

In this test, we consider an example with zero initial velocities on both sides, driving by the gradient of the pressure, there are rarefaction waves produced into the higher pressure side and shock waves generated into the lower pressure side. The initial condition is given as

$$\begin{cases} \text{L: Al}, \quad \rho = 2785\text{kg/m}^3, \quad u = 0.0\text{m/s}, \quad p = 1.0 \times 10^{10}\text{Pa}, \quad s_{xx} = 0.0\text{Pa}, \\ \text{R: Al}, \quad \rho = 2785\text{kg/m}^3, \quad u = 0.0\text{m/s}, \quad p = 1.0 \times 10^{2}\text{Pa}, \quad s_{xx} = 0.0\text{Pa}. \end{cases} \tag{6.8}$$

Shown in Fig.16, we can see there are two shocks in the right side and two rarefaction waves on the left side.

Test 9

Now we will consider two multi-material tests with different materials on both sides. In this test, on the left side, the lighter material of aluminum impacts the heavier material of Copper. The initial condition is given as

$$\begin{cases} \text{L: Al}, \quad \rho = 2785\text{kg/m}^3, \quad u = 40\text{m/s}, \quad p = 0.1\text{Pa}, \quad s_{xx} = 0.0\text{Pa}, \\ \text{R: Copper}, \quad \rho = 8930\text{kg/m}^3, \quad u = 0.0\text{m/s}, \quad p = 0.1\text{Pa}, \quad s_{xx} = 0.0\text{Pa}. \end{cases} \tag{6.9}$$

Shown in the Fig.14, there is a large jump of density at the material interface and both the elastic shock and the plastic shock exist in each side of the interface. Comparing with the numerical results of the scheme with MHLLCEP approximate solver, we can find that our exact Riemann solver can solve the Riemann problem with multi-materials very well.

Test 10

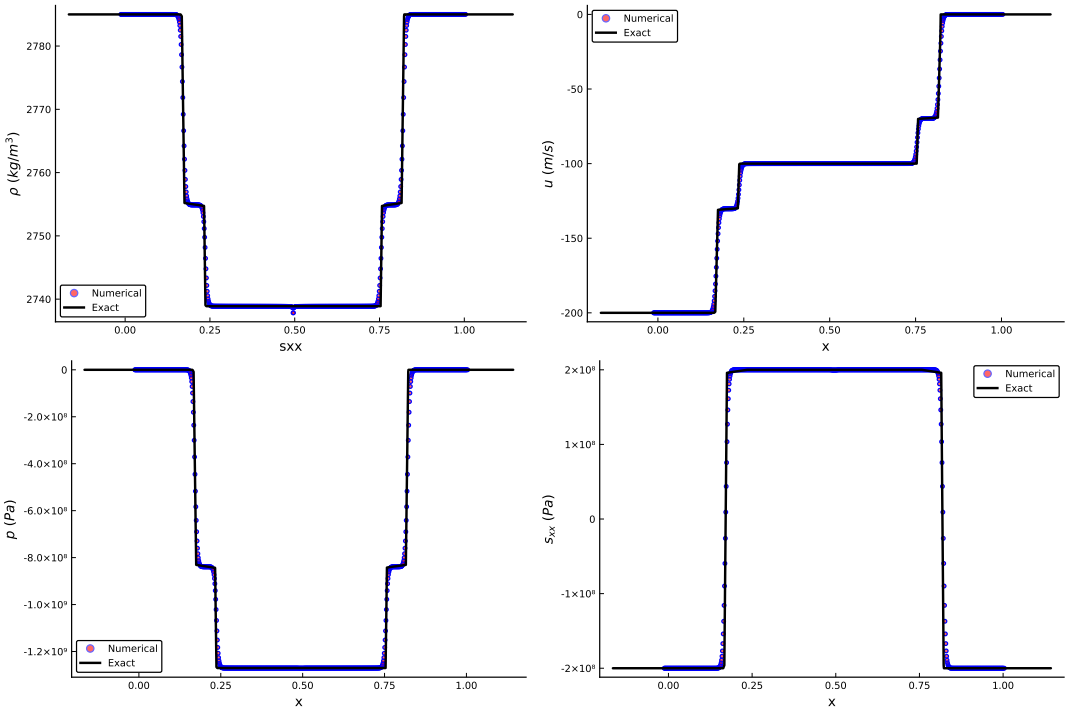

Figure 9: Comparison results for Test 5 with the structure of $R^E R^P | R^P R^E$.

Here we test another multi-materials case. In this test the initial condition is given as

$$\begin{cases} \text{L: Copper}, \quad \rho = 8930\text{kg/m}^3, \quad u = 0.0\text{m/s}, \quad p = 1.0 \times 10^{10}\text{Pa}, \quad s_{xx} = 0.0\text{Pa}, \\ \text{R: Al}, \quad \rho = 2785\text{kg/m}^3, \quad u = 0\text{m/s}, \quad p = 10.0\text{Pa}, \quad s_{xx} = 0.0\text{Pa}. \end{cases} \tag{6.10}$$

Shown in Fig.15, there are two rarefaction waves on the left side and two shocks on the right side. Moreover, we can find that there is the discontinuity of pressure on the interface, and the Cauchy stress is continuous, which satisfies the theoretical analysis.

Test 11

This test is the half Riemann problem with a given velocity $u^* = -20\text{m/s}$ on the left, and the right initial condition is

$$\text{Copper}, \quad \rho = 8930\text{kg/m}^3, \quad u = 0.0\text{m/s}, \quad p = 0.1\text{Pa}, \quad s_{xx} = 0.0\text{Pa}. \tag{6.11}$$

In Fig.16, comparison results are given by the exact half Riemann solver and the numerical method. We can see that the exact solver can resolve both the elastic shock and the plastic shock wave very well.

Test 12

The second half Riemann case is with a given Cauchy stress $\sigma^* = 0\text{Pa}$ on the left, and the right initial condition is

$$\text{Copper}, \quad \rho = 8930\text{kg/m}^3, \quad u = 0.0\text{m/s}, \quad p = 1.0 \times 10^9\text{Pa}, \quad s_{xx} = 0.0\text{Pa}. \tag{6.12}$$

In Fig.17, we give the results computed by the exact Riemann solver and the numerical simulation. From

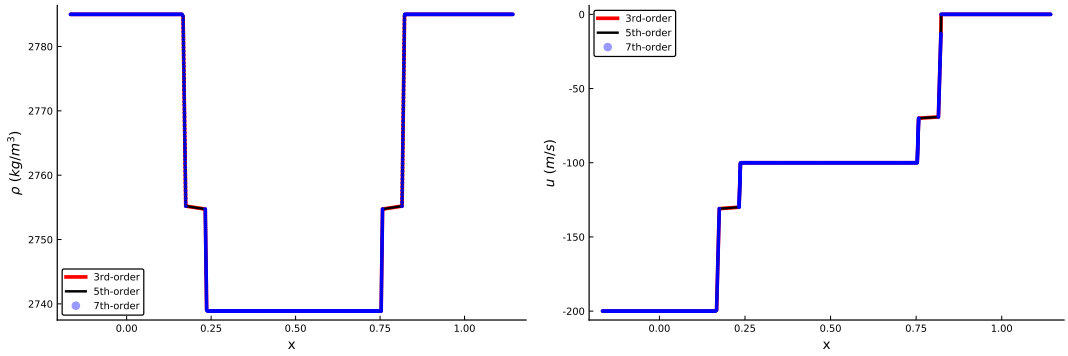

Figure 10: Comparison results for Test 5 with different orders of the Gaussian quadrature method.

this figure one can see, the exact solver can resolve the elastic and plastic rarefaction waves well.

7. Conclusions

In this paper, we have analyzed the Riemann problem in detailed for one-dimensional multi-material elastic-plastic flows with the Mie-Grüneisen EOS, hypo-elastic constitutive model and the von Mises' yielding condition and found

1. The sonic speed periods a significant jump when the material is yielding.
2. the plastic wave is always faster than the elastic wave for the reason of the sonic speed jump.
3. There are only thirty-six possible cases of the wave structure in the Riemann problem.
4. All the variables after the non-linear waves can be written as functions of the density theoretically.
5. If the initial material is in the negative plastic state, after being expanded, the material may be into the elastic state or the positive plastic state and vice versa.

Then, based on the above analysis, we have constructed exact Riemann solvers for both the Riemann problem and the half Riemann problem, separately.

Because of the iteration process, the CPU cost of the exact Riemann solver is of course more expensive than approximate ones. However, the main purpose of the exact Riemann solver is used to study the structures of the Riemann problem itself and give reference results to construct high performance approximate solvers. Tested by a large number of examples, the exact Riemann solver is reasonable and its solutions are matching well with the numerical results for both single material problems and multi-material Riemann problems.

Acknowledgement

We thank Professor Jiequan Li for many useful and insightful discussions. This work has been supported by Science Challenge Project (Grant No. TZ2016002) and NSFC (Grant No. 11672047).

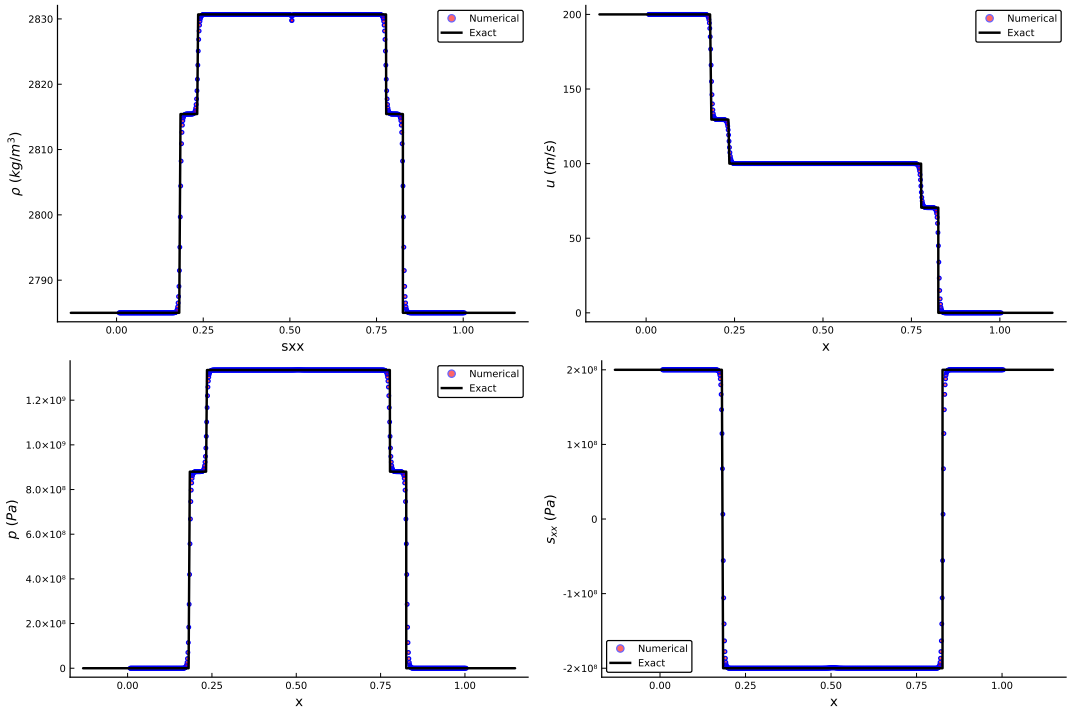

Figure 11: Comparison results for Test 6 with the structure of $S^E S^P | S^P S^E$.

References

[1] K. M. Shyue, A fluid-mixture type algorithm for compressible multicomponent flow with Mie-Grneisen equation of state, Journal of Computational Physics 171 (2) (2001) 678–707.

[2] S. B. Segletes, Thermodynamic stability of the Mie–grüneisen equation of state, and its relevance to hydrocode computations, Journal of applied physics 70 (5) (1991) 2489–2499.

[3] M. L. Wilkins, Calculation of elastic-plastic flow, Tech. rep., California Univ Livermore Radiation Lab (1963).

[4] P.-H. Maire, R. Abgrall, J. Breil, R. LoubèRe, B. Rebourcet, A nominally second-order cell-centered Lagrangian scheme for simulating elastic–plastic flows on two-dimensional unstructured grids, Journal of Computational Physics 235 (2013) 626–665.

[5] S. N. Atluri, On constitutive relations at finite strain: hypo-elasticity and elasto-plasticity with isotropic or kinematic hardening, Computer methods in applied mechanics and engineering 43 (2) (1984) 137–171.

[6] D. Steinberg, C. Lund, A constitutive model for strain rates from 10^{-4} to 10^{6} s^{-1}, Journal of Applied Physics 65 (4) (1989) 1528–1533.

[7] E. J. Lieberman, N. R. Morgan, D. J. Luscher, D. E. Burton, A higher-order Lagrangian discontinuous Galerkin hydrodynamic method for elastic-plastic flows, Computers & Mathematics with Applications 78 (2) (2019) 318–334.

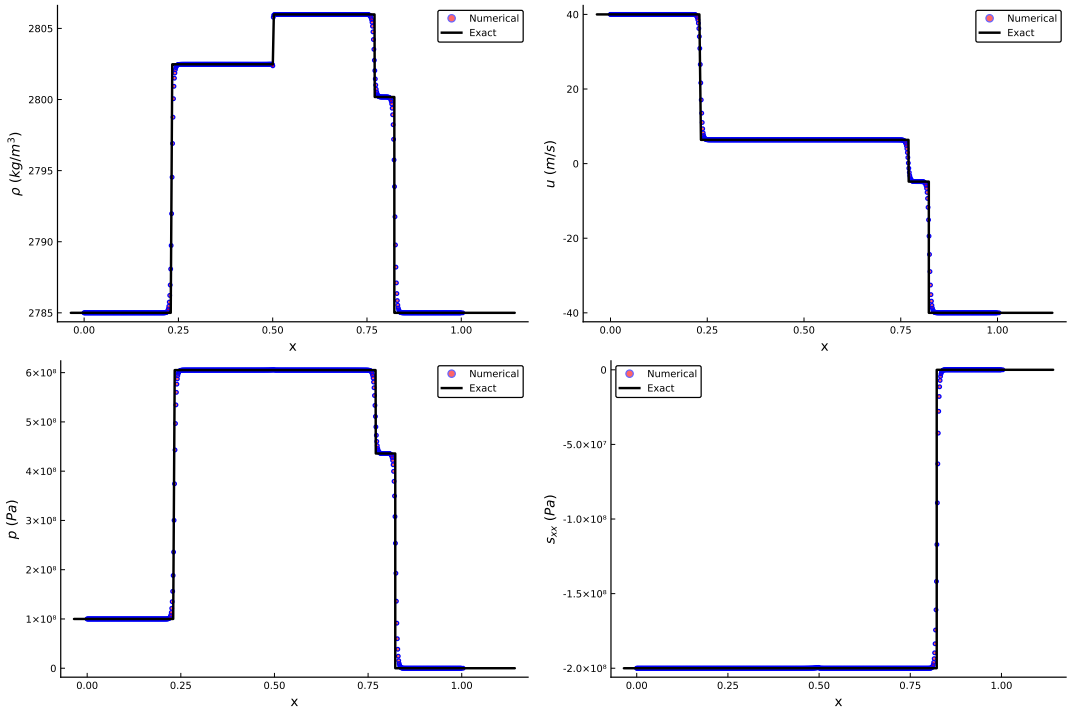

Figure 12: Comparison resutls for Test 7 with the structure of $R^P|R^P R^E$.

[8] J.-B. Cheng, W. Huang, S. Jiang, B. Tian, A third-order moving mesh cell-centered scheme for one-dimensional elastic-plastic flows, Journal of Computational Physics 349 (2017) 137–153.

[9] S. Thomson, Mathematical modelling of elastoplasticity at high stress, Ph.D. thesis, University of Oxford (2017).

[10] S. K. Godunov, A difference method for numerical calculation of discontinuous solutions of the equations of hydrodynamics, Matematicheskii Sbornik 89 (3) (1959) 271–306.

[11] B. Leer, Toward the ultimate ultimate conservative difference scheme. V. A second-order sequel to Godunov's method, Journal of Computational Physics 32 (101).

[12] P. L. Roe, Discrete models for the numerical analysis of time-dependent multidimensional gas dynamics, Journal of Computational Physics 63 (2) (1986) 458–476.

[13] A. Harten, P. D. Lax, B. Van Leer, On upstream differencing and Godunov-type schemes for hyperbolic conservation laws, Siam Review 25 (1) (1983) 53–79.

[14] E. F. Toro, M. Spruce, W. Speares, Restoration of the contact surface in the HLL-Riemann solver, Shock Waves 4 (1) (1994) 25–34.

[15] B. Einfeld, On Godunov-type methods for gas dynamics, SIAM Journal on Numerical Analysis 25 (2) (1988) 294–318.

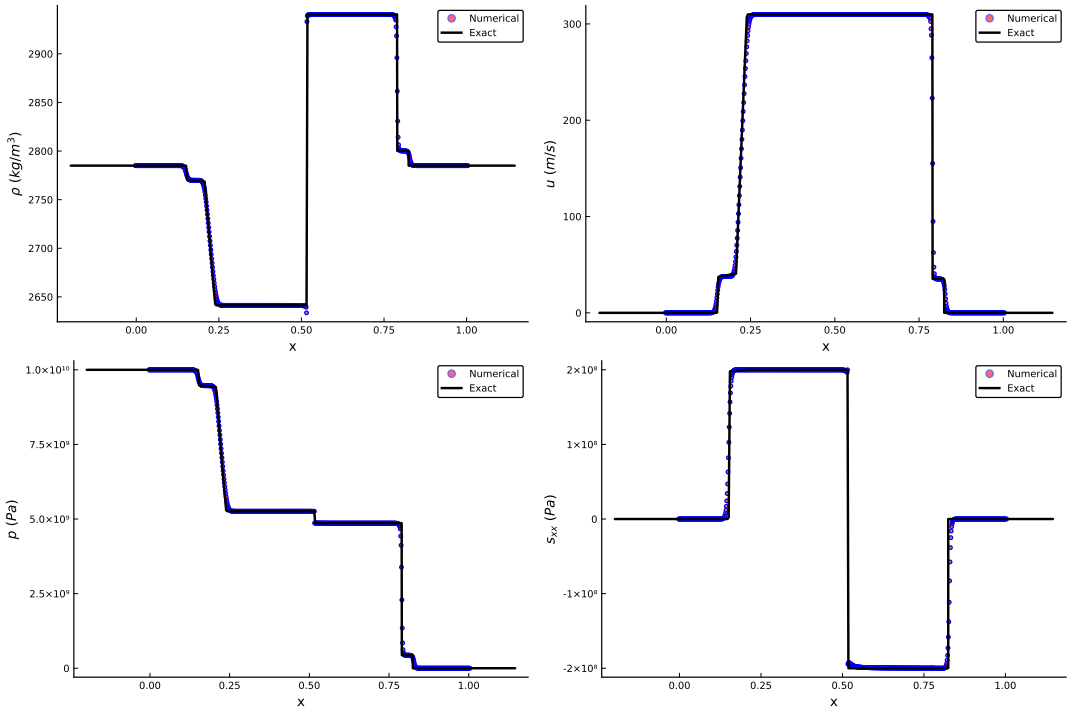

Figure 13: Comparison resutls for Test 8 with the structure of $R^E R^P | S^P S^E$.

[16] X. Deng, P. Boivin, F. Xiao, A new formulation for two-wave Riemann solver accurate at contact interfaces, Physics of Fluids 31 (4) (2019) 046102.

[17] S. Simon, J. C. Mandal, A simple cure for numerical shock instability in the HLLC Riemann solver, Journal of Computational Physics 378 (2019) 477–496.

[18] D. S. Balsara, A two-dimensional HLLC Riemann solver for conservation laws: Application to Euler and magnetohydrodynamic flows, Journal of Computational Physics 231 (22) (2012) 7476–7503.

[19] J. Vides, B. Nkonga, E. Audit, A simple two-dimensional extension of the HLL Riemann solver for hyperbolic systems of conservation laws, Journal of Computational Physics 280 (2015) 643675.

[20] J.-B. Cheng, L. Liu, S. Jiang, M. Yu, Z. Liu, A second-order cell-centered Lagrangian scheme with a HLLC Riemann solver of elastic and plastic waves for two-dimensional elastic-plastic flows, Journal of Computational Physics (2020) 109452.

[21] F. Bouchut, C. Klingenberg, K. Waagan, A multiwave approximate Riemann solver for ideal MHD based on relaxation II: numerical implementation with 3 and 5 waves, Numerische Mathematik 115 (4) (2010) p.647–679.

[22] S. L. Gavrilyuk, N. Favrie, R. Saurel, Modelling wave dynamics of compressible elastic materials, Journal of computational physics 227 (5) (2008) 2941–2969.

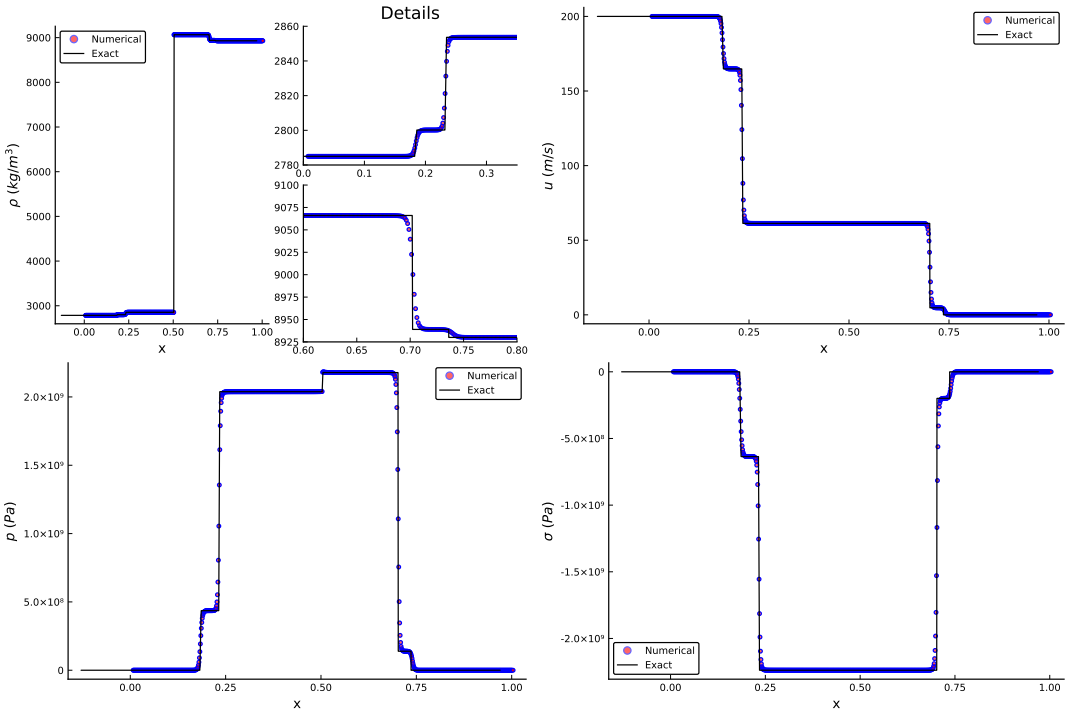

Figure 14: Comparison results for Test 9 with the structure of $R^E R^P | R^P R^E$.

[23] J.-B. Cheng, E. F. Toro, S. Jiang, M. Yu, W. Tang, A high-order cell-centered Lagrangian scheme for one-dimensional elastic–plastic problems, Computers & Fluids 122 (2015) 136–152.

[24] J. Cheng, Harten-Lax-van Leer-contact (HLLC) approximation Riemann solver with elastic waves for one-dimensional elastic-plastic problems, Applied Mathematics and Mechanics 37 (11) (2016) 1517–1538.

[25] L. Liu, J.-B. Cheng, Z. Liu, A multi-material HLLC Riemann solver with both elastic and plastic waves for 1D elastic-plastic flows, Computers & Fluids 192 (2019) 104265.

[26] F. Kerger, P. Archambeau, S. Erpicum, B. J. Dewals, M. Pirotton, An exact Riemann solver and a Godunov scheme for simulating highly transient mixed flows, Journal of Computational and Applied Mathematics 235 (8) (2011) 2030–2040.

[27] V. Deledicque, M. V. Papalexandris, An exact Riemann solver for compressible two-phase flow models containing non-conservative products, Journal of Computational Physics 222 (1) (2007) 217–245.

[28] R. Bernetti, V. A. Titarev, E. F. Toro, Exact solution of the riemann problem for the shallow water equations with discontinuous bottom geometry, Journal of Computational Physics 227 (6) (2008) 3212–3243.

[29] P. T. Barton, D. Drikakis, E. Romenski, V. A. Titarev, Exact and approximate solutions of Riemann problems in non-linear elasticity, Journal of Computational Physics 228 (18) (2009) 7046–7068.

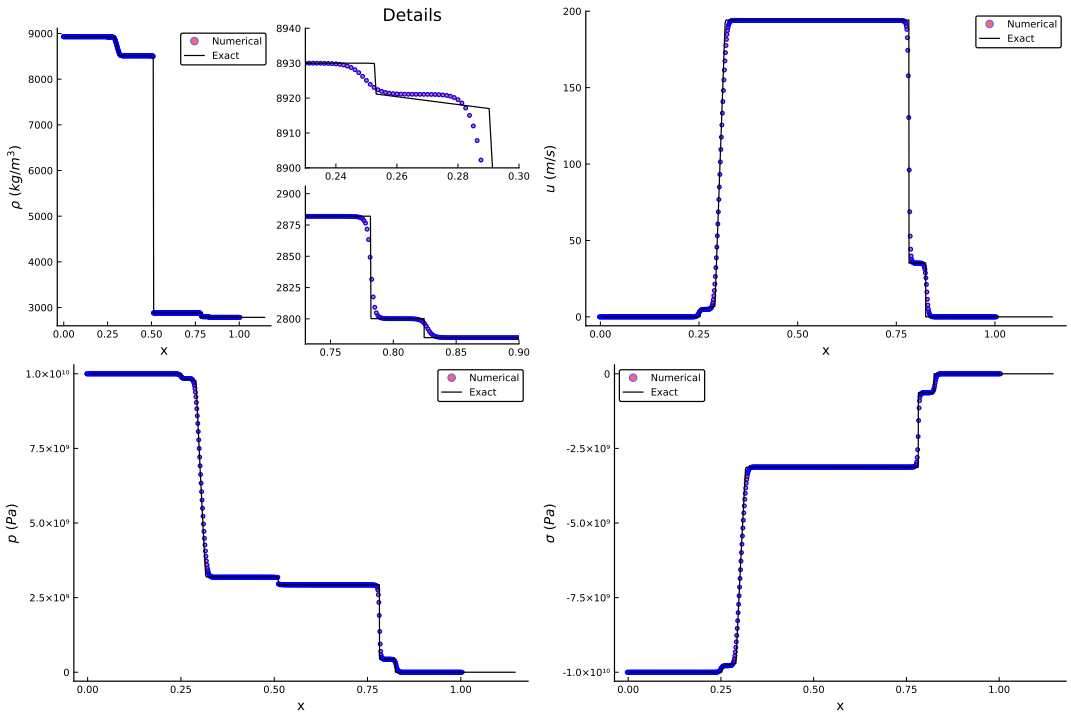

Figure 15: Comparison results for Test 10 with the structure of $R^E R^P | S^E S^P$.

[30] G. H. Miller, An iterative Riemann solver for systems of hyperbolic conservation laws, with application to hyperelastic solid mechanics, Journal of Computational Physics 193 (1) (2004) 198–225.

[31] Q. Zhan, Q. Ren, M. Zhuang, Q. Sun, Q. H. Liu, An exact Riemann solver for wave propagation in arbitrary anisotropic elastic media with fluid coupling, Computer Methods in Applied Mechanics and Engineering 329 (2018) 24–39.

[32] X. Garaizar, Solution of a Riemann problem for elasticity, Journal of elasticity 26 (1) (1991) 43–63.

[33] S. Gao, T. Liu, 1d exact elastic-perfectly plastic solid Riemann solver and its multi-material application, Advances in Applied Mathematics and Mechanics 9 (3) (2017) 621–650.

[34] S. Gao, T. Liu, C. Yao, A complete list of exact solutions for one-dimensional elastic-perfectly plastic solid Riemann problem without vacuum, Communications in Nonlinear Science and Numerical Simulation 63 (2018) 205–227.

[35] M. B. Tyndall, Numerical modelling of shocks in solids with elastic-plastic conditions, Shock Waves 3 (1) (1993) 55–66.

[36] J. Wang, K. Liu, D. Zhang, An improved CE/SE scheme for multi-material elasticplastic flows and its application, Computers and Fluids 38 (3) (2009) 544–551.

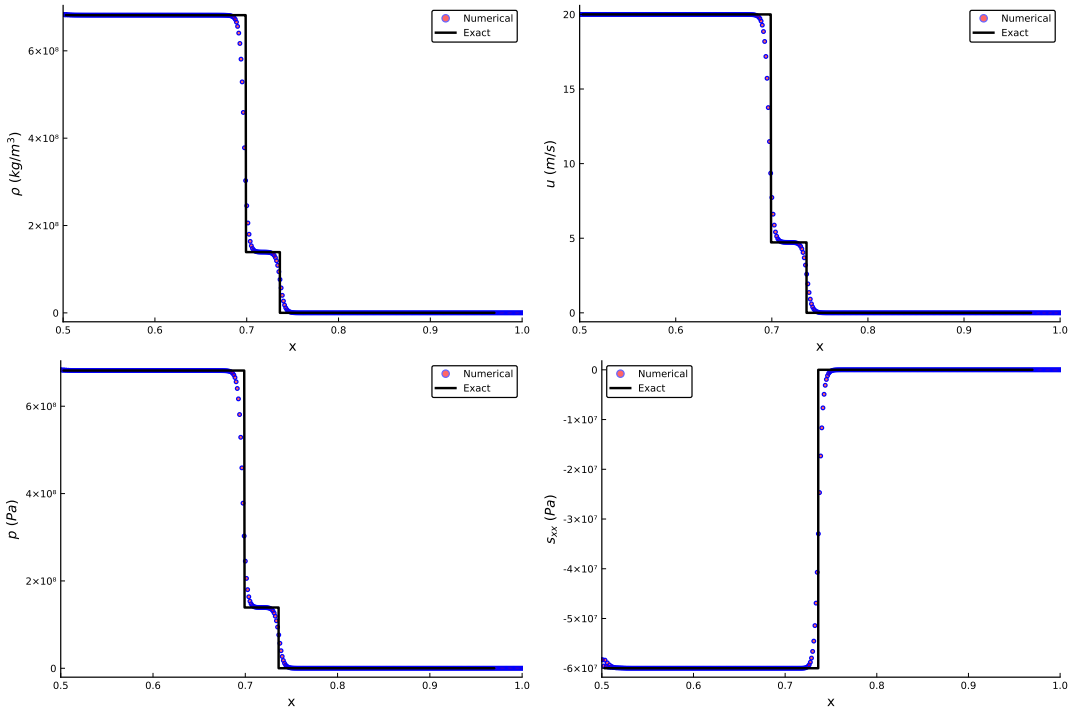

Figure 16: Comparison results for Test 11 with the structure of $S^E S^P$.

[37] A. L. Ortega, M. Lombardini, D. Pullin, D. I. Meiron, Numerical simulation of elastic–plastic solid mechanics using an Eulerian stretch tensor approach and HLLD Riemann solver, Journal of Computational Physics 257 (2014) 414–441.

[38] N. Favrie, S. Gavrilyuk, Dynamics of shock waves in elastic-plastic solids, in: ESAIM: Proceedings, Vol. 33, EDP Sciences, 2011, pp. 50–67.

[39] A. S. Khan, S. Huang, Continuum theory of plasticity, John Wiley & Sons, 1995.

[40] R. Batra, Linear constitutive relations in isotropic finite elasticity, Journal of Elasticity 51 (3) (1998) 243–245.

[41] E. F. Toro, Riemann solvers and numerical methods for fluid dynamics: a practical introduction, Springer Science & Business Media, 2013.

[42] A. G. Kulikovskii, N. V. Pogorelov, A. Y. Semenov, Mathematical aspects of numerical solution of hyperbolic systems, CRC Press, 2000.

[43] R. Saurel, R. Abgrall, A multiphase Godunov method for compressible multifluid and multiphase flows, Journal of Computational Physics 150 (2) (1999) 425–467.

[44] X. Deng, S. Inaba, B. Xie, K.-M. Shyue, F. Xiao, High fidelity discontinuity-resolving reconstruction for compressible multiphase flows with moving interfaces, Journal of Computational Physics 371 (2018) 945–966.

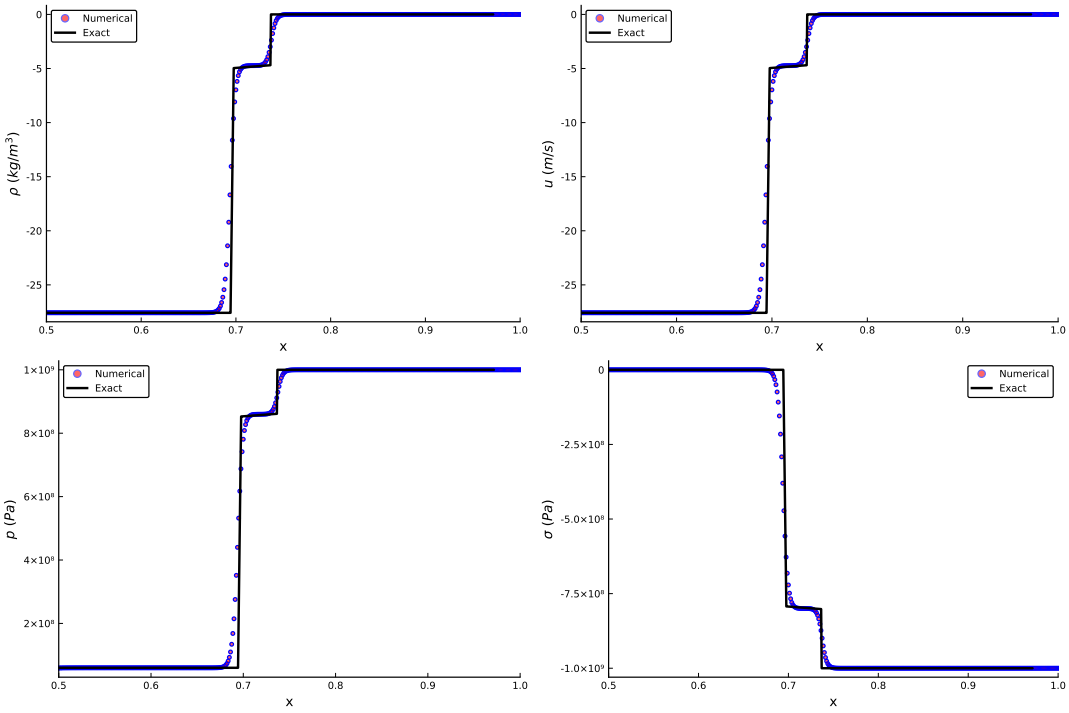

Figure 17: Comparison results for Test 11 with the structure of $R^E R^P$.

A. Numerical integration for the rarefaction wave

There are two integrations in functions $p(\rho)$ and $u(\rho)$ in the rarefaction wave, for example, in the equations (4.14) and (4.15). In this paper, we use a seventh-order (with 4 integrating points) Gaussian quadrature to make numerical integrations. For a function $g(x)$, the Gaussian integration from -1 to 1 is given as

$$\int_{-1}^{1} g(x)dx \approx \sum_{i=1}^{n} \omega_i g(x_i),$$

ω_i is the weight, and x_i is the integrating point, n is the number of the Gaussian quadrature points. Here $n = 4$. For the 7th-order Gaussian quadrature, integrating points and corresponding weights are

$$x_1,\ x_2 = \pm\sqrt{\frac{3}{7} - \frac{2}{7}\sqrt{\frac{6}{5}}} \quad \left(\omega_1,\ \omega_2 = \frac{18+\sqrt{30}}{36}\right),$$

$$x_3,\ x_4 = \pm\sqrt{\frac{3}{7} + \frac{2}{7}\sqrt{\frac{6}{5}}} \quad \left(\omega_3,\ \omega_4 = \frac{18-\sqrt{30}}{36}\right).$$

For the function $g(x)$ over $[\rho_0, \rho]$, this change of interval can be done in the following way:

$$\int_{\rho_0}^{\rho} g(x)dx = \frac{\rho-\rho_0}{2}\int_{-1}^{1} g\left(\frac{\rho-\rho_0}{2}x + \frac{\rho_0+\rho}{2}\right)dx.$$

At last, we can get

$$\int_{\rho_0}^{\rho} g(x)dx \approx \frac{\rho-\rho_0}{2}\sum_{i=1}^{n}\omega_i g\left(\frac{\rho-\rho_0}{2}x_i+\frac{\rho_0+\rho}{2}\right). \tag{A.1}$$

A.1. Integrating of $p(\rho)$

Taking Equation (4.14) as an example,

$$p(\rho) \approx p_{L(R)}e^{\frac{\lambda}{\rho_{L(R)}}-\frac{\lambda}{\rho}} + e^{-\frac{\lambda}{\rho}}\mathrm{Intg}_1, \tag{A.2}$$

where

$$\mathrm{Intg}_1 = \frac{\rho-\rho_{L(R)}}{2}\sum_{n=1}^{4}\omega_i f_2(\rho_i)e^{\lambda/\rho_i},$$

and $\rho_i = \frac{\rho-\rho_{L(R)}}{2}x_i + \frac{\rho_{L(R)}+\rho}{2}$.

Obviously, we can use (A.2) to evaluate all the values of $p(\rho_i)$ on all Gaussian quadrature points.

A.2. Integrating of $u(\rho)$

Taking Equation (4.15) as an example, if the wave is on the left side

$$u(\rho) = u_L - \int_{\rho_L}^{\rho}\frac{c_e(x)}{x}dx.$$

The numerical integration of $u(\rho)$ is given as

$$u(\rho) \approx u_L - \mathrm{Intg}_2 \tag{A.3}$$

where

$$\mathrm{Intg}_2 = \frac{\rho-\rho_{L(R)}}{2}\sum_{n=1}^{4}\omega_i\frac{c_e(\rho_i)}{\rho_i},$$

Different from (A.2), the sonic speed $c_e(\rho_i)$ is dependent on $p(\rho_i)$:

$$c_e(\rho_i) = \sqrt{a_0^2\frac{\partial f}{\partial\eta}\left(\frac{\rho_i}{\rho_0}\right) + \frac{p(\rho_i)}{\rho_i^2}\rho_0\Gamma_0 - \frac{\rho_0}{\rho_i^2}\Gamma_0 s_{xx}(\rho_i) + \frac{4}{3}\frac{\mu}{\rho_i}}. \tag{A.4}$$

After finishing the evaluation of $p(\rho_i)$, we can evaluate $c_e(\rho_i)$ by using the same process as (A.2).